[redacted]

1991-01-23

Measuring the Source Level of Wind Generated Ambient Noise in the Ocean

by

James W Cornish
B Sc , Royal Roads Military College, 1988

A Thesis Submitted in Partial Fulfillment of the
Requirements for the Degree of

MASTER OF SCIENCE

in the Department of Physics and Astronomy

We accept this thesis as conforming
to the required standard

[redacted]

Dr N R. Chapman, Supervisor (Defence Research Establishment Pacific)

[redacted]

Dr R W Stewart, Co-Supervisor (Department of Physics and Astronomy)

[redacted]

Dr R M Clements, Departmental Member (Department of Physics and Astronomy)

[redacted]

Dr J W. Wegner, Outside Member (Department of Mechanical Engineering)

[redacted]

Dr S R. Waddell, External Examiner (Royal Roads Military College)

University of Victoria

Supervisor Dr N Ross Chapman

ABSTRACT

Measurements of the source level of wind-generated ambient noise in the ocean at low frequencies (10-340 Hz) are presented in this paper The data were obtained using a vertical line array of hydrophones deployed in the deep water sound channel at various sites in the Northeast Pacific Ocean The array response was steered vertically upward to measure the locally generated sea-surface noise and eliminate the effect of distant shipping noise The beamforming was carried out with a frequency-domain beamforming algorithm using a spatial Kaiser-Bessel window function to reduce side-lobe levels in the beam pattern The beam power levels obtained were referenced to a source level at the sea surface using a simple propagation model An analysis of the relation between the measured surface source levels and measured wind speed data suggest that the noise level is dependent on local wind speed and is influenced by the presence of breaking waves in the ocean The source levels are compared with measurements reported in the literature

Examiners

[redacted]

Dr N R. Chapman, Supervisor (Defence Research Establishment Pacific)

[redacted]

Dr R W Stewart, Co-Supervisor (Department of Physics and Astronomy)

[redacted]

Dr R M Clements, Departmental Member (Department of Physics and Astronomy)

[redacted]

Dr J W Wegner, Outside Member (Department of Mechanical Engineering)

[redacted]

Dr S R Waddell, External Examiner (Royal Roads Military College)

Contents

List of Tables

List of Figures

Acknowledgements

The author acknowledges Dr N R. Chapman for his supervision and guidance in the analysis and interpretation of the data presented in this report The author also acknowledges the scientists and technicians of the Ocean Acoustics Group at the Defence Research Establishment Pacific and the crew of the CFAV Endeavour for their efforts in the data aquisition phase of the experiment

Special thanks to my wife for her patience, support, and proof-reading skills and efforts

Chapter 1

Introduction and Background

I. Preamble

In the study and prediction of deep-ocean acoustic ambient noise fields at low frequencies (below 200 Hz), it is becoming increasingly apparent [1, 2] that it is necessary to account for the effect of wind-generated ambient noise The wind speed dependence of the ambient noise field at high frequencies (above 200 Hz) is relatively easy to study and has been quantified by Urick [3] and Wenz [4] At lower frequencies, however, the wind-generated noise is more difficult to measure due to the predominance of shipping traffic noise, and the wind dependence of the ambient noise in this area of the spectrum is not well understood It is these problems which prompted the investigation to determine the source level of wind-generated noise that is presented in this thesis

II. High Frequency Noise

In his review of the available literature up to 1962, Wenz [4] was able to establish a composite of ambient noise spectra (see Figure 1 1) in the frequency band from 1 Hz to 100 kHz based on omni-directional measurements of the noise field in both shallow and deep water, at different wind speeds and in different locations He suggests that the ambient noise field (in the absence of biological or other spatially-dependent noise sources) is a combination of three main components

i a wind-dependent component with a broad maximum between 100 and 1000 Hz (He suggests that the most probable source of this component is bubbles and spray from surface agitation),

ii a wind-independent component with a broad maximum between 10 and 200 Hz and a steep negative slope for frequencies above the maximum (He suggests that this component is mostly attributable to shipping traffic noise), and

iii a thermal noise component which only affects the spectrum appreciably at very high frequencies

At frequencies between 200 and 1000 Hz, a major component of the ambient noise is the wind-dependent component, which makes it possible in many cases to observe the wind-dependence of the noise field with only an omni-directional hydrophone and without sophisticated processing In fact, at somewhat higher frequencies (above

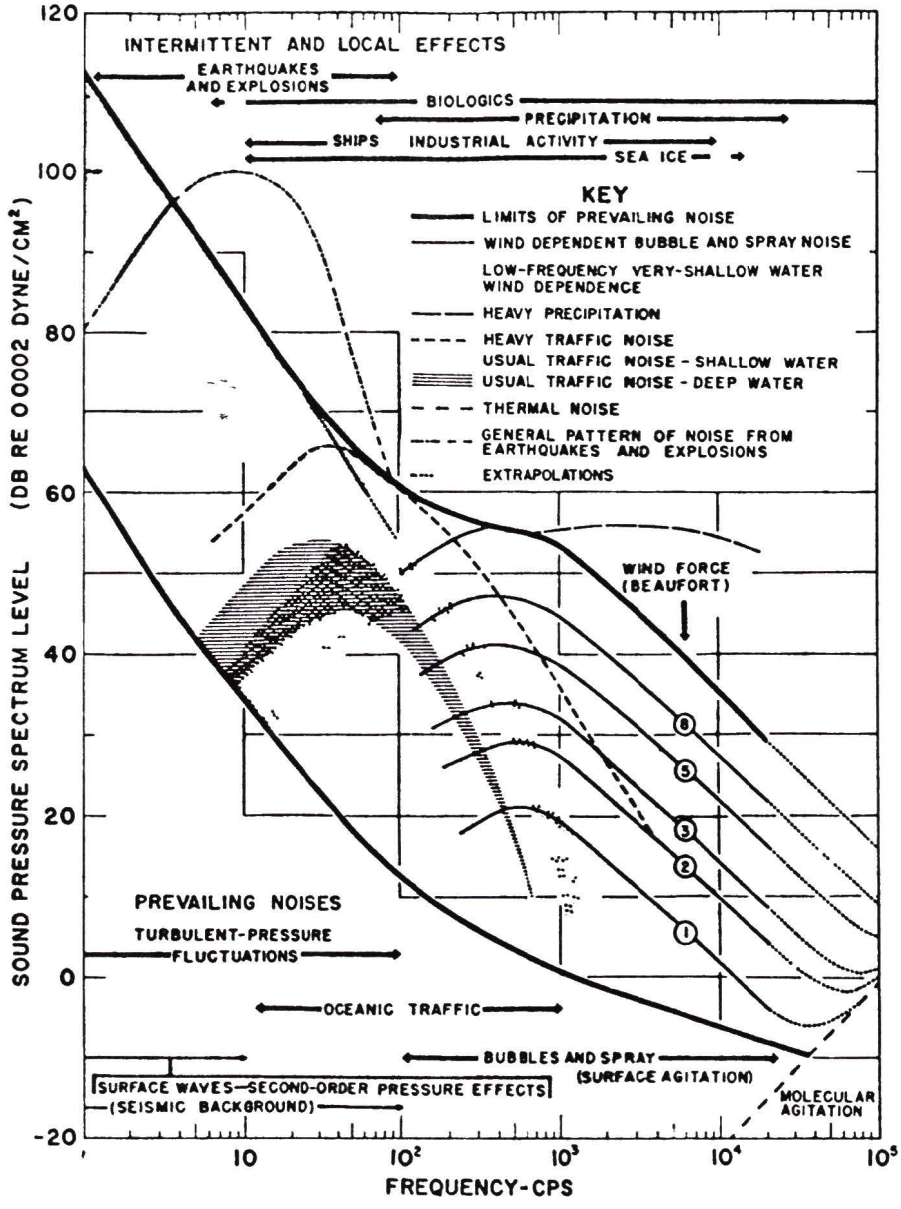

Figure 1 1 Wenz's composite diagram of ocean ambient noise

1000 Hz), Lemon et al [5] were able to devise a system of measuring local wind speeds and precipitation from hydrophone data in order to eliminate the need to place anemometers in the hostile environment of the sea surface

In his study of ambient sea noise off the Scotian Shelf, Piggott [6] used an omnidirectional hydrophone to determine the noise levels over a period of one year in 1959 and 1960 He related the noise levels in a number of frequency bands to the measured wind speed, using a linear least-squares regression in log space, according to

$$L(f,v) = A(f) + 20n(f)\log_{10} v \qquad (1\,1)$$

where $L(f,v)$ was the noise spectrum level in decibels, $A(f)$ and $n(f)$ were constant for a particular frequency f, and v was the wind speed in nautical miles per hour In this formulation, $n(f)$ is related to the power of the dependence of the noise level on wind speed For example, a value for $n(f)$ of 1 5 would correspond to the noise level being proportional to v^3F He found that the slope $n(f)$ was dependent on the frequency, and the model fitted his data well for all wind speeds at frequencies above 200 Hz At lower frequencies, he found that the noise levels tended to a constant at low wind speeds and suggested that this was possibly due to two different components in the noise field a background noise which is independent of wind speeds and a wind dependent noise with level varying linearly with the logarithm of the wind speed This two-component model is consistent with more recent results reported by Burgess and Kewley [7] Piggott could not, however, rule out the possi-

bility that the constant noise he found at low wind speeds was due to system noise The values which he obtained for the slope $n(f)$ at frequencies above 100 Hz varied between 1 53 and 1 20, and decreased with increasing frequency

The relation between wind speed and the transfer of wind energy into the ocean also lends support to the idea of a two–component model As Gill [8] points out, this tranfer depends on the wind stress which is a function of v^2 at wind speeds below approximately 10 knots and v^3 at higher wind speeds Thus, if the noise level were directly proportional to this energy transfer, with no non-linear effects due to the actual noise generation mechanism, the value of $n(f)$ should be equal to 1 for the low wind speeds and 1 5 for the higher wind speeds

III. Low Frequency Noise

At low frequencies (10-200 Hz) Wenz [4] suggests that the ambient noise field is composed of the wind-dependent and shipping noise components mentioned above, and also an additional low-frequency component which he attributes to ambient turbulence pressure fluctuations and seismic disturbances In this frequency band, however, he points out that the noise field is dominated by the shipping noise contributions unless the area in which the measurements are made is acoustically isolated from shipping traffic Because of this domination of the spectrum by shipping noise, it is very difficult to observe a wind dependence in the noise spectrum using only omni-

directional noise data.

Three different methods [2] have been developed for studying source levels at low frequencies The first method uses omni-directional noise measurements and relies on calculations of local propagation conditions to determine the strengths of the sources The conditions required for this method [1] include bathymetric blockage of long-range acoustic propagation paths, high bottom reflection loss to eliminate contributions from multiple bottom bounces, and location of the receivers below the depth of the turnaround point of the limiting ray for long-range propagation from the surface These conditions apply considerable restrictions on experimental location and do not eliminate the possibility of contamination of the data by sources not accounted for in the calculations [2]

Shooter and Gentry [9] used this method to measure ambient noise levels in the Parece Vela Basin Even though the above environmental conditions were satisfied by the location chosen for this experiment, they were only able to get good correlation between noise levels and wind speed for frequencies above 150 Hz due to contamination by shipping noise originating within the basin

Marrett and Chapman [10] also used this method in a study conducted using a towed line array in the South Fiji Basin. The basin satisfies all the conditions required for this method with the additional advantages of very low shipping densities and weak convergence zone propagation from surface sources They studied the omni-directional noise levels in 5 Hz bands centered at 18, 145, and 250 Hz and compared

them to wind speeds measured aboard the research vessel The correlation between the wind speed and the noise levels was good for the 250 Hz data and reasonably good for the 18 Hz data. The noise level in the 145 hz band did not follow the wind speed closely, however, and showed a diurnal variation– relatively constant levels during the day which were uncorrelated with wind speed, and night-time levels which dropped by as much as 10 dB They found some correlation between the wind speed and the night-time levels and attributed the diurnal variation in this band to biological activity

In the analysis of the noise data at 250 Hz, Marrett and Chapman [10] used the model which Piggott [6] used (Eqn 1 1), applied to the data from wind speeds above 15 knots They obtained a value for n of 1 5 using this model By applying this same model to beamformed noise data, using the lowest beam levels observed for a particular frequency and wind speed in the regression (assuming that any contamination would raise the levels), they were able to increase the correlation in the 125 to 180 Hz band They found that the value of n=1 5 was relatively constant over the entire band for high wind speeds In addition to these results, they also found a better correlation between the wind speeds and the measured noise at 250 Hz if a time delay of between 40 minutes and 2 hours was applied to the wind data. This suggests that there is a time lag between a change in the wind speed and a change in the noise level which is quite reasonable since surface agitation depends on the duration of the wind as well as the wind speed

The second method [11] requires the use of environmental data including bottom reflection losses, sound propagation paths and losses, a surface reflection model, and a description of the depth of the source and its directionality characteristics This environmental information is used to model the noise field and the modelled field is compared to the measured field to determine source levels Using this method in their study of source levels in the Mediterranean Sea, Kuperman and Ferla [11] were able to show wind-dependence in the noise field at frequencies above 400 Hz, but at lower frequencies shipping noise contamination prevented them from getting good results with the method even though they monitored shipping traffic by radar and included estimates of the effect of this traffic in their model

The third, and to date most successful, method, used by Burgess and Kewly [7] and Bannister et al [12], utilizes the directional capabilities of a vertical linear array of hydrophones By steering the array response and comparing the beam power in the upward looking beam to the beam power in the downward looking beam, Burgess and Kewley [7] were able to make direct measurements of the local noise generated at the surface In a slightly different approach, Bannister et al [12] used measured power in the upward looking beam and a model for the propagation from the surface, including bottom loss data to eliminate bottom reflected paths, to determine the source level of the noise generated at the surface As long as contamination from side-lobes in the beam pattern is understood and accounted for, it is possible to make direct measurements of locally generated noise levels [2] It is this last approach which

was chosen for use in this study

IV. Vertical Structure of Low–Frequency Noise

One of the first investigations of the vertical structure of the ambient noise field in the ocean was conducted by Axelrod et al [13] in 1964 Using a bottom–moored vertical line array of hydrophones, they measured the vertical directivity of the ambient noise field at various frequencies by performing time-delay beamforming and band-pass filtering the beam outputs At low frequencies (100-200 Hz) they found that the noise arriving from the horizontal (around 90° to the array axis)was greater than that arriving at the vertical (along the array axis) and vice-versa at high frequencies They also found that the cross-over point, where the noise from the vertical was at the same level as the noise from the horizontal, varied in frequency depending on the wind force– occuring at 100 Hz for a Beaufort wind force of 7 and at 550 Hz for a wind force of 4 (see Figure 1 2) They suggested that this behaviour was quite reasonable, since noise arriving from distant sources comes into the array at the horizontal with much of its high frequency component attenuated by propagation loss The vertical noise, on the other hand, emanates from sources nearly above the array and is subject to much less attenuation In addition, though it is not evident from the figure due to the scaling used for the vertical axis, they found that the noise from the vertical exhibited a high dependence on sea-state while the horizontal noise did not This

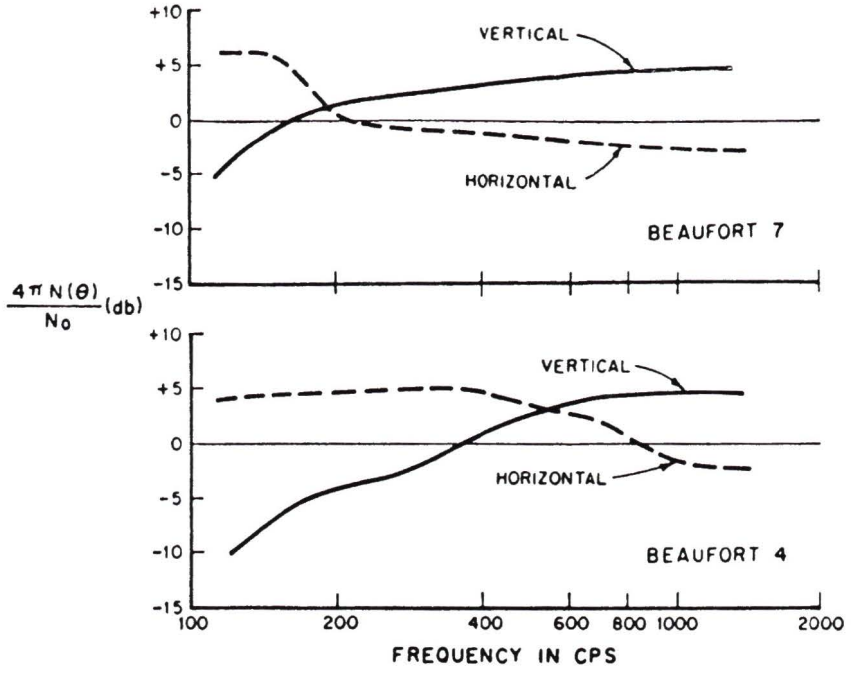

Figure 1 2 Axelrod et al 's plot of horizontal and vertical noise levels vs frequency

behaviour is consistent with the theory that the vertical noise is locally generated by surface agitation while the horizontal noise is primarily the result of distant shipping

The results of this early experiment have been confirmed and expanded upon by several investigations conducted with more sophisticated equipment and data processing techniques In their review of ambient noise directionality data available up to 1986, Carey and Wagstaff [14] found that the vertical noise field at low frequencies was characterized by a broad hump or pedestal centered at the horizontal and with a width of 10 to 15 degrees on either side They state that this pedestal is a result of SOFAR (sound channel refracted paths) propagation of sound from deep-ocean shipping which arrives at $\pm 10°$ to $\pm 15°$ and from down-slope enhancement of noise (mainly shipping) from the continental shelf or sea-mounts which fills in the noise at the horizontal The noise falls off rapidly at angles to the horizontal greater than $\pm 15°$ to minimum values in the vertical both upwards and downwards from the array Hodgkiss and Fisher [15] found similar results and one of their plots of array response vs vertical arrival angle is included as Figure 1 3 Burgess and Kewley [7] added that the noise in the vertical from above the array was slightly higher than that from below the array, with the difference depending on the magnitude of the bottom loss at the site This is due to the fact that there is one direct path from the surface to the upward-looking beam, while all paths to the downward beam undergo at least one bottom reflection This characteristic was essential to their determination of the source levels at the surface in the absence of bottom-loss measurements

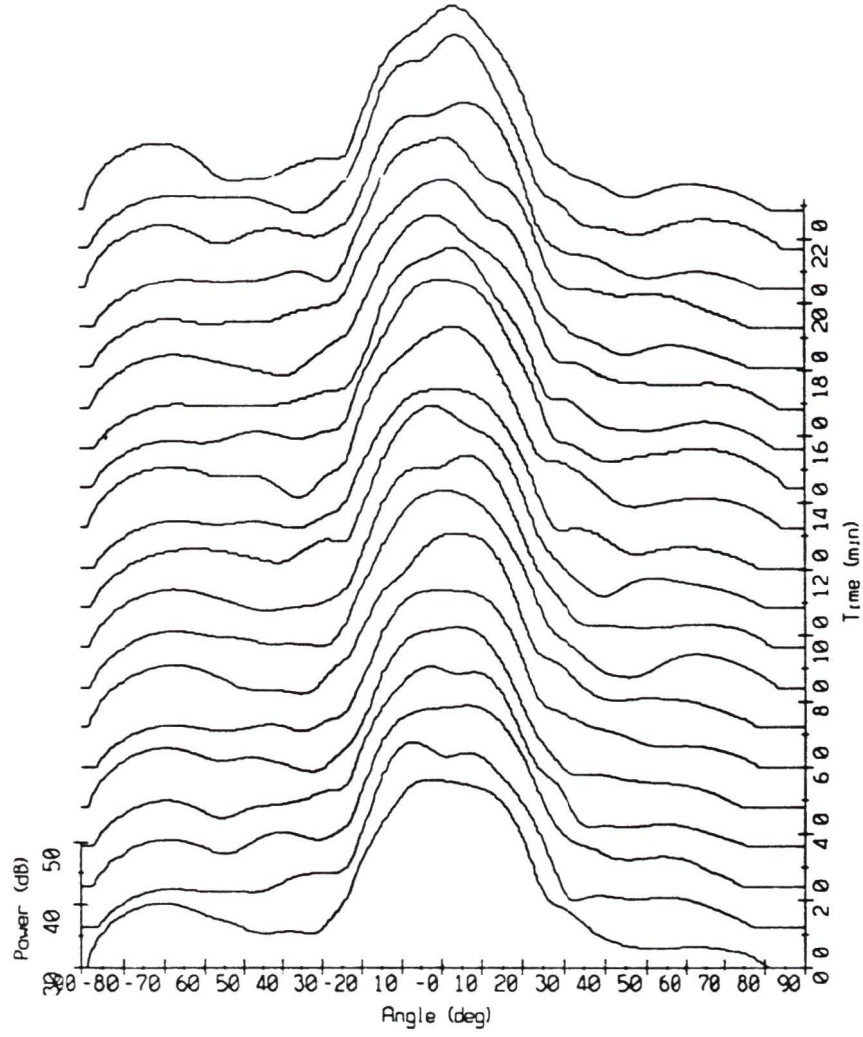

Figure 1 3 Hodgkiss and Fisher's plot of array response vs vertical arrival angle at 100 Hz

More recently, these general results were confirmed by Sotirin and Hodgkiss [16] using a large-aperature, 120 element array suspended from the research platform FLIP Their results are in agreement with those previously reported with regard to spectral shape They were also able, with the increased angular resolution due to the large number of elements used, to produce finer-scaled plots of the vertical directionality of the noise field which confirmed the broad pedestal at $\pm 15°$ to the horizontal

V. Wind-Noise Generation Mechanisms

The mechanism responsible for the generation of underwater ambient noise from surface sources is not well understood [17] In his review of underwater ambient noise sources, Wenz [4] studied the source characteristics of bubble oscillations, impacting water droplets, surface wave interactions, and turbulence effects He concluded that the most probable noise generation mechanisms at high frequencies were bubble oscillations and spray impact He also pointed out that bubbles have a natural frequency of oscillation which is inversely proportional to the size of the bubble and that the sound pressure amplitude is directly proportional to the amplitude of oscillation of the bubble Since there is a practical limit to bubble size, and it is quite possible that there would be a predominance of bubbles of nearly the same size, he pointed out that in general the spectrum should have a maximum at some frequency associated

with the predominant bubble size

Wilson [1] quantified this further by suggesting that the surface-noise generation mechanism could be separated into three frequency regimes

i 5-10 Hz, where the dominant mechanism is wave-wave interaction (production of standing waves for which the pressure amplitude effects are not inversely proportional to depth as with surface gravity waves),

ii 10-80 Hz, where turbulent pressure fluctuations in the atmosphere near the ocean surface are the dominant mechanism, and

iii 80-1000 Hz, where the impact of ocean spray streaks and whitecaps with the ocean surface dominate

Kerman [17] examined several different models of noise generation at high frequencies spray noise, bubble cavitation, and bubble oscillations He found that none of the models studied were complete in their formulation of a physical model of the noise generated by wind forcing He therefore chose to study noise produced by bubbles entrained by breaking waves oscillating at frequencies other than their resonant frequency as a result of turbulent pressure fluctuations at or near the surface These turbulent pressure fluctuations cause cavitation, and therefore volume fluctuations, of the the entrained bubbles, thereby generating noise The entrainment of large amounts of bubbles is dependent upon breaking waves, which would suggest that this mechanism is only active at wind speeds high enough to cause whitecaps

Prosperetti [18] examined the generation of noise by entrained bubbles in three frequency ranges- below 100-200 Hz, between 100 Hz and 1 kHz and above 1 kHz In the high frequency range (above 1 kHz), he suggests that the noise is a result of single bubble oscillations When the bubble is entrained by the breaking wave, it is presumed to have some initial mechanical energy associated with its velocity of penetration of the water This initial energy is dissipated through damped free oscillations of the bubble in the water which produce acoustic waves at the natural frequency of oscillation of the bubble This mechanism is not viable in the intermediate frequency range (100 Hz to 1 kHz), however, since it would require bubbles with a diameter of 1 cm or more which is not physically realistic

In this medium-frequency range, Prosperetti [18] suggests a possible noise generation mechanism is the collective oscillation of large bubble clouds When two or more oscillators are coupled together in some way, they are capable of oscillating in collective modes at much lower frequencies than their individual natural frequencies The physical mechanism involved is essentially the oscillation of a volume which contains both bubbles and fluid which has different properties from either a large bubble or a volume of fluid and therefore different resonant characteristics For these collective, low-frequency oscillations to occur, Prosperetti states that the bubble clouds would have to be excited coherently but he points out that this would not be unreasonable in the presence of breaking waves

In the low-frequency range (below 100-200 Hz), Prosperetti [18] suggests that

the noise generation mechanism is the amplification of turbulent noise by bubbles present in the turbulent region He points out that turbulence itself is not a good radiator of sound, but if bubbles are present in the turbulent region, they respond to the turbulent pressure fluctuations with volume pulsations as was mentioned by Kerman [17] and these radiate more effectively In breaking waves, regions of intense turbulence coincide with regions of large bubble population [18] so this mechanism is quite plausible in the presence of breaking waves

In the mechanisms discussed above, there is a reliance on breaking waves for bubble formation, turbulence, or spray Since waves generally do not break at wind speeds below about 10 knots, it is reasonable to assume that there should be two regimes of wind speed with different processes generating the noise and a different wind-speed dependence in each regime Kewley et al [2] examined the literature on the theory of noise generation mechanisms and suggested that at frequencies above about 10 Hz, the noise level should be proportional to v for low wind speeds and proportional to v^3 for wind speeds above about 10 knots This would seem to indicate that the noise generated is not proportional to the wind-energy transfer [8] at low wind speeds They also observed that the measured dependences reported in the literature varied widely between v^1 and v^4 and suggested that this could be due to the narrow range of wind speeds studied in each case If two processes were operating in different wind-speed regimes, as suggested above, then results would be different for different studies if the range of wind speeds used was not the same

VI. Scope of Thesis

The aim of this thesis is to use a vertical line array of hydrophones to measure the local wind-generated noise by steering the array response in the vertically upward (or up end-fire) direction, and to study the wind-speed dependence of this noise Acoustic noise data were collected from selected sites in the North-East Pacific Ocean and processed using a frequency-domain beamforming algorithm to determine beam powers in the vertical in the frequency range 10-350 Hz The beam powers are scaled for system and processing gains and referenced to a source level at the surface using a propagation model developed by Bannister et al [12] The source levels obtained are compared with measured wind data and the wind-speed dependence of the local noise is examined

Chapter 2

Experimental Method

I. Data Collection

Data for this study were collected in experiments carried out in 1977, 1978, 1981, 1983, 1984, 1985, and 1986 using various configurations of a multi-element vertical line array (MEVA) The MEVA was deployed at the depth of the deep-water sound channel axis from the CFAV Endeavour

The variations of the MEVA used in this experiment were designed and constructed by the Ocean Acoustics Group at the Defence Research Establishment Pacific (DREP) The system was designed to collect data for a number of different experiments and can be broken down into eight main parts

1 the surface float, which contained a radar transponder, a radar reflector, the surface electronics unit, and a battery pack, and provided the FM radio link to

the CFAV Endeavour,

ii a distributed source of surface bouyancy,

iii a damper plate to isolate the array from surface wave action,

iv a sub-surface float from which the array was suspended,

v the lower electronics unit (which contained the power gain amplifier (PGA), digitizer, tilt sensor, and multiplexer),

vi a horizontal circular array (not always present and not used in this experiment),

vii the multi-element vertical array, and

viii weights to hold the array in a vertical attitude

A diagram of the entire system is shown in Figure 2 1 and the variations of the MEVA for each year are shown in Figures 2 2 to 2 5 The experiments were carried out at selected sites in the Northeast Pacific

During data collection periods, all mechanical systems aboard CFAV Endeavour and, when possible, other ships involved in the experiments were shut down to reduce the possibility of nearby ship noise contaminating the data. During these 'quiet periods', data from the hydrophones in the band 0-500 Hz were sampled at 1500 Hz, submultiplexed along with array status information, and transmitted to the CFAV Endeavour by an FM radio link. Aboard the Endeavour, the data were recorded on a

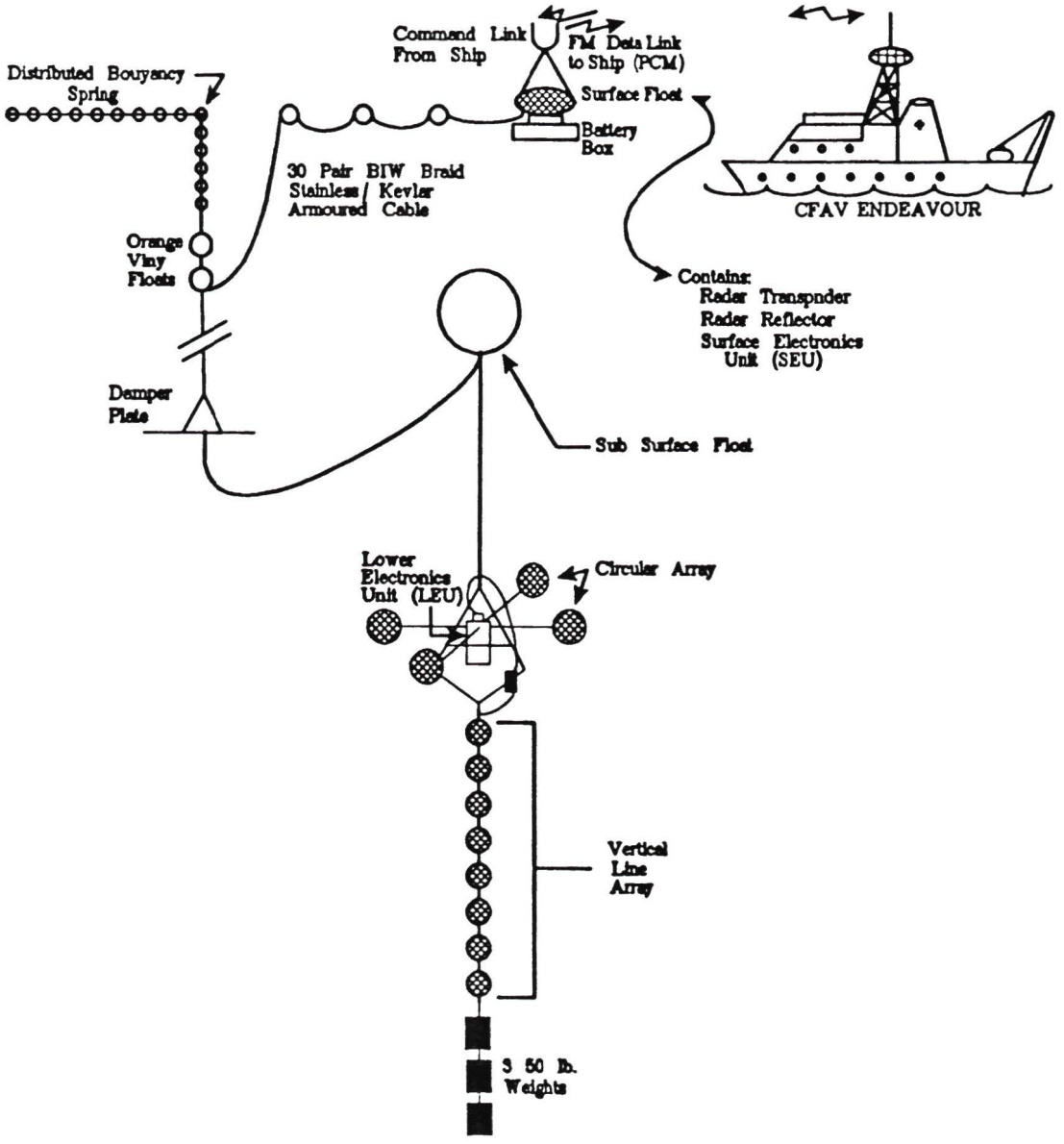

Figure 2 1 Diagram of MEVA system.

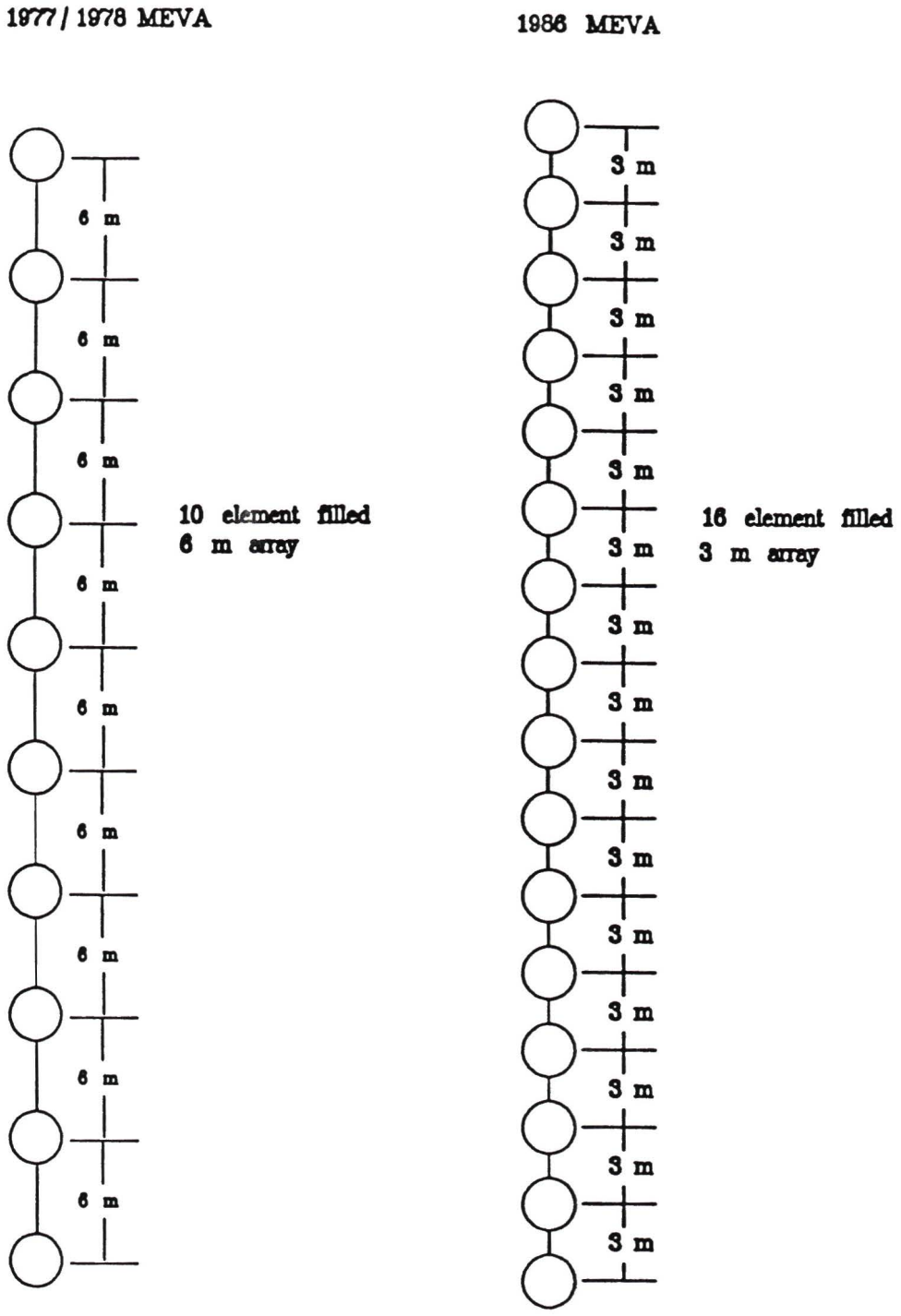

Figure 2 2 1977/78 and 1986 MEVA

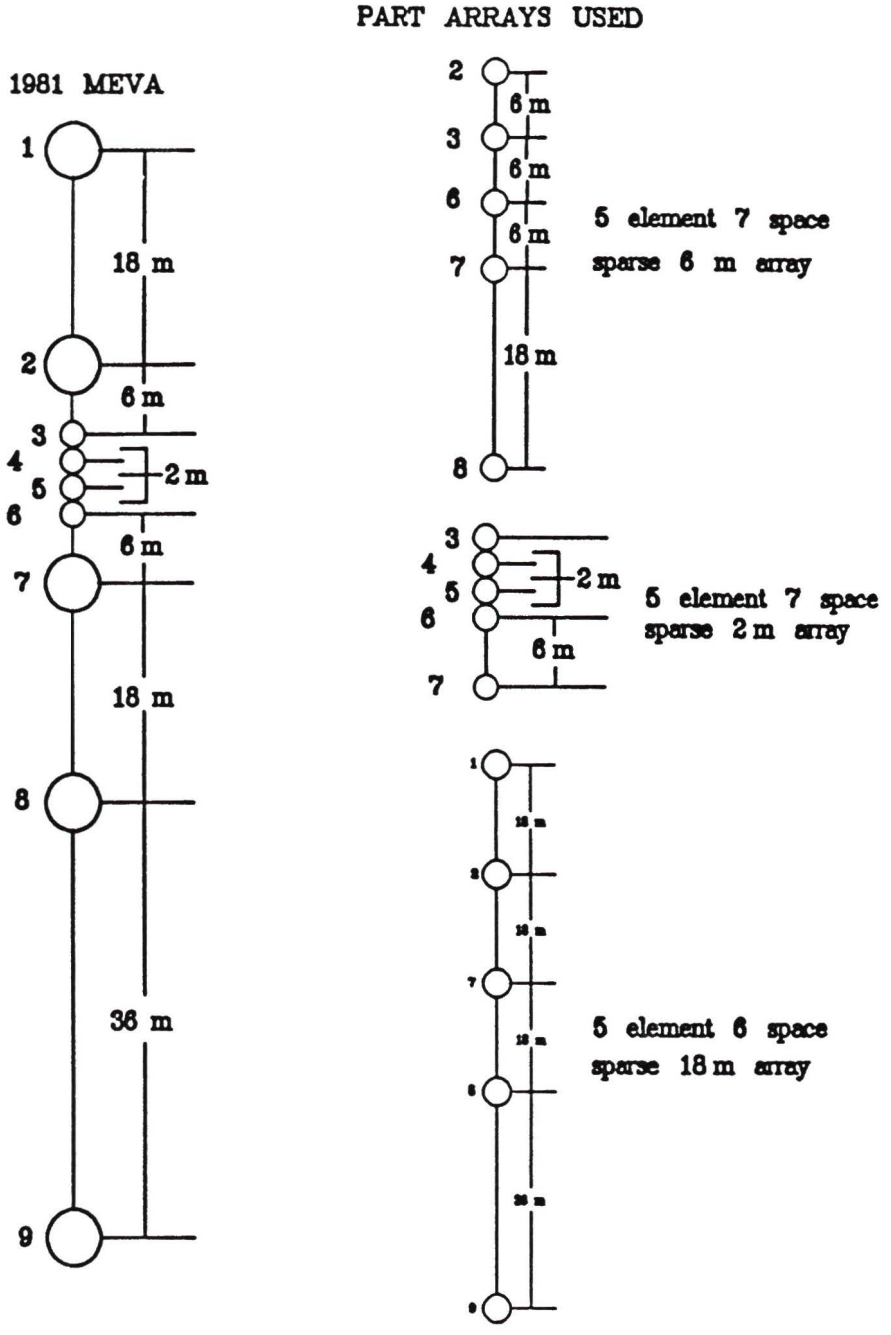

Figure 2 3 1981 MEVA

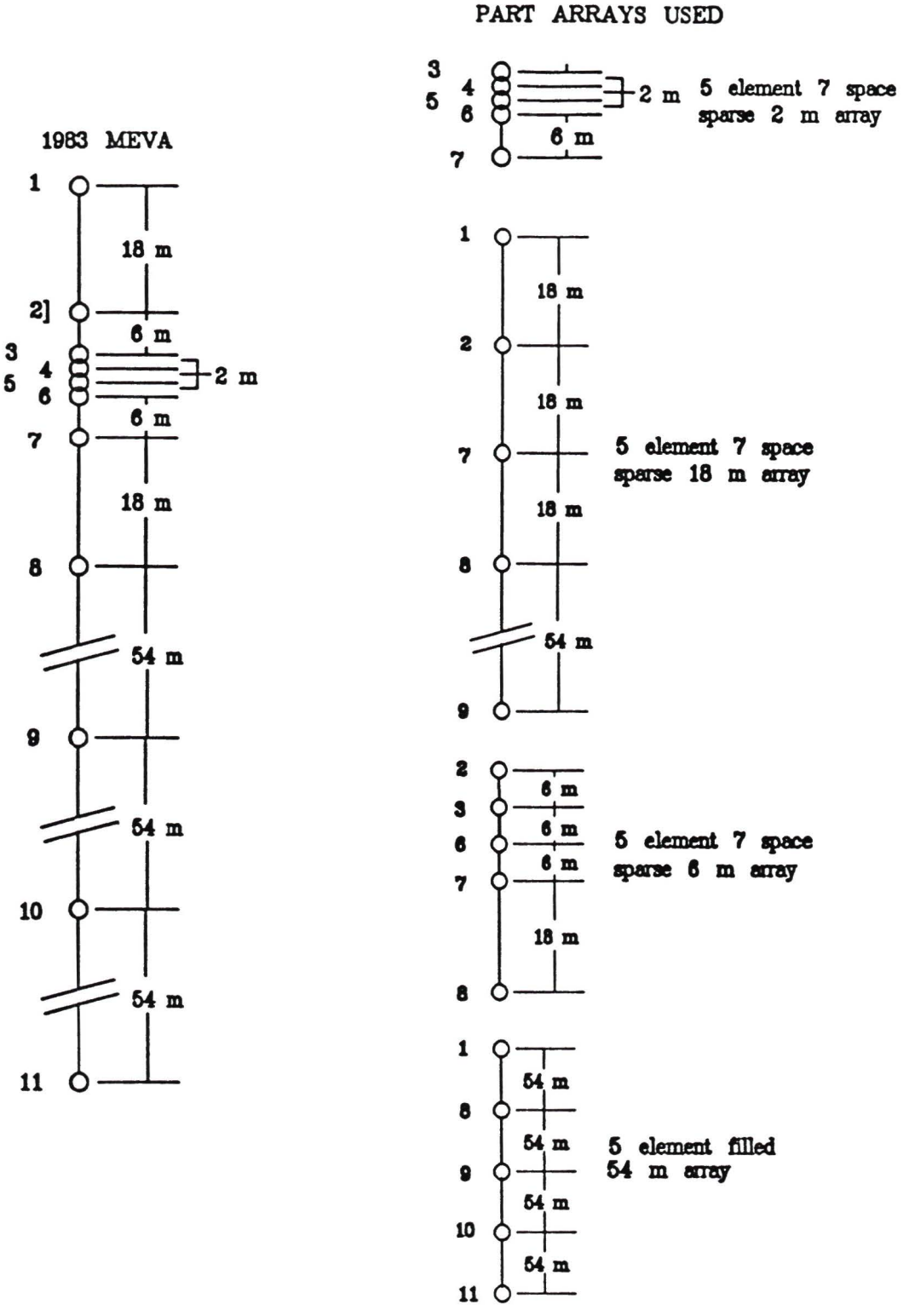

Figure 2 4 1983 MEVA

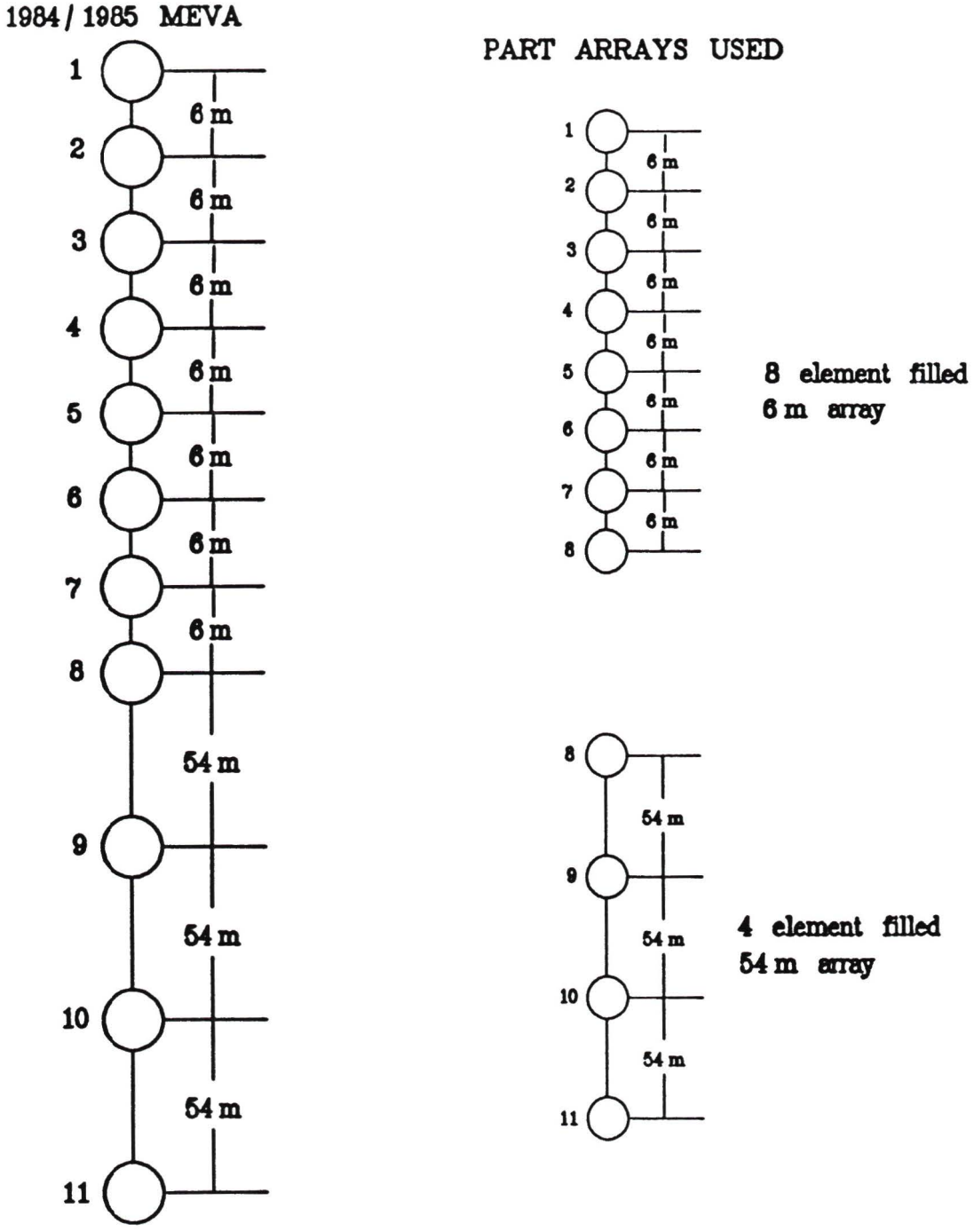

Figure 2 5 1984/85 MEVA

master magnetic tape and later transcribed to tapes readable by the data management system at DREP A schematic of the electronics from the sampling hydrophone to the recording tape is shown in Figure 2 6 and the system gains are listed in Table I

The bridge crew of the Endeavour were requested to record wind speed and direction measurements at two or four hour intervals from readings of the ship's anemometer These measurements represent the deck officers' best interpretation of the wind speed at the time of the measurement and no time averaging was possible other than the time actually taken for the deck officer to determine the wind speed As such, there is likely to be considerable variance in these measurements This data was retrieved from the bridge logs and used to determine wind speeds during observation intervals by plotting the wind speed versus time and interpolating between measured points Unfortunately, the relatively large time interval between wind-speed observations precluded an investigation of the time-lagged cross correlation between wind-speed and noise level and it was impossible to confirm the 40 minute to 2 hour time lag reported by Marrett and Chapman [10] which was discussed in the introduction

II. Data Processing

Figure 2 7 shows a schematic diagram of the steps taken in processing and analyzing the hydrophone noise data in order to obtain estimates of the array beam powers in the vertical direction A discussion of the processing system is given in the following

	YEAR				
	1977/78	1981	1983	1984/85	1986
Hydrophone Sensitivity (dB)	-187 7	-187 7	-187 7	-193 1	-193 1
Freq (Hz)	SYSTEM GAINS (dB)				
1	11 2	16 0	11 2	7 4	2 4
5	24 3	24 3	24 3	15 5	—
6	26 4	—	26 4	—	—
7	—	—	—	—	—
11	26 4	—	26 4	25 2	25 2
13	—	25 5	—	—	—
19	26 5	—	26 5	27 3	28 0
29	—	—	—	28 3	—
57	25 9	—	25 9	28 4	—
97	25 6	—	25 6	28 7	—
200	25 4	25 5	25 4	28 3	28 0
325	—	—	—	—	24 0
400	—	24 0	—	26 3	15 0

Table 2 1 Summary of system gains

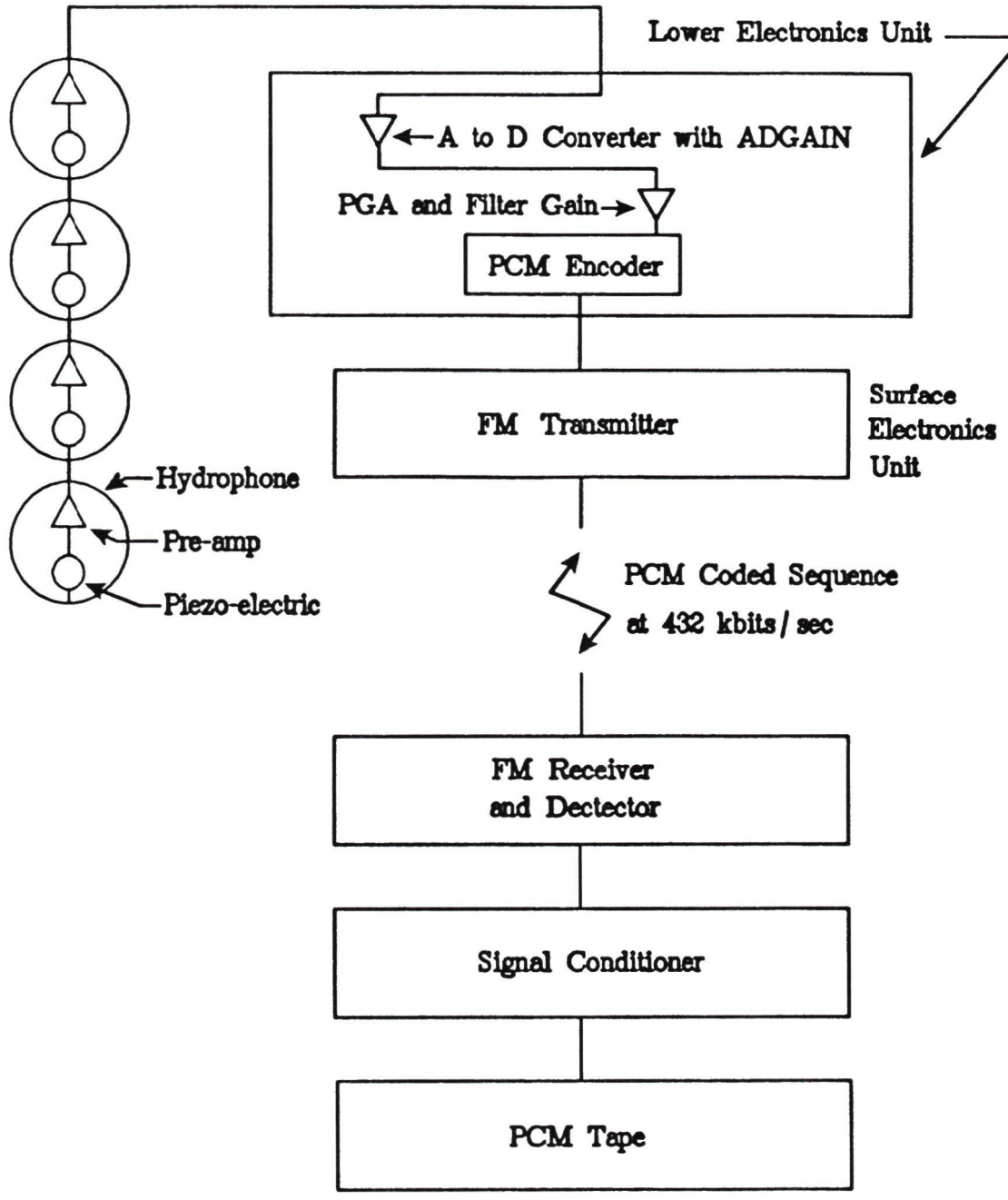

Figure 2 6 Schematic of electronics

sections, beginning with a description of the beamforming algorithm.

A. Beamforming Algorithm

The forming of beams using a multi-element array is a well-established technique which essentially maximizes the sensitivity of the array to signals arriving from a particular angle to the axis of the array The process can also be called spatial filtering and is analogous to the frequency filtering accomplished with Fourier Transforms [19] In fact, discrete Fourier techniques can be used to carry out the beamforming, and the use of windows and averaging have the same effects on the properties of the transform

The simplest example of beamforming using only two hydrophones is illustrated in Figure 2 8 using a two-element array If the signals received at each hydrophone are simply added together, the resultant beam pattern is omni-directional as shown in the figure However, for frequencies with wavelengths greater than or equal to twice the hydrophone separation, if the signal from one of the hydrophones is subtracted from that of the other, the resultant beam pattern has the characteristic dipole pattern with two main lobes along the axis to the array and nulls at 90° to the axis This simple method of beamforming is highly suitable when processing power and hydrophone number are limited, and is extensively used in directional sonobouys deployed from ships and aircraft where size and operating channels for transmission of data are limited The steering of beams using this method, however, must be accomplished by physically changing the direction of the axis of the array, which limits its applications

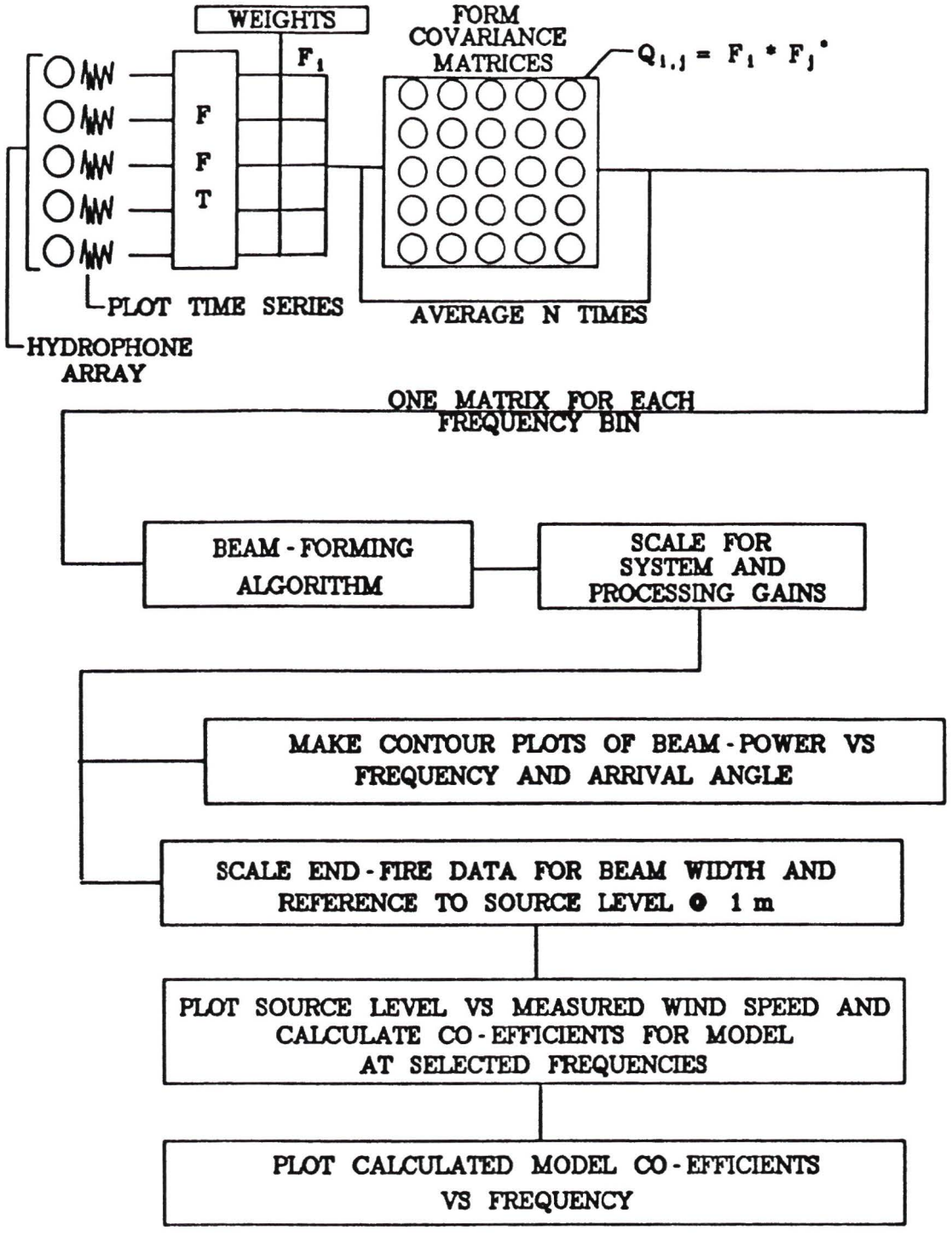

Figure 2 7 Schematic diagram of steps in signal processing

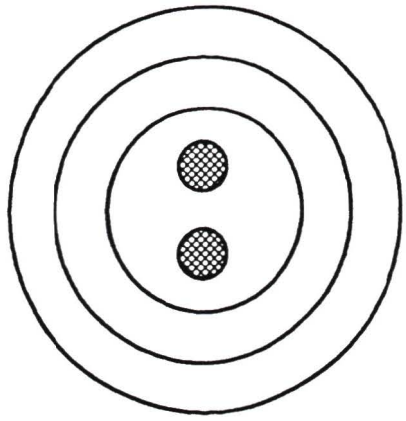

When the signals are simply summed, the resultant beam pattern is omni-directional.

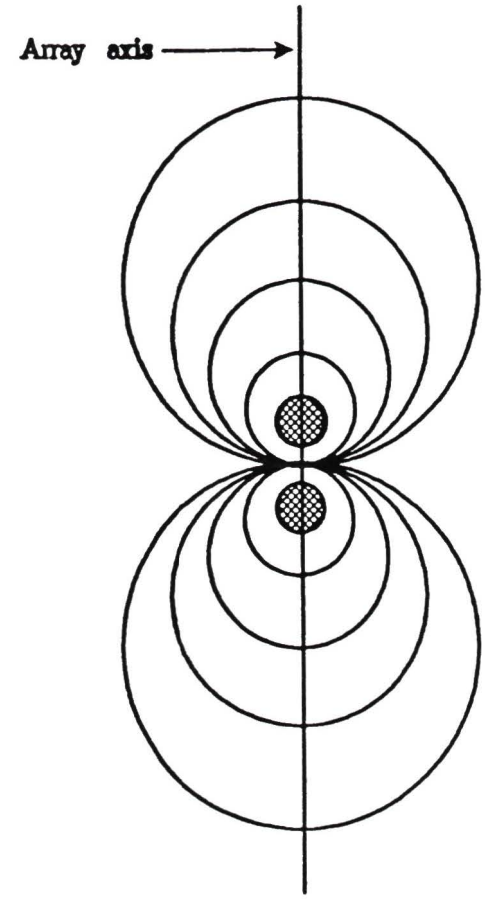

When one of the signals is multiplied first by -1, however, and the signals are then summed, the resultant beam pattern is the characteristic dipole pattern.

Figure 2 8 Beam patterns for simple, two-element array

A more sophisticated method of beamforming, which steers the beams electronically, is more useful when the limitations of processing power and hydrophone number are not as serious a factor

The geometry of a plane-wave signal arriving at a multi-element array from a distant source is illustrated in Figure 2 9 As the wave front travels in the direction of propagation, it is clear that the signal will arrive at each hydrophone at a different time In the case illustrated in the figure, it will arrive at the top hydrophone first, and the arrival at each subsequent hydrophone will be delayed by a time factor τ which depends on the angle θ, the hydrophone separation d, and the speed of propagation of the wave front c according to

$$\tau_n = \frac{d_n * cos(\theta)}{c} \tag{2 1}$$

where d_n is the distance to the n^{th} sensor It is easy to see, then, that by applying a succesive time lag of τ_n to the output from the n^{th} hydrophone and summing the lagged outputs, it is possible to maximize the sensitivity of the array to signals arriving at the angle θ [20] The actual process of forming the beam is defined by

$$y(t) = \sum_{n=0}^{N-1} W_n x_n(t - \tau_n) \tag{2 2}$$

where y(t) is the beam output, N is the total number of sensors in the array, W_n is the weighting function applied to the n^{th} sensor, $x_n(t)$ is the output from the

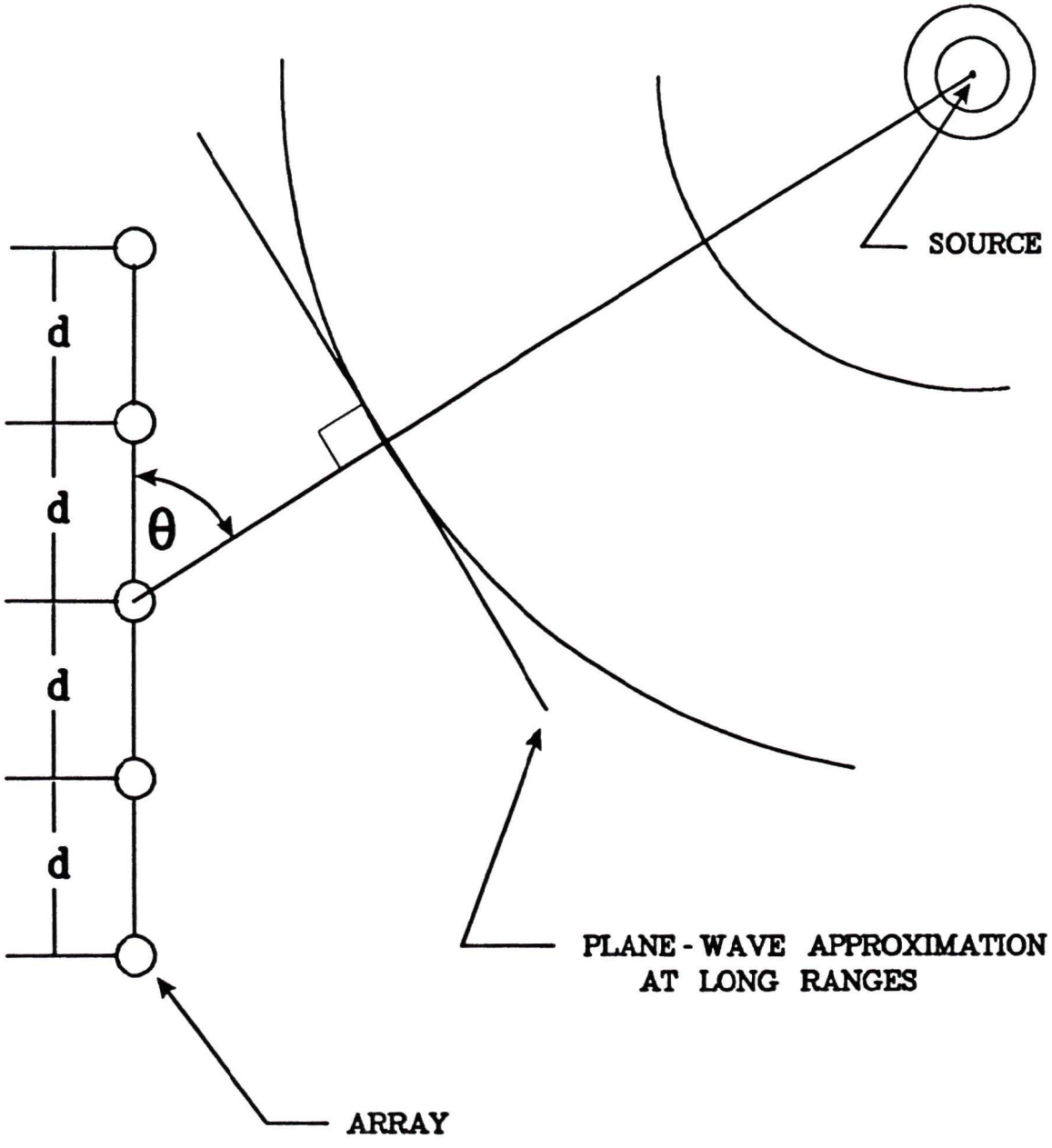

Figure 2 9 Geometry of plane wave arriving at array

n^{th} sensor, and τ_n is the time delay defined above for the n^{th} sensor This procedure is called time-delay beamforming and can be accomplished with either software or hardware, but is very time or hardware intensive depending on the method used

Another way of acheiving the same result with less effort utilizes the properties of the Fourier Transform[22] and is called frequency-domain beamforming A time lag in the time domain is equivalent to a phase shift in the frequency domain [20] and therefore if the time signals from each hydrophone are first transformed to the frequency domain and then a phase shift corresponding to the required time lag is applied before the power is computed from the transformed signals, the result will be a maximization of the sensitivity of the array at an angle θ The phase shift ϕ_n to be applied between the first hydrophone and the n^{th} hydrophone depends upon the frequency f, the angle θ, the sound speed c, and the distance to the n^{th} hydrophone d_n according to

$$\phi_n = 2\pi d_n \frac{f}{c} cos(\theta) \tag{2 3}$$

The relation between time-delay beamforming and frequency-domain beamforming is seen by taking the fourier transform of Equation 2 2 [21]

$$\mathcal{F}(y(t)) = Y(f) = \sum_{n=0}^{N-1} (W_n e^{-2\pi i f \tau_n} X_n(f)) \tag{2 4}$$

and substituting for τ_n

$$Y(\theta, f) = \sum_{n=0}^{N-1} W_n e^{\frac{-2\pi i d_n f}{c} cos(\theta)} X_n(f) \quad (2\,5)$$

and the beam strength is defined as

$$B(\theta, f) = \vec{j}^* \mid Y(\theta, f) \mid^2 \vec{j} \quad (2\,6)$$

where $\vec{j}$ is an N-dimensional unit vector

The beamforming of the data for this thesis was accomplished in this way using a frequency domain beamforming program [21] which was originally developed for DREP by Barrodale Computing Services and was modified to suit the requirements of this study The program implements an efficient algorithm for conventional frequency-domain beamforming as outlined by Bucker [22] and developed above Equation 2 6 can be simplified using matrix notation to[21]

$$B(\theta, f) = \vec{j}^* D_\theta^* Q D_\theta \vec{j} \quad (2\,7)$$

where Q is the N×N cross-covariance matrix with the weights W_n already included and D_θ is an N×N beam-steering matrix defined by

$$\begin{matrix} e^{\phi_1} & 0 & 0 \\ 0 & e^{\phi_2} & 0 \\ & & 0 \\ 0 & 0 & e^{\phi_n} \end{matrix}$$

where ϕ_k is the phase lag to the k^{th} sensor defined by

$$\phi_k = (\frac{2\pi d_n f}{c})cos(\theta) \tag{2 8}$$

The method actually implemented in the program [21] makes use of the fact that the matrix Q is hermitian and can be factored by Cholesky decomposition into arrays U and L such that

$$LU = Q \quad and \quad L = U^* \tag{2 9}$$

Thus, equation 2 7 can be expressed as

$$B(\theta) = \vec{j}^* D_\theta^* U^* U D_\theta \vec{j}$$

$$B(\theta) = \mid U D_\theta \vec{j} \mid^2 \tag{2 10}$$

Using equation 2 10, the beamforming algorithm produced beams for 181 directions equally spaced in $\cos(\theta)$ from 0° (pointing straight up at the surface) to 180° (pointing straight down at the bottom)

B. Beamforming Window

In using a vertical linear array to steer beams towards the surface and look at locally generated noise, what is effectively being done is applying a spatial filter to the incoming noise so as to ignore noise arriving at angles near the horizontal (presumably coming from distant sources) and maximize the sensitivity to noise arriving at vertical angles (from the surface) As with any filtering operation of this type, the major

factors affecting performance are the filter band width and the side-lobe suppression As was discussed in the introduction, the noise level arriving at the horizontal to the array is usually greater than that arriving at the vertical, and, as Burgess and Kewley [7] point out, it is necessary to ensure that side-lobe suppression in the beamforming filter is large enough that the ratio of near-horizontal noise to vertical noise is less than the inverse of the array peak side-lobe levels when the array is steered to end-fire If this condition is not met, the noise included through the side-lobes at the horizontal will exceed that arriving from the vertical and contaminate the results With this in mind, it is apparent that the side-lobe suppression was a critical factor in this study The side-lobe suppression of a standard rectangular window (i e $W_n = 1$ for all n) is only -13 dB, and does not always meet the above criterion, therefore it is necessary to employ some technique to reduce side-lobe levels Unfortunately, when dealing with a filter of this type, there is always a trade-off between side-lobe suppression and main-lobe width [23] When side-lobe suppression is increased, main-lobe width also increases As was explained in the introduction, however, the width of the noise pedestal is confined to within $\pm 15°$ of the horizontal, so as long as the main lobe width is much less than 75°, noise from the pedestal should not significantly affect the results by entering through the side of the main lobe

As with conventional Fourier filtering in the frequency domain, the main-lobe width and the side-lobe suppression are controlled by applying weights (a window function) to the elements in the filter[23] Side lobes in the filter are caused by dis-

continuities in the derivatives of the window function [19], which show up as the side lobes when the window function is transformed By applying a different window function to the elements in the filter, it is possible to smooth out these discontinuities and thereby reduce side-lobe levels The choice of which window function is appropriate under any given set of circumstances is determined by consideration of the side-lobe suppression required, the trade-off between side-lobe suppression and main-lobe width, and the side-lobe roll-off or the decrease in side-lobe peak height for successive side-lobes away from the main lobe Harris [23] studied and listed the characteristics of most of the window functions available Although these windows were developed for the transform from the time domain to the frequency domain, Harris[23] points out that they also apply to beamforming The window function chosen for use in this study was the Kaiser-Bessel window and is defined by

$$W_n = \frac{I_0(\pi\alpha\sqrt{1\,0 - (\frac{n}{N/2})^2})}{I_0(\pi\alpha)} \tag{2 11}$$

where

$$0 \leq n \leq N/2$$

$$I_0(X) = \sum_{k=0}^{\infty}(\frac{(\frac{x}{2})^k}{k!})^2$$

With $\alpha = 2$ the theoretical characteristics of this window for a beam steered broadside to the array are [23]

1 a first side-lobe peak suppression of -46 dB,

ii a side-lobe fall-off of -6 dB/octave, and

iii a coherent gain of 0 49

This window was also used by Sotirin and Hodgkiss [16] and Hodgkiss and Fisher [15]

Figures 2 10 to 2 16, show the beam patterns obtained using the STARPACK [21] simulation program for the arrays used in this study Although the theoretical side-lobe suppression of -46 dB was not achieved (mostly due to the fact that these beams were steered to end-fire and not broadside), the suppression in each case is much greater than the -13 dB attainable using a rectangular window function A sensor spacing of $d = 0\,4\lambda$ (λ = the wavelength in metres) was assumed for each of these plots

C. Array Design

In the design of the array (i e the positioning of the sensors along the array axis), three main factors must be taken into consideration

i the frequency range over which the array is to be effective,

ii the desired angular resolution of the array, and

iii the availability of hydrophones and the ability to collect and store the signals from them.

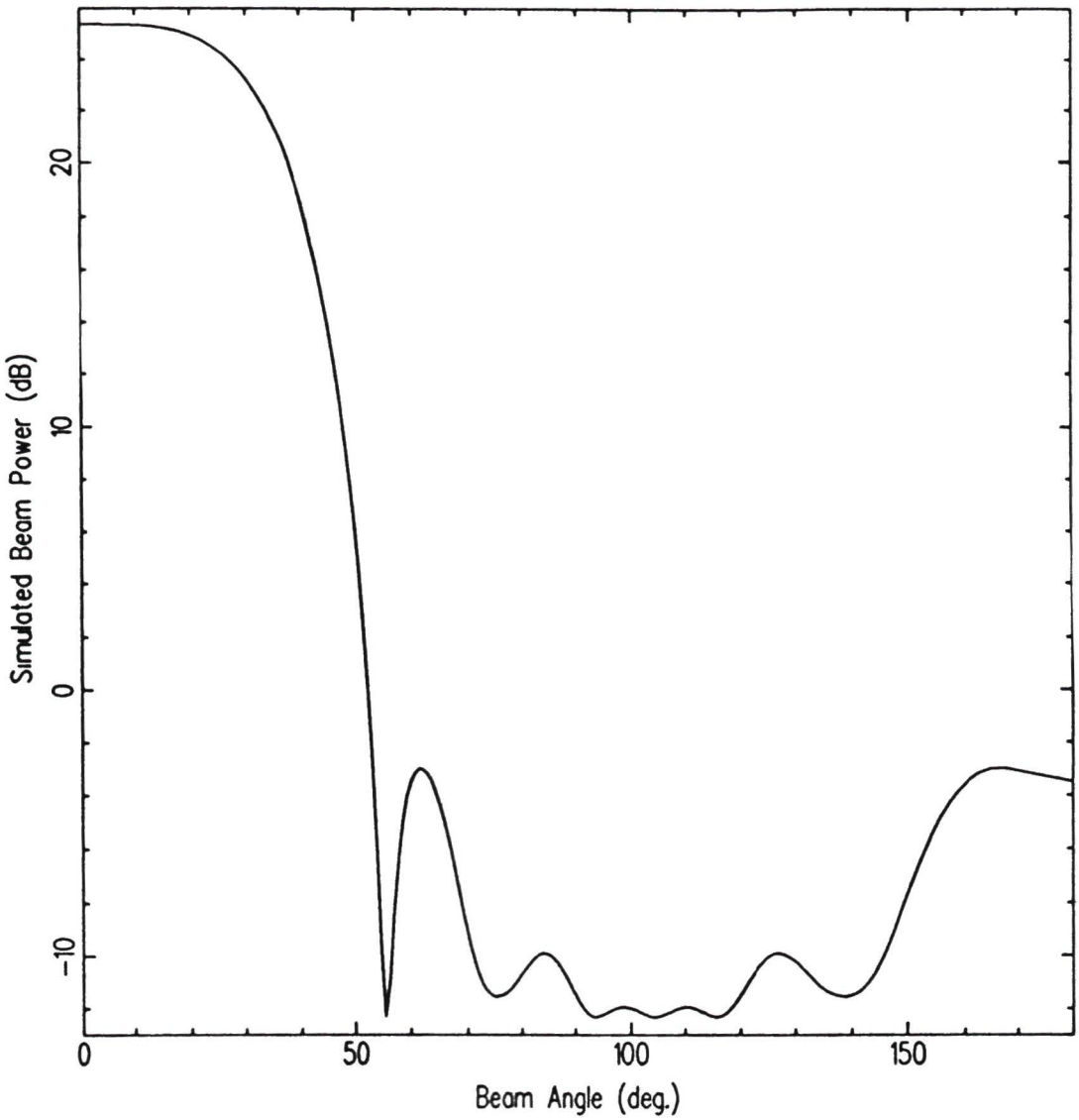

Figure 2 10 Beam pattern for 1977/78 6m array

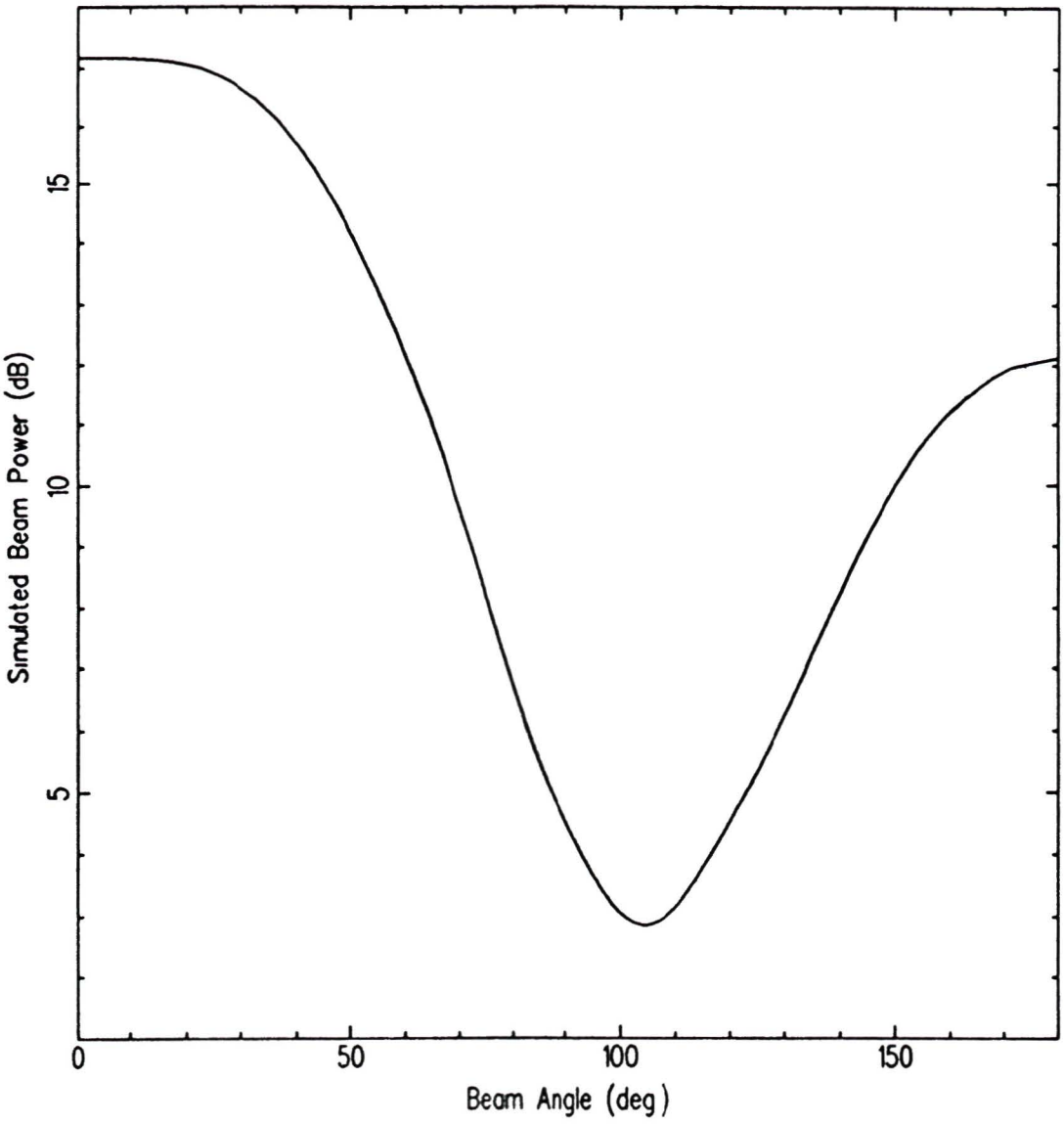

Figure 2 11 Beam pattern for 1981 and 1983 2m and 6m arrays

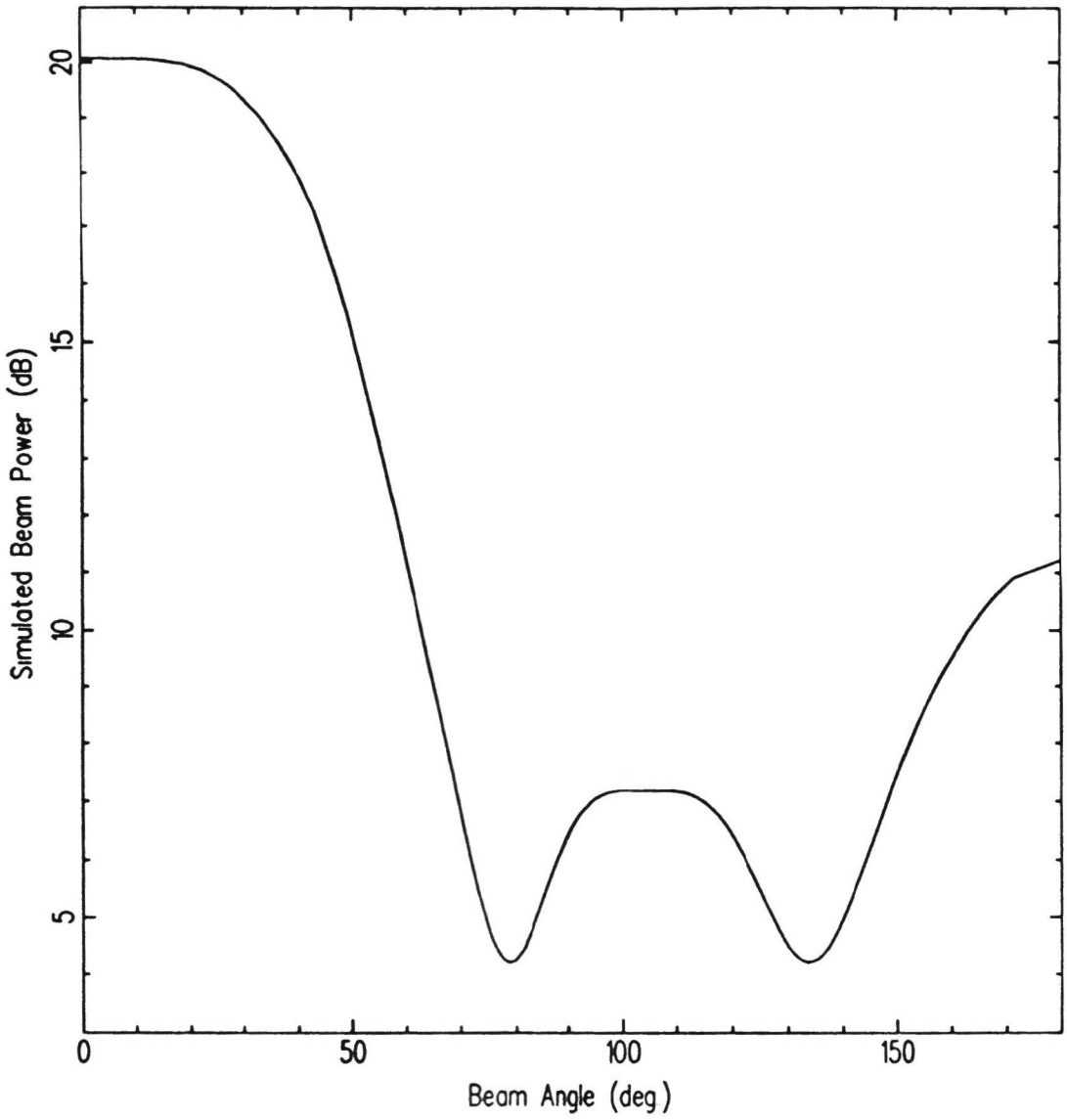

Figure 2 12 Beam pattern for 1981 18m array

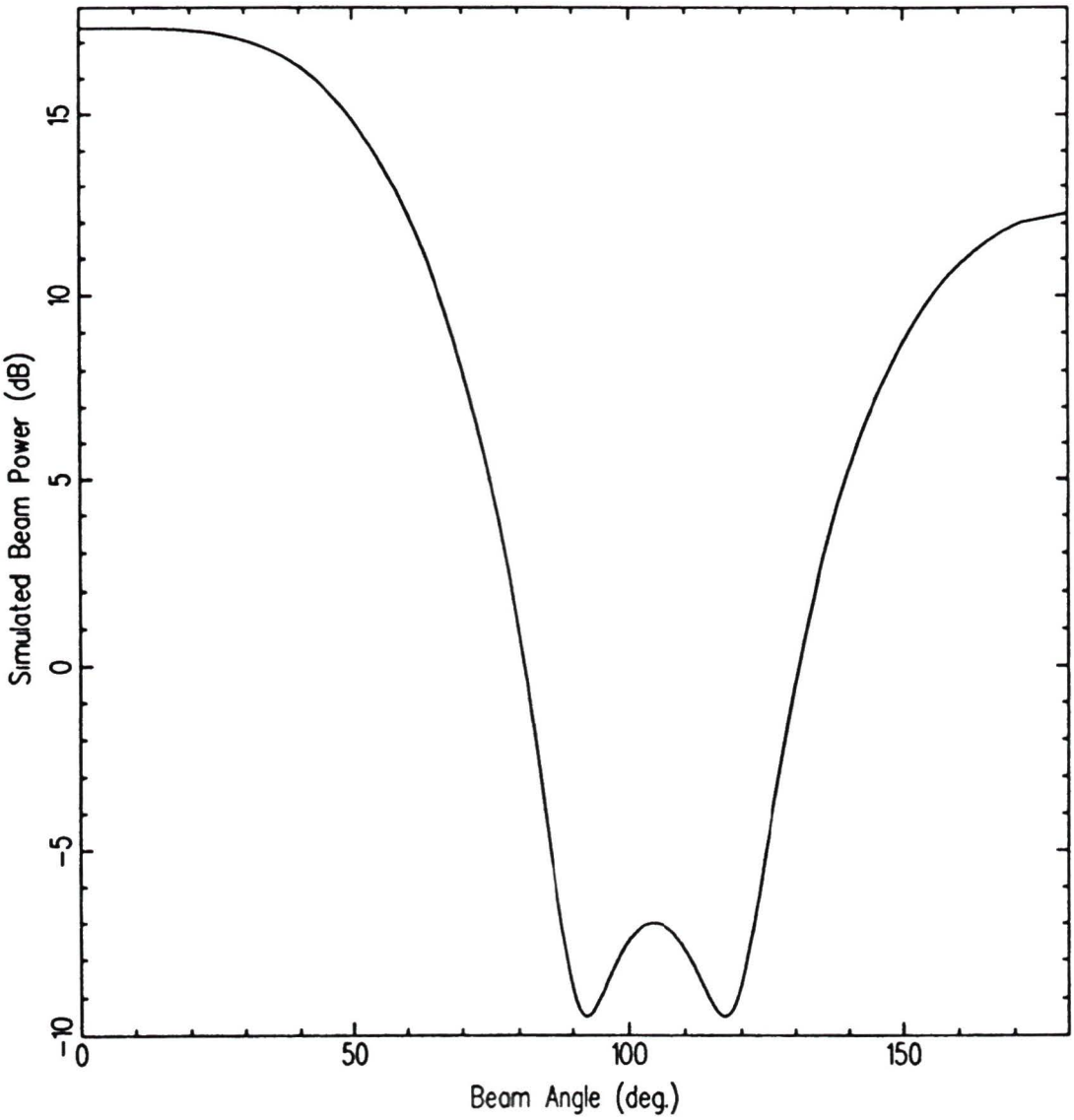

Figure 2 13 Beam pattern for 1983 18m array

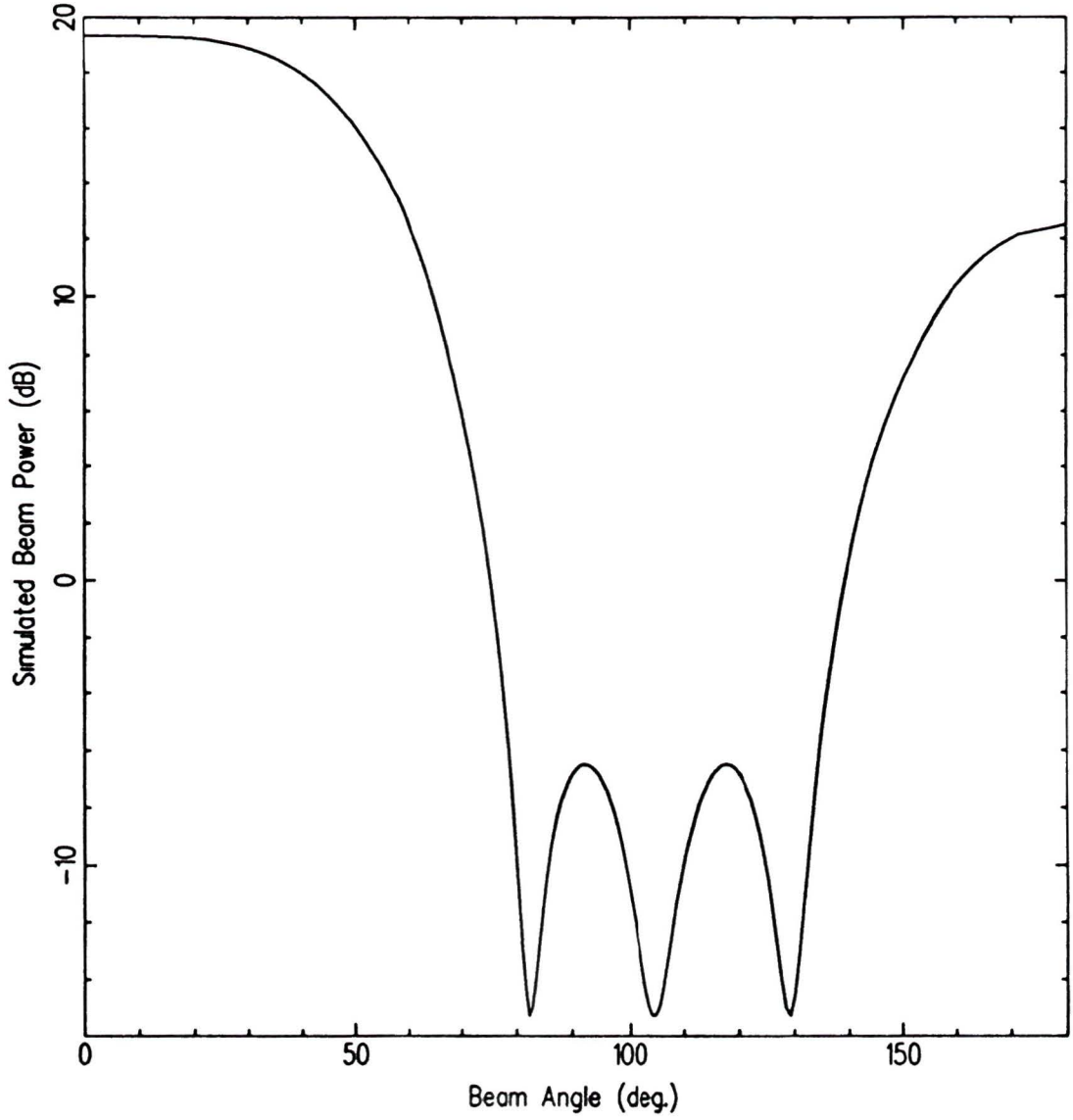

Figure 2 14 Beam pattern for 1983 and 1984/85 54m arrays

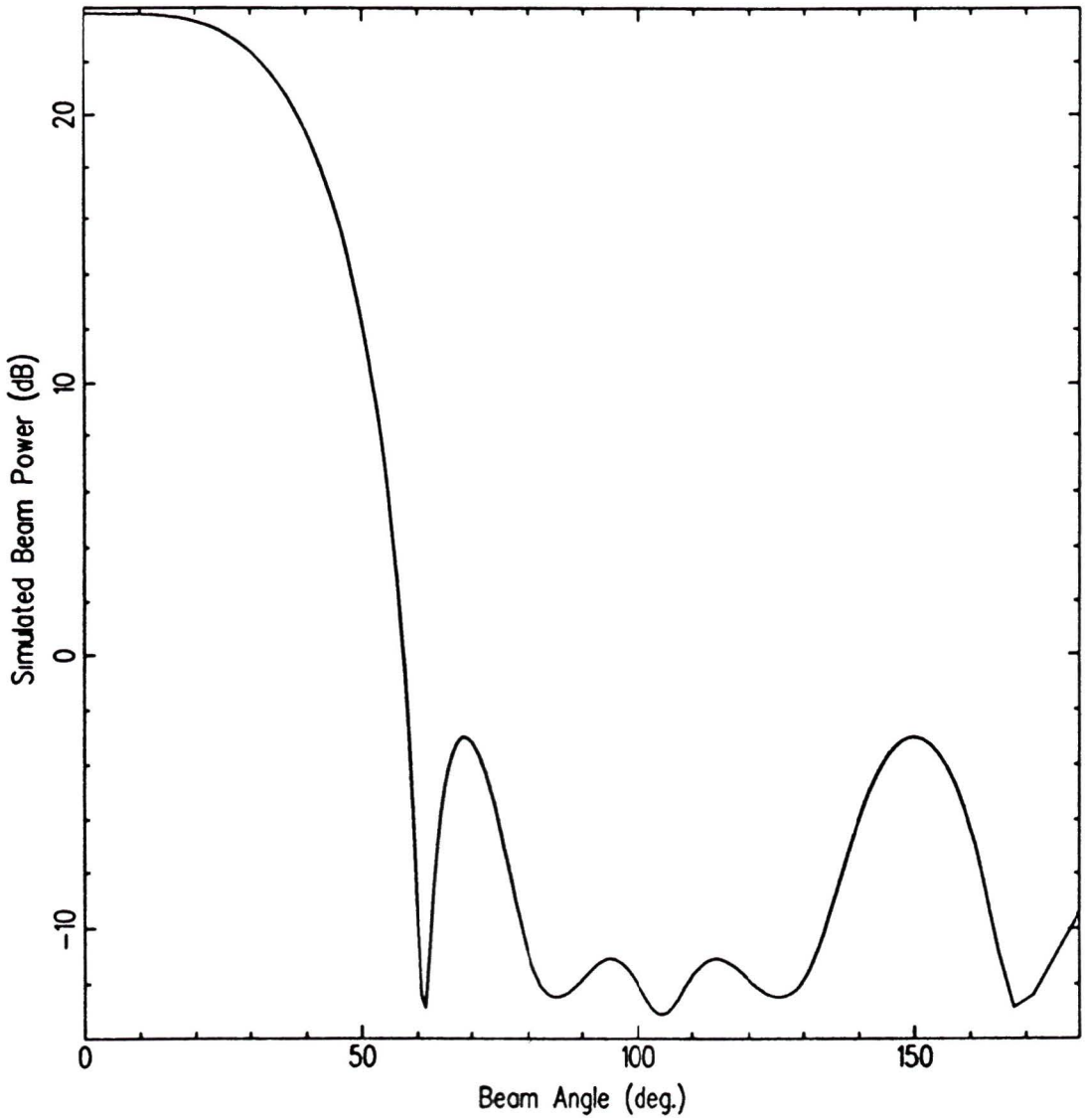

Figure 2 15 Beam pattern for 1984/85 6m array

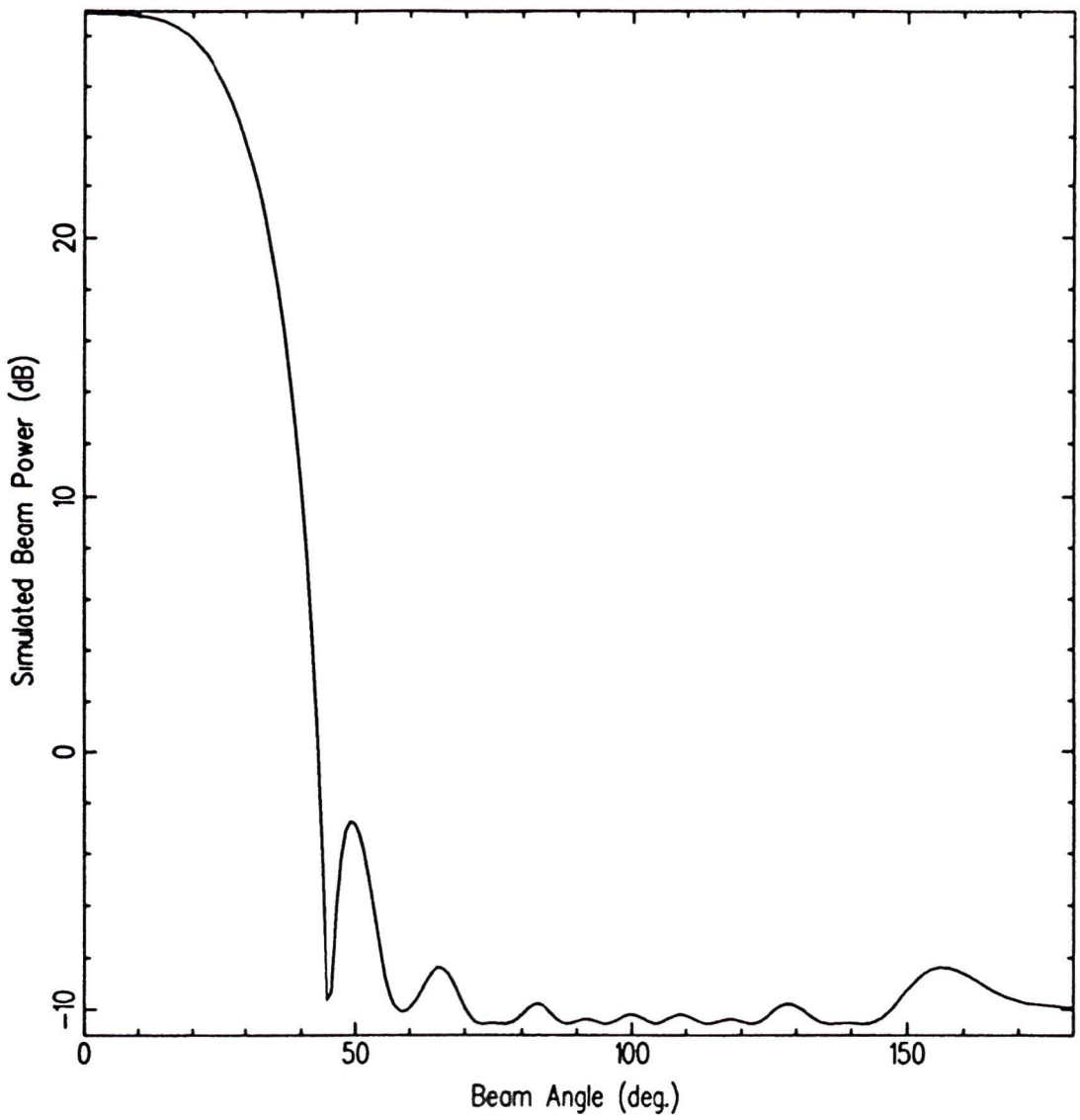

Figure 2 16 Beam pattern for 1986 3m array

These three factors are inter-linked and a balance must be found between them in order to optimize array performance for the desired results

The effective frequency range of the array is dependent on the array spacing and the number of hydrophones or the aperture of the array Just as aliasing can occur in the transform from the time domain to the frequency domain if frequencies higher than the Nyquist frequency (1/2 the sampling rate) are present in the signal, so can aliasing occur in the forming of beams depending on the wavelength of the signal and the spacing of the hydrophones The effect of this aliasing on the beam pattern for the array is to produce large lobes at directions other than the steering direction which are called grating lobes [20] The upper limit of frequency (the cut-off frequency) for forming a broadside (perpendicular to the array axis) beam without aliasing is defined by[20] $f_u = c/2d$ where d is the hydrophone spacing in metres and c is the sound speed in metres per second In other words, it is when $\lambda = d/2$ where λ is the wavelength in metres When the beam is steered to end-fire (along the array axis), however, the effective maximum frequency is even lower than the cut-off frequency This is easily illustrated and is due to the geometry of a plane- continuous-wave signal arriving along the axis to the array The beam-former is unable to distinguish between a signal arriving from one end of the array and a signal arriving from the other end, as the phase difference for any hydrophone spacing is the same for both

The lower limit of the effective frequency range of the array is less well-defined, and is dependent on the required angular resolution The best angular resolution is

obtained at the cut-off frequency of the array and it deteriorates as the frequency decreases At some frequency, the angular resolution deteriorates to the point that the array is no longer capable of adequately performing its function of spatial filtering The angular resolution at all frequencies can be improved by increasing the number of hydrophones in the array and therefore the array aperture (this is similar to increasing the number of points in a Fourier transform from the time domain to the frequency domain to decrease the frequency bin width), but there is a practical limit to the number of hydrophones which can be deployed due to both hardware limitations and considerations of spatial stationarity of the noise field

Bucker [22] outlined a method for improving the angular resolution of an array and making one array suitable for several different frequency ranges by building what is called a sparse array This is an array in which there are M spaces but only N hydrophones where N<M In this way it is possible to increase the aperture or length of the array while working within hydrophone number constraints Arrays can also be built which have different parts with spacings suitable for different frequency ranges and any one hydrophone can be used for more than one part array The power of this technique is limited, however, by a requirement that each diagonal of the cross-covariance matrix must have at least one non-zero element In other words, there must be at least one pair of sensors in the part array which has a spacing of m d where m=1,2 M-1, M is the number of positions including those with no hydrophone, and d is the spacing for that part array If this condition is not satisfied, aliasing can occur

This is illustrated by Figure 2 17 which is the beam pattern for an array steered to end-fire which has one hydrophone separation missing The aliasing is evident in the large lobe at around 100° The array design used to simulate this incorrect sparse array is illustrated in Figure 2 18 The figure shows a 5 element, 10 space sparse array with no hydrophone pair corresponding to a hydrophone spacing of 7d Thus, the seventh diagonal away from the main diagonal in the cross-covariance matrix is filled with zeros

For the purposes of this study, arrays with spacings of 54m (f_u = 14 Hz), 45m (f_u = 17 Hz), 18m (f_u = 42 Hz), 6m (f_u = 125 Hz), 3m (f_u = 250 Hz), and 2m (f_u = 375 Hz) were used The low-frequency cut-off point was taken to be when the array half-power beam width (defined here as the angular separation between the peak of the main lobe and the half-power point of the beam pattern) exceeded approximately 50 – 60° as determined by the STARPACK beam simulation program [21] Plots of end-fire beam width vs frequency for the various arrays and part-arrays used are included as Figures 2 19 to 2 26

As the number of hydrophones was limited to between 10 and 16, depending on the year, extensive use was made of the sparse array technique mentioned above as is illustrated by Figures 2 2, to 2 5 In all cases, as can be determined from the array geometry shown in the figures, the requirement of at least one non-zero element in each diagonal of the cross-covariance matrix was satisfied

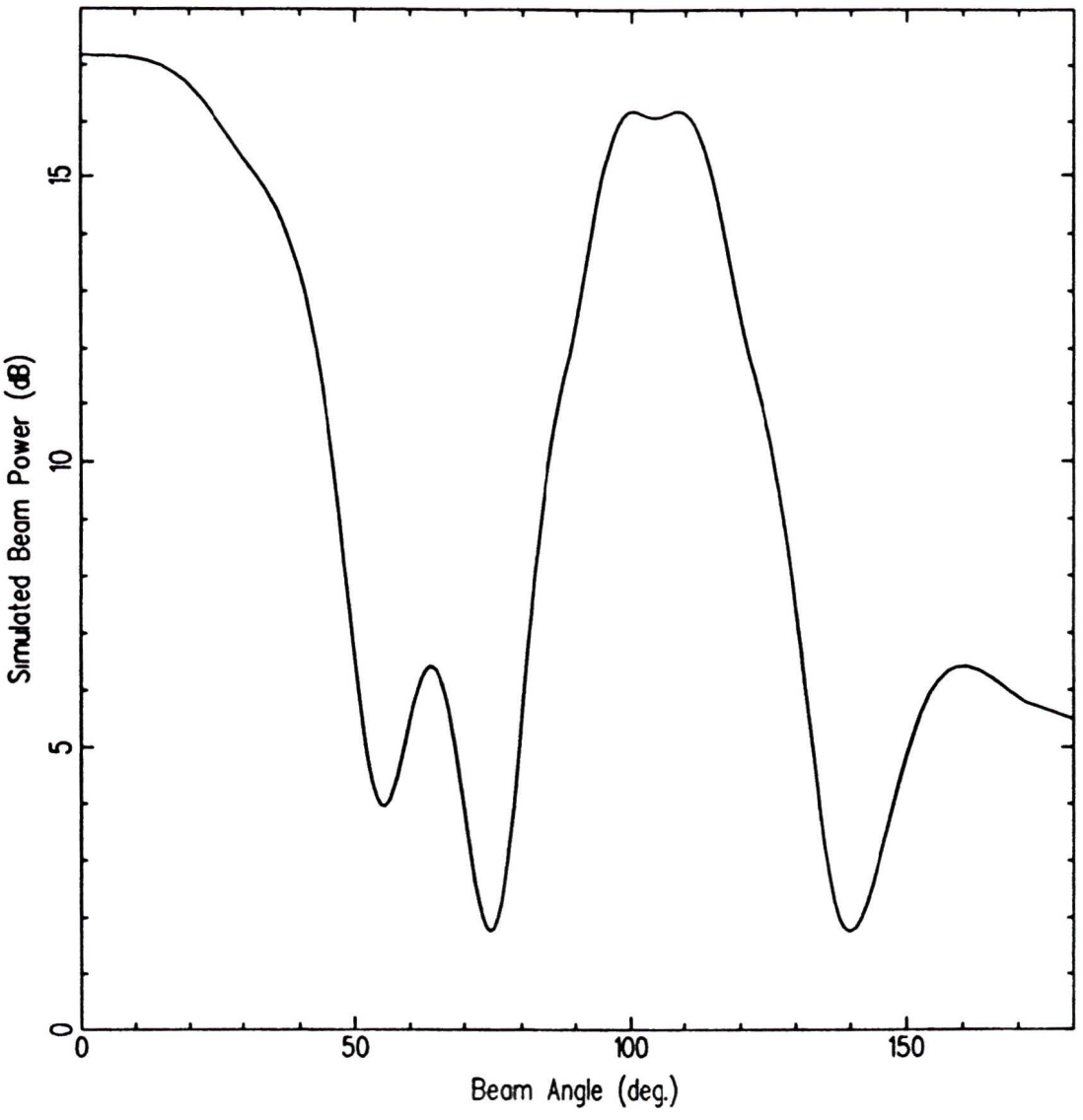

Figure 2 17 Beam pattern of an array with one diagonal of the covariance matrix filled with zeros

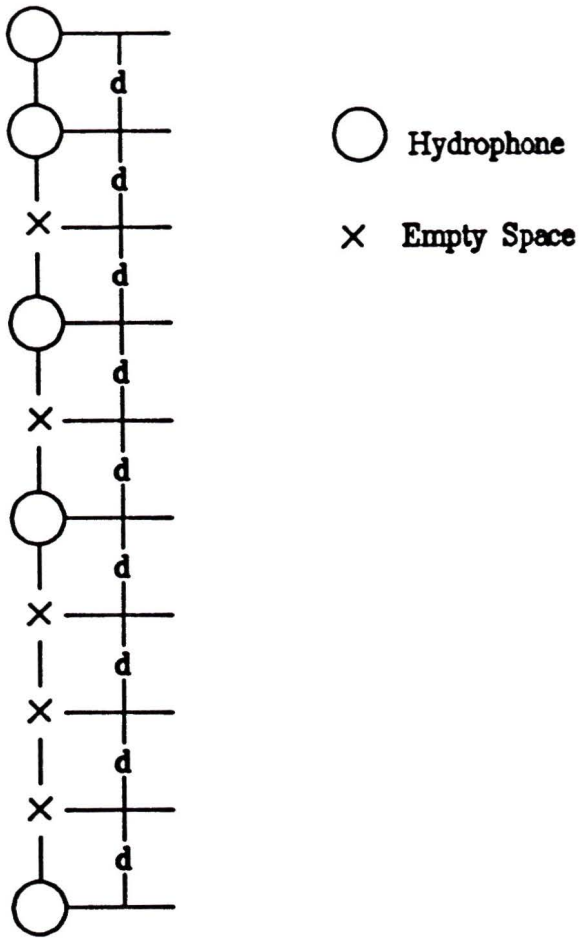

Figure 2 18 Array configuration used to simulate incorrect sparse array

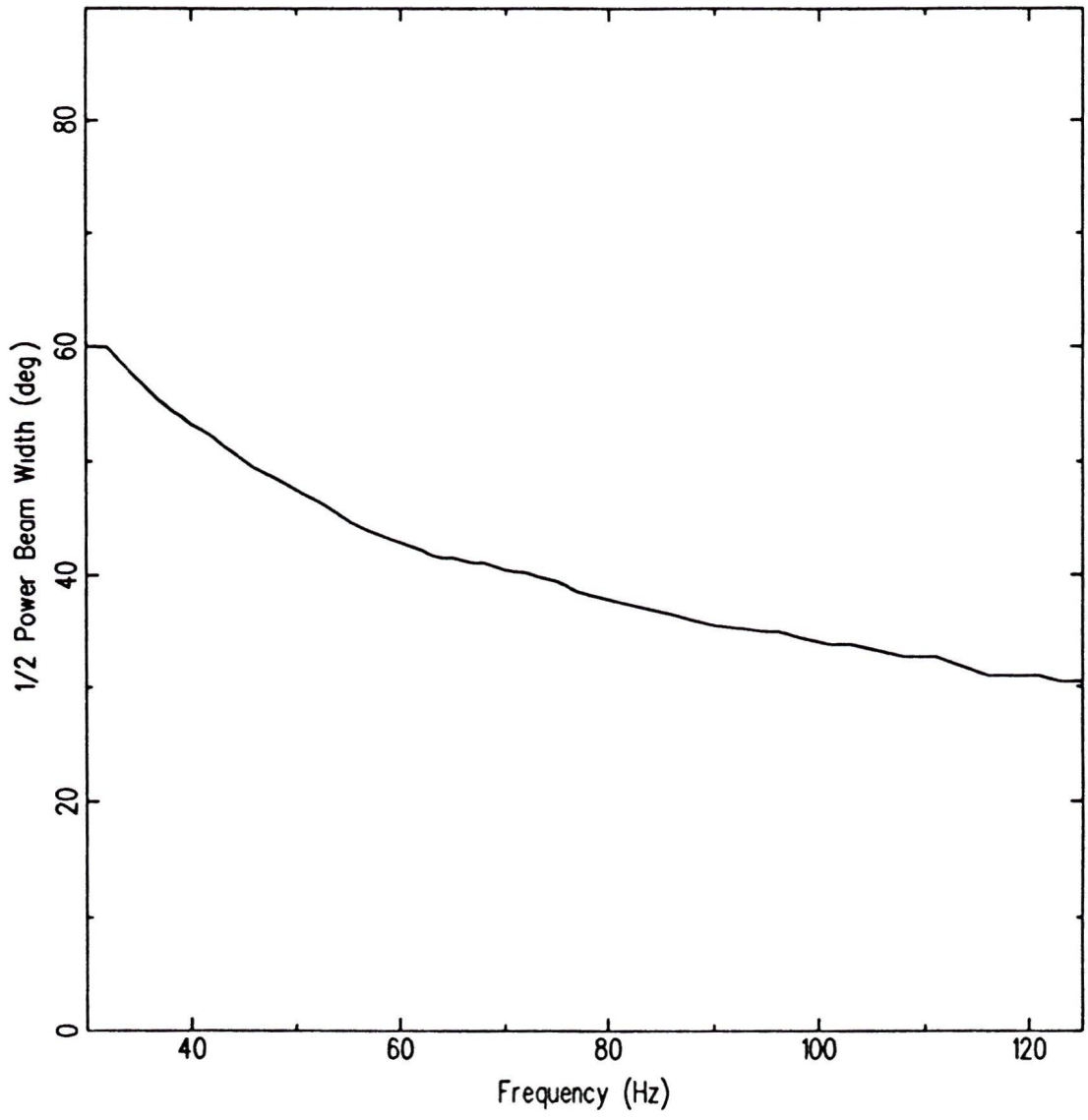

Figure 2 19 Beam width vs frequency for 1977/78 6m array

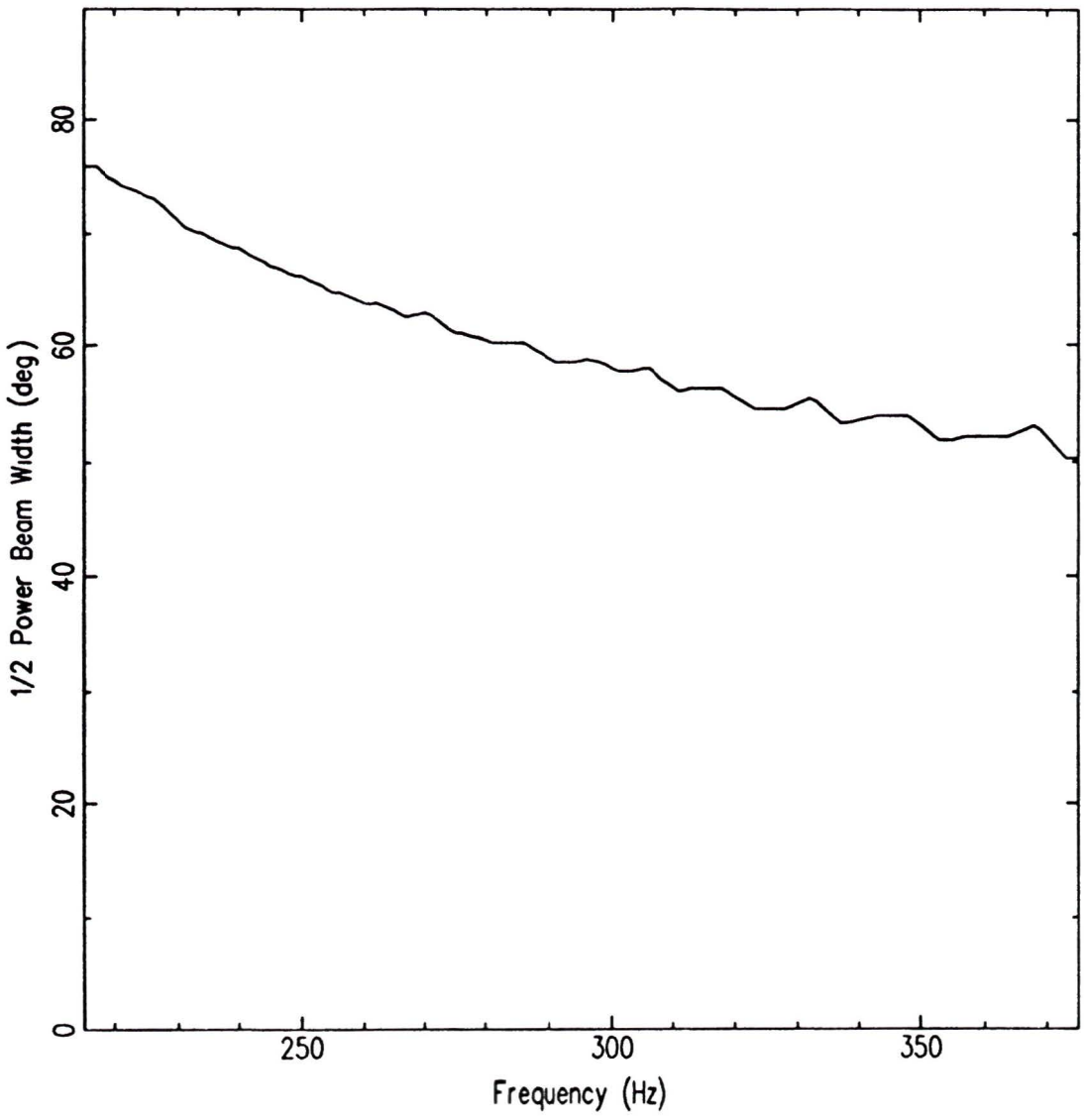

Figure 2 20 Beam width vs frequency for 1981 and 1983 2m arrays

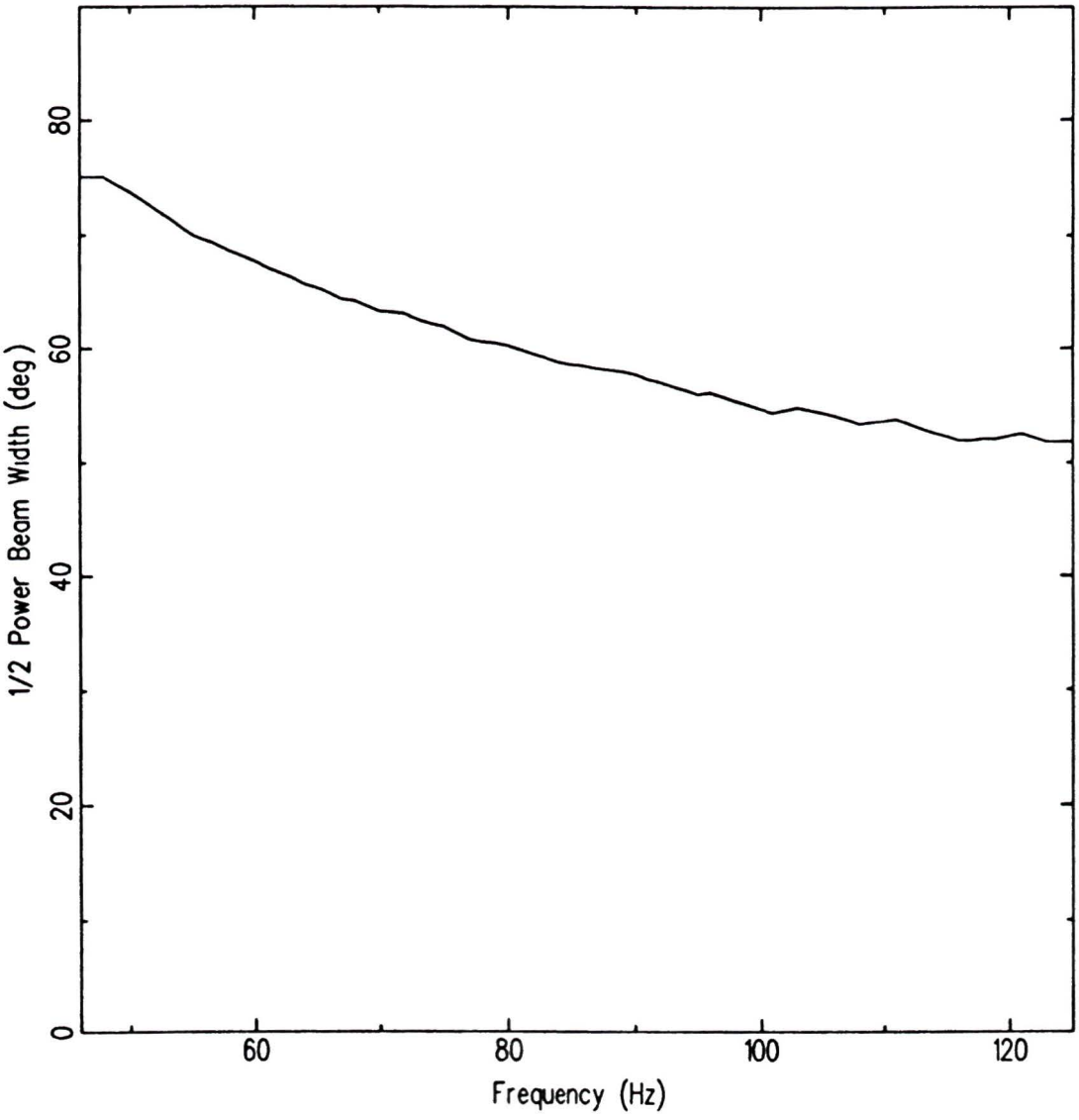

Figure 2 21 Beam width vs frequency for 1981 and 1983 6m arrays

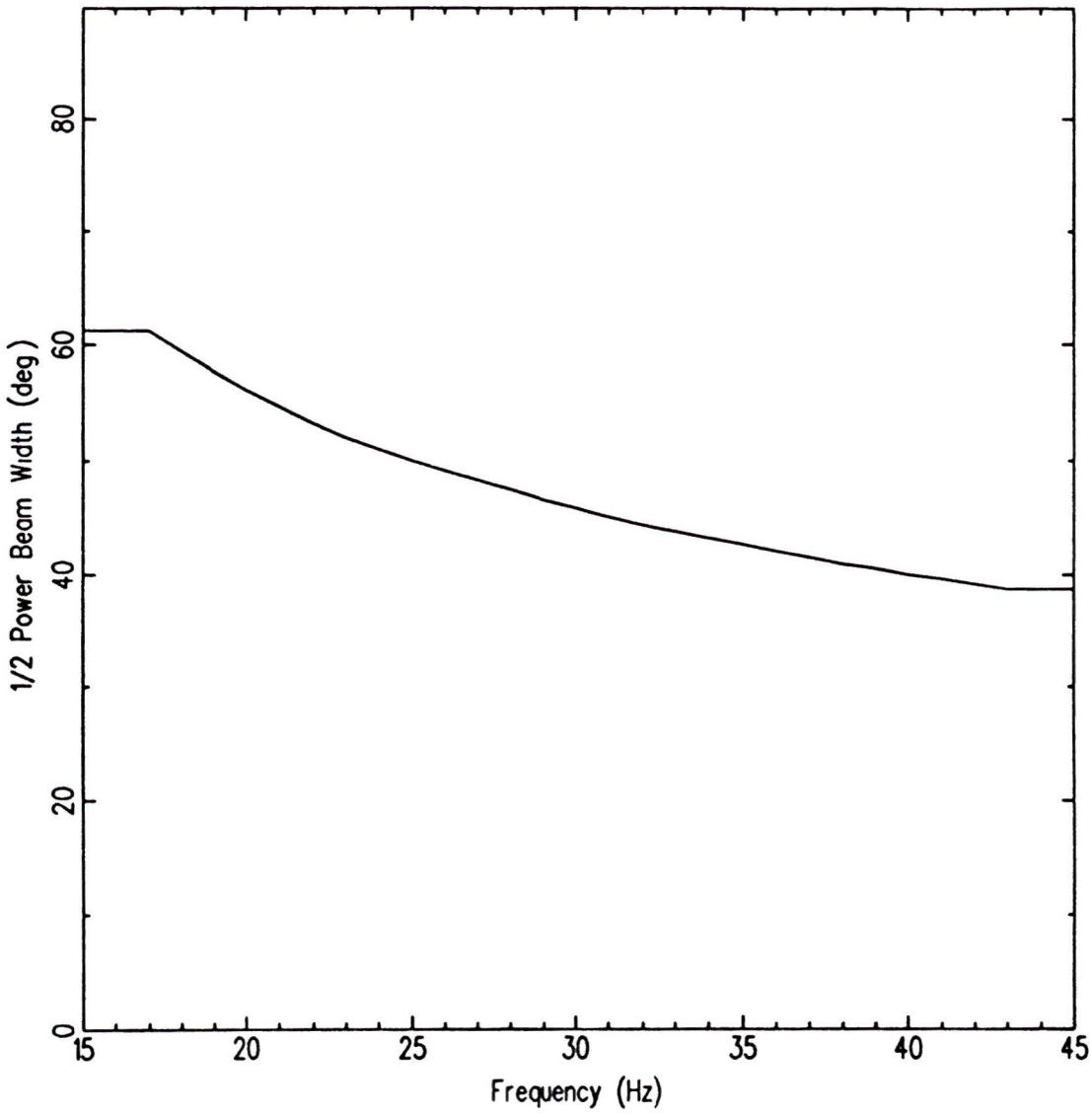

Figure 2 22 Beam width vs frequency for 1981 18m array

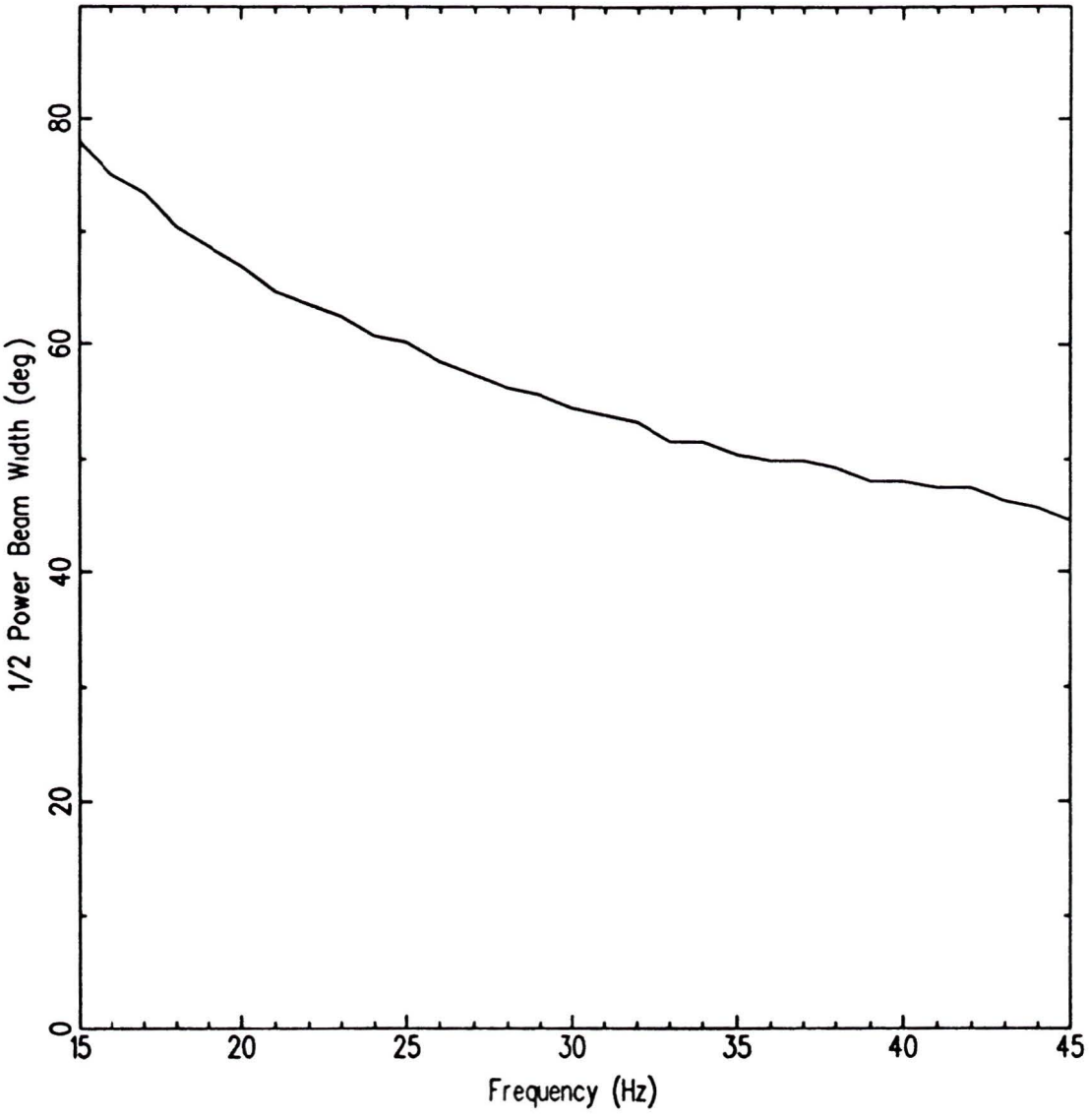

Figure 2 23 Beam width vs frequency for 1983 18m array

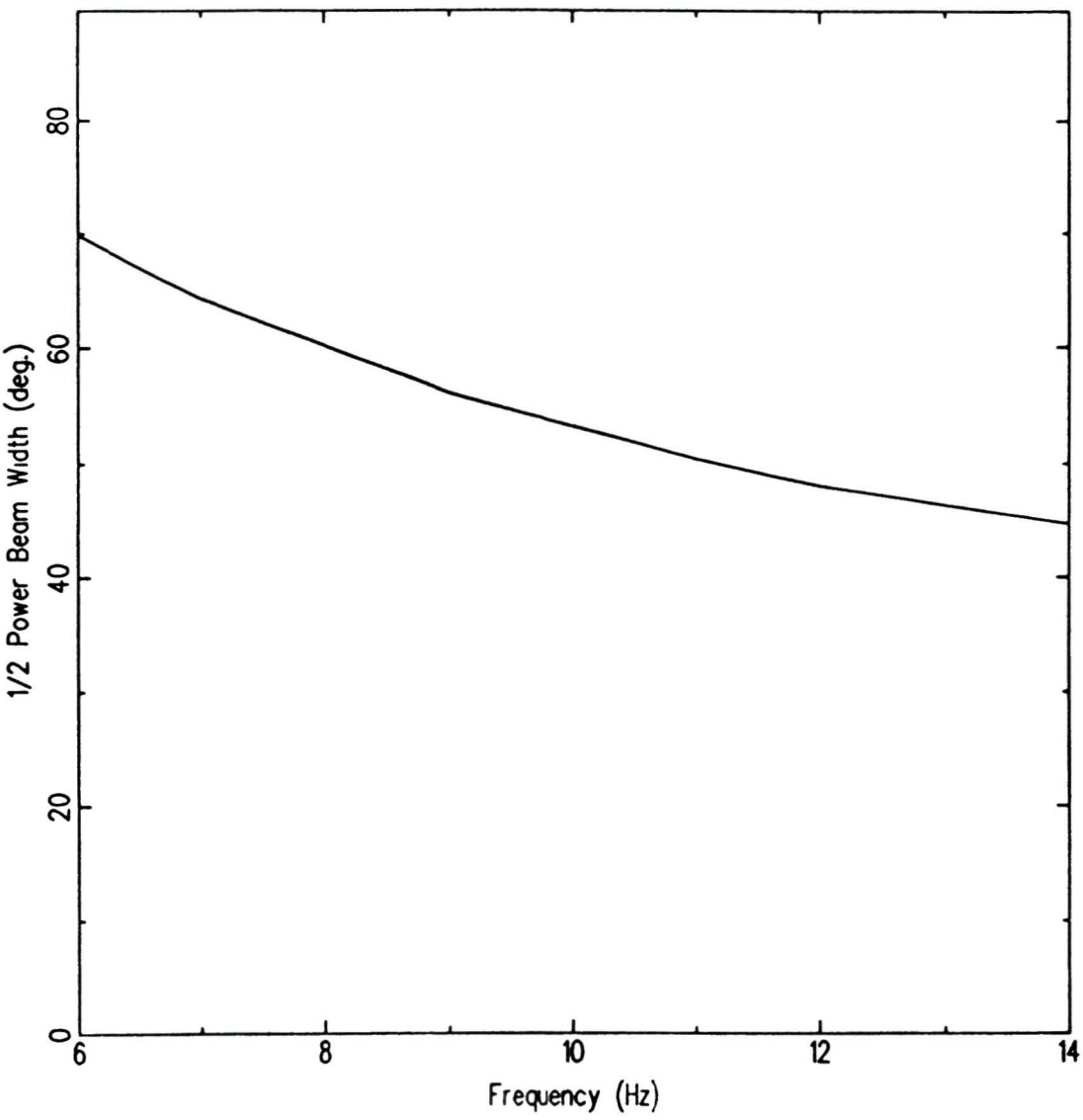

Figure 2 24 Beam width vs frequency for 1983 and 1984/85 54m arrays

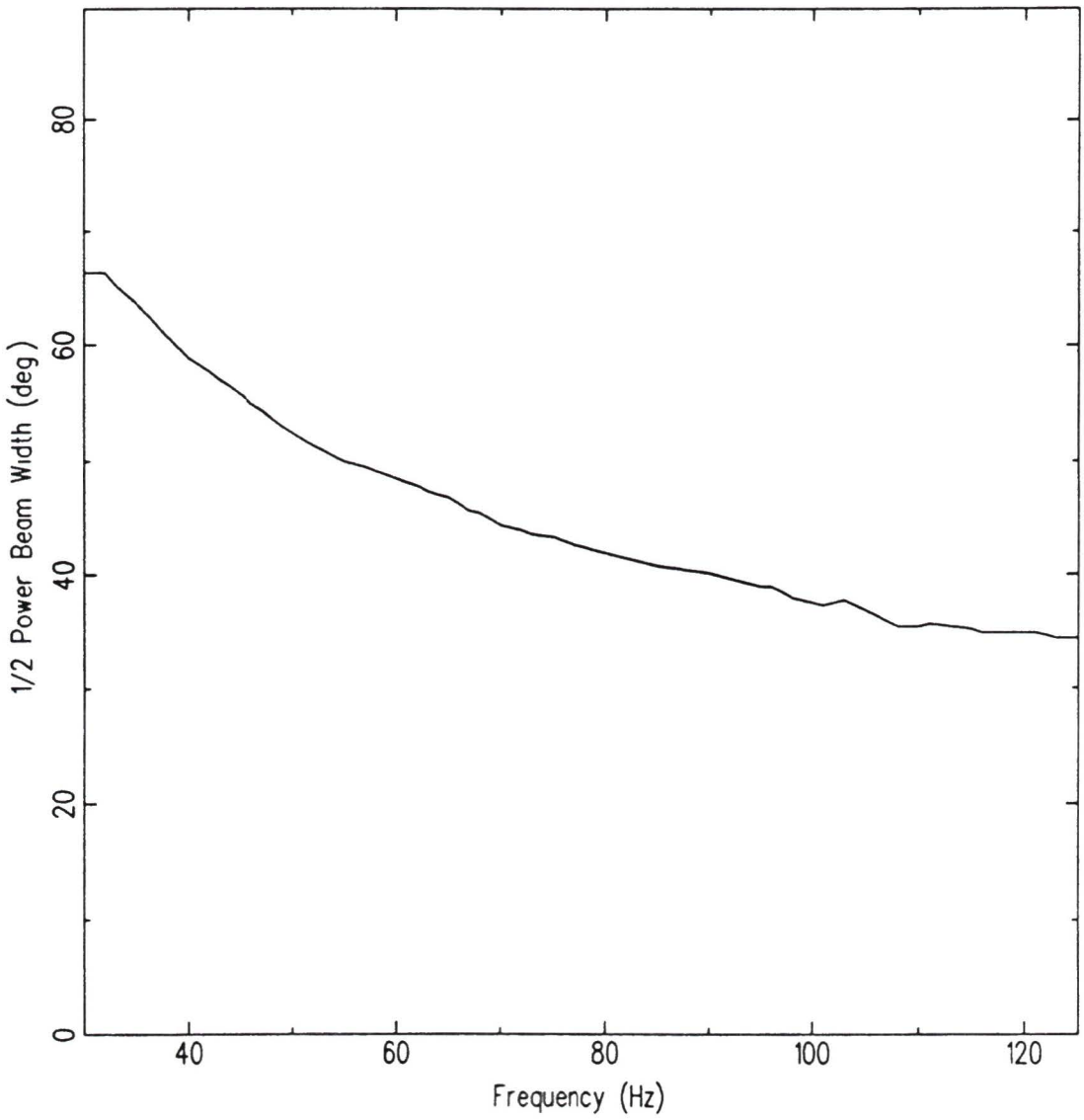

Figure 2 25 Beam width vs frequency for 1984/85 6m array

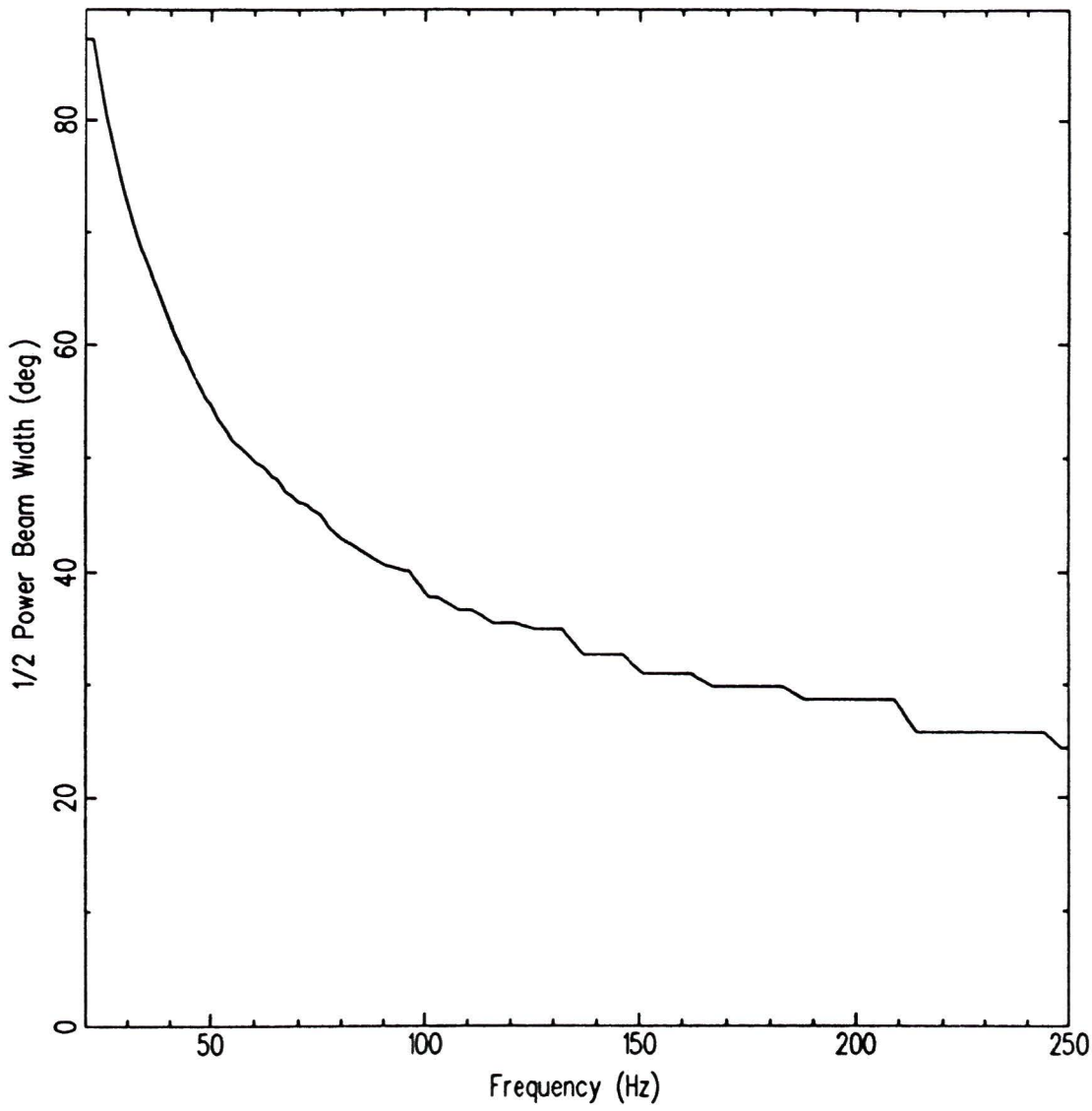

Figure 2 26 Beam width vs frequency for 1986 3m array

D. Data Processing Method

The hydrophone noise data were retrieved from the magnetic tapes using the data management system at DREP Time series of all the hydrophones used were examined for selected observation intervals to ensure there were no problems such as faulty hydrophones or long dropouts in the radio link which could affect the transform to the frequency domain The data were also demultiplexed and stored in a suitable format for further processing

The time series for each hydrophone were transformed to the frequency domain through a standard fast Fourier transform (FFT) algorithm from the NAG Fortran Library [24] An FFT size of 2048 points was used which, with a sampling frequency of 1500 Hz, led to a frequency resolution (bin width) of approximately 7 Hz In the final results, only specific frequencies were required, therefore a rectangular window was used in the time domain and the data at the required frequencies were smoothed in the frequency domain using a Daniell spectral window [19] This smoothing in the frequency domain is equivalent [19] to windowing in the time domain to reduce spectral leakage When windowing in the time domain, the time series are multiplied by a window function When this operation is transformed into the frequency domain, the multiplication of the time series with the window becomes a convolution operation with the transform of the time series and the transform of the spatial window function The convolution operation is effectively the smoothing of the transform of the time

series with the spectral window This method of smoothing in the frequency domain required fewer operations than windowing in the time domain since only the selected frequencies needed to be smoothed

The Fourier spectra produced by the FFT routine were used to determine a power spectrum for each hydrophone and a covariance matrix (used in beamforming) for the array These spectra and the matrix were block averaged over 40 blocks in order to reduce the variance in the estimates

A covariance matrix was formed for each frequency bin according to

$$Q_{i,j}(f) = X_i(f)X_j^*(f)W_iW_j \tag{2 12}$$

where $Q_{i,j}(f)$ is the covariance matrix, $X_i(f)$ is the complex Fourier transform of the time series of the i^{th} hydrophone at the frequency for which the matrix is being built, $X_j^*(f)$ is the complex conjugate of the transform of the j^{th} hydrophone, and W_i is the Kaiser-Bessel window weighting factor applied for the i^{th} hydrophone Since these matrices are Hermetian, i e $Q = Q^*$, they were stored in lower triangular form to reduce disk space requirements Beam strengths were then determined according to equation 2 10

E. Scaling for System and Processing Gains

The beam strength results were converted to beam powers $P(f,\theta)$ in dB re $\mu Pa^2/Hz$ according to

$P(f,\theta) = 10\log_{10} B(f,\theta) + 10\log_{10} 2$ - ADGAIN - HPSENS - SYSGAIN - FREQGAIN - PGA - NGAIN - WINDOWGAIN - AVEGAIN where

i ADGAIN is the gain associated with the conversion of the signal from analog to digital = 46 2 dB,

ii HPSENS is the hydrophone sensitivity in dB as listed in Table 2 1,

iii SYSGAIN is the system gain in dB determined from calibration of the array and also listed in Table 2 1,

iv FREQGAIN is $10\log_{10} s$ where s is the sampling frequency in Hz (required because FFT was not normalized),

v PGA is the gain in the power gain amplifier which was varied according to the noise level present from 0 to 60 dB in steps of 12,

vi NGAIN is the gain in the beamforming algorithm which is $10\log_{10} N^2$, where N is the number of hydrophones in the array,

vii WINDOWGAIN is the negative gain associated with the reduction in power due to the spatial weighting function used = $10\log_{10} 0\,49^2$ [23], and

viii AVEGAIN is $10\log_{10}$NAVE where NAVE is the number of time averages taken = 40

As a cross-check on the scaling process used, beams for the angle range from vertically upwards to vertically downwards, overlapping at the half-power points, were integrated and the sum was compared to the average omni-directional power of the hydrophones The results agreed to within 1 dB

Once the beam power results were scaled for system and processing gains as outlined above, contour plots of scaled beam power versus frequency and arrival angle were produced These plots were used to examine the vertical structure of the noise field, to confirm the pedestal structure as discussed in the introduction, and to check for contamination of the data by close-in, non-wind-generated sources with arrival angles near the vertical Any sources, such as nearby ships or sound sources used in conjunction with other experiments, which produced noise at arrival angles close to the vertical would cause contamination of the data, since the beamforming system was designed to filter out only the noise coming from angles close to the horizontal direction All data sets which showed contamination of this type were eliminated from the analysis

In order to reference the beam powers calculated by the above method to a source level at the surface, it was necessary to determine the beam widths in the vertical beam for each frequency and to account for bottom losses The beam widths were calculated using a beam simulation algorithm incorporated in the original STARPACK program[21] used to perform the beamforming Bottom losses were determined from shot-run experiments which were conducted by the Ocean Acoustics Group at DREP

in conjunction with the data collection for this study [25] The beam width calculations were used to scale the power in the upward looking beam to dB re $\mu Pa/srHz$, and then the bottom loss data were used to reference these beam powers to a source level at the surface in dB re $\mu Pa/Hz * m^2$ @1m using the propogation model [12] which will be developed in the next section

Chapter 3

Models

I. Surface Noise Propagation Model

Once the vertical beam power results, referenced to $\mu PA/srHz$, were obtained, it was necessary to reference them to a source level at the surface in $\mu Pa/m^2Hz@1m$ To do this, a simple propagation model developed by Bannister [12] was used

Figure 3 1 shows the geometry of the propagation of noise from a distributed surface source to a receiver at some depth via a general cone of rays The received intensity i_d per unit of solid angle from this cone can be estimated as [12]

$$i_d = S * A_3 * g * L * a * t/\Omega \tag{3 1}$$

where

S is the monopole (omni–directional) distributed source level per m^2,

a is the source directivity function,

A_3 is the surface area intersected,

g is the geometrical losses– A_1/A_2,

t is the backward transmission loss– $\cos^2\theta_r/\cos^2\theta_s = 1$,

Ω is the number of steradians in the cone $\equiv$ 1 since i_d is referenced to a level per steradian, and

L is the total absorption loss

The total loss L includes both the loss due to bottom interactions (surface interactions are assumed to be loss-less since it is a free surface) and due to attenuation losses in the water column Bannister [12] points out that attenuation losses are a second order term and can be ignored for simplicity so that L can be set equal to the bottom reflection coefficient b Also, it can be seen from the geometry in Figure 3 1 that $A_3 = A_2/\sin\theta_s$ and equation 3 1 can be expressed as

$$i_d = \frac{S * a * b * n}{\sin\theta_s} \tag{3 2}$$

where n is the number of bottom interactions

Equation 3 2 gives the received intensity in the cone from one particular propagation path– i e the path which undergoes n bottom interactions If all the paths with

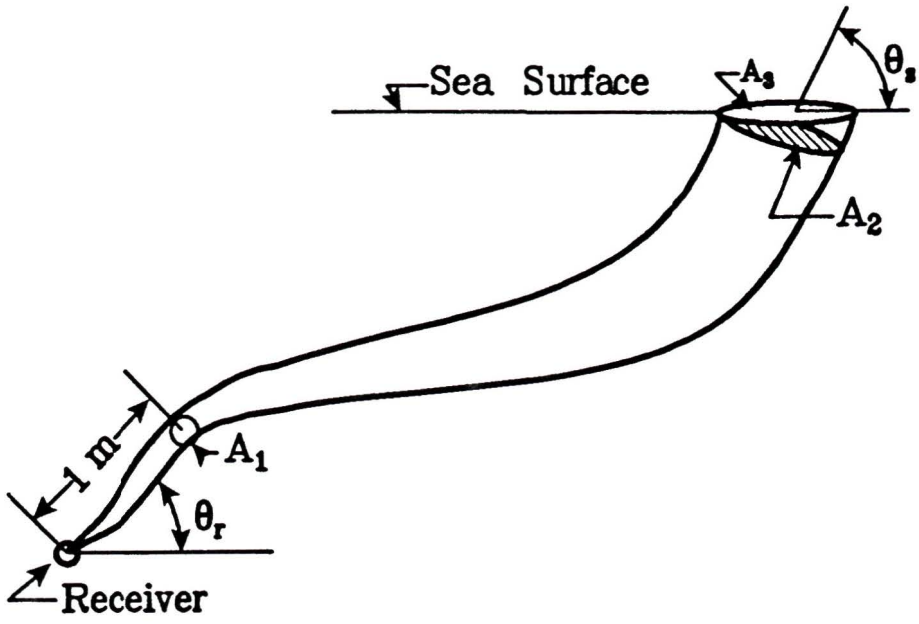

Figure 3 1 Diagram of Bannister et al 's noise propagation model

n bottom interactions where $n = 0, \quad , N$ are summed, the total energy arriving at the array from above is given by

$$I_d(\theta_r) = S * a * (\frac{1 + b + b^2 + \quad + b^N}{\sin\theta_s}) \tag{3 3}$$

where θ_s and θ_r are connected through Snell's Law Since the bottom reflection coefficient b is less than 1, this can be further simplified to

$$I_d(\theta_r) = S * A * \frac{(\frac{1-b^n}{1-b})}{\sin\theta_s} \tag{3 4}$$

and for $n \rightarrow \infty$ this becomes

$$I_d(\theta_r) = \frac{S * a}{\sin\theta_s(1-b)} \tag{3 5}$$

Since the vertical beams are under consideration, the angle at the receiver is $= 90°$, therefore $\cos\theta_s = \cos\theta_r = 0$ and is independent of the sound speed profile Also, $\theta_s = 90°$ and $\sin\theta_s = 1$ Then, rearranging equation 3 5

$$S = \frac{I_d}{a(1-b)} \tag{3 6}$$

Using equation 3 6, it is possible to reference the beam powers measured in the upward looking beam to a source level in dB re $\mu Pa/m^2Hz$ @1m, as long as the bottom reflection coefficient is known for the area under study

The factor a in equation 3 6 accounts for the source directivity function which depends on whether the source is radiating as a dipole or as a monopole [12] In order to remove this factor from the results, it is necessary to have a system which

is capable of distinguishing the fine structure of the vertical directionality of the noise However, the angular resolution of the arrays used in this study was not good enough to distinguish this fine structure because the arrays consisted of relatively few hydrophones As a result, the results quoted for the surface source levels are actually a combination of a monopole source level and a radiation distribution pattern, and no attempt has been made to separate the two effects

II. Wind-Noise Generation Model

The process used to model the effect of wind speed on the measured source levels was similar to that used by Piggott [6], Kewley et al [2], and Crouch and Burt [26] It is assumed that a noise generation mechanism is linear with respect to the logarithm of the wind speed according to

$$N(f,v) = A(f) + 20n(f)/log_{10}v \tag{3 7}$$

where $N(f,v)$ is the noise source level in dB, and $A(f)$ and $n(f)$ are constant for a particular frequency f

As was discussed in the introduction, however, it is reasonable to assume that there are two noise generation mechanisms involved in wind-generated noise The first mechanism is assumed to be present at all wind speeds and is given the form

$$N_L(f,v) = A_L(f) + 20n_L(f)log_{10}v \tag{3 8}$$

The second mechanism is only effective in the presence of breaking waves and therefore does not contribute to the noise field when wind speeds are below about 10 knots, but dominates the noise field at greater wind speeds This second mechanism is given the form.

$$N_H(f,v) = A_H(f) + 20n_H(f)log_{10}v \tag{3 9}$$

The total wind-generated noise power is modelled by a combination of these two processes At wind speeds of 10 knots or less, the noise is assumed to be generated only by the first mechanism (equation 3 8), while at wind speeds above 10 knots, it is assumed that the total wind-generated noise power is a combination of the two processes (equations 3 8 and 3 9) The addition of the two processes, however, does not occur in log space and equations 3 8 and 3 9 must be converted from decibel notation back to linear space before they can be summed to obtain the modelled total noise power

Expressed in standard notation, the modelled total wind-generated noise power $N_r(f,v)$ can then be expressed as

$$N_r(f,v) = \begin{cases} 10^{\frac{A_L}{10}} v^{2n_L} & \text{for } v \leq 10 \text{ knots} \\ 10^{\frac{A_L}{10}} v^{2n_L} + 10^{\frac{A_H}{10}} v^{2n_H} & \text{for } v > 10 \text{ knots} \end{cases} \tag{3 10}$$

For the frequencies between 80 and 120 Hz, where enough low wind-speed data were available to calculate $A_L(f)$ and $n_L(f)$, both mechanisms were used to model

the wind-speed dependence of the noise field The parameters $A_L(f)$ and $n_L(f)$ in equation 3 10 were determined from the data for wind speeds equal to or less than 10 knots using the Levenberg-Marquardt iterative non-linear regression technique [27] Once the low wind-speed parameters were obtained in this way, the data for wind speeds of 10 knots or greater were fitted to equation 3 10 using the Levenburg-Marquardt technique and holding $A_L(f)$ and $n_L(f)$ constant at the values obtained from the low wind-speed data to obtain $A_H(f)$ and $n_H(f)$ The regression coefficient, r, was also calculated for both fits

For all the other frequencies studied, not enough low wind-speed data were available to calculate the low wind parameters, and all that could be done was to model the data for wind speeds greater than or equal to 10 knots by fitting to the high wind mechanism only, ignoring the low-wind component Depending on the value of $n_L(f)$ for these frequencies, the values obtained for $n_H(f)$ may be strongly biased, but, due to the limitations of available data, this problem could not be resolved For instance, if $n_L(f) \gg 0\,0$, then the estimates obtained for $n_H(f)$ will be biased to lower values

When performing the regressions outlined above, there was some question as to whether all the points in the regression should be weighted equally In considering the possibility of contamination of the data by sources other than wind-driven mechanisms, it is reasonable to assume that any contaminating sources would raise the observed noise level above that which would be observed if only wind-generated sources were present Therefore, when more than one observation of noise level was

available at a particular wind speed, it was assumed that the lower values were more reliable and a weighting function was included in the regression procedure to account for this The lowest value at a particular wind speed was given a weight of unity, the second was given a weight of $1/2^2$, the third a weight of $1/3^2$, and so on This weighting function was also included in the calculation of the correlation coefficient r as outlined by Press et al [27]

Chapter 4

Results

I. Contour Plots of Sound Intensity vs Arrival Angle and Frequency

The contour plots which were produced showing sound intensity vs arrival angle and frequency provided a useful means for comparison with the results of other investigators regarding spectral shape and vertical directionality, as well as for confirming that the arrays were performing as expected and for identifying data sets with excessive contamination due to close-in shipping or other, high arrival-angle sources

In these plots, the sound intensity is quoted from the scaled beam powers in dB re $1\mu Pa/Hz$ In order to reduce processing requirements, the beam powers were not scaled for beam width and were not smoothed with the Daniell spectral window This

does not, however, affect the general discussion of spectral shape, vertical directionality, and array performance presented in this section The beam number scale on the vertical axis corresponds to beams equally spaced in $\cos\theta$ from beam 0 (end-fire looking up at the surface) to beam 180 (end-fire looking down at the bottom) Because the beams were equally spaced in the cosine of the vertical angle (as is standard in beam-forming due to the variation in beam widths with steering angle [20]), the density of the beams in θ-space is greater at the horizontal than at end-fire This must be taken into consideration when using the plots to study the pedestal width Figure 4 1 shows the relationship between beam number and sound arrival angle for these plots

A. 54m Arrays

Figure 4 2 is a representative contour plot for a 54m array In the figure, it is apparent that even at very low frequencies (around 10 Hz), the pedestal is present in the noise level around the horizontal and that the noise level decreases with increasing frequency The effective frequency range for this array is between approximately 8 and 13 Hz Below about 8 Hz the beam width is very large and noise from the pedestal at the horizontal affects the measurement of noise in the end-fire beams Above 13 Hz, the aliasing effect (described in section 2 II C) is very apparent in the folding of noise from the horizontal into the end-fire beams through the grating lobes

Figure 4 3, which is from a 45m array, illustrates how the contour plots were used

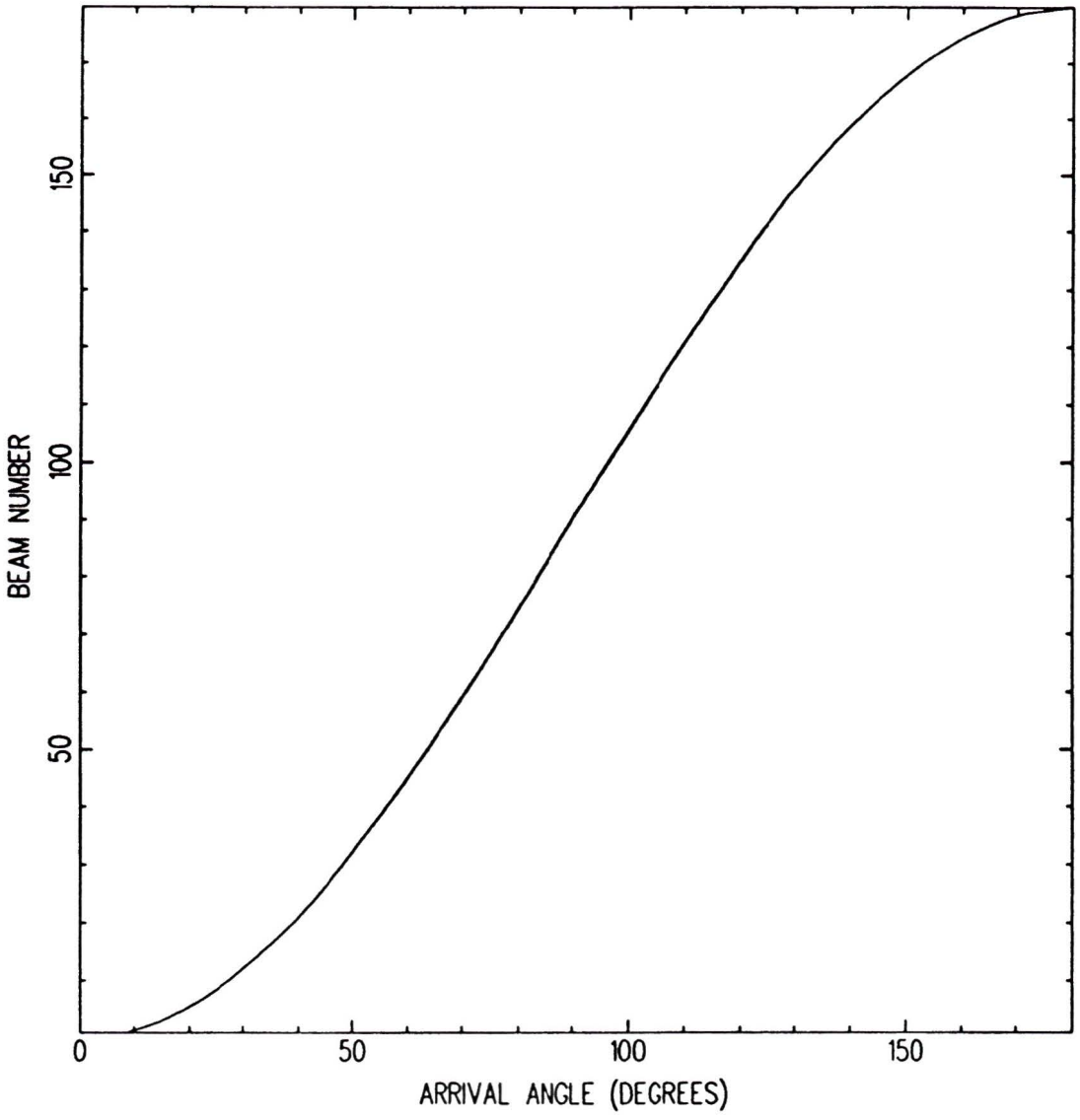

Figure 4 1 Beam number vs sound arrival angle for contour plots

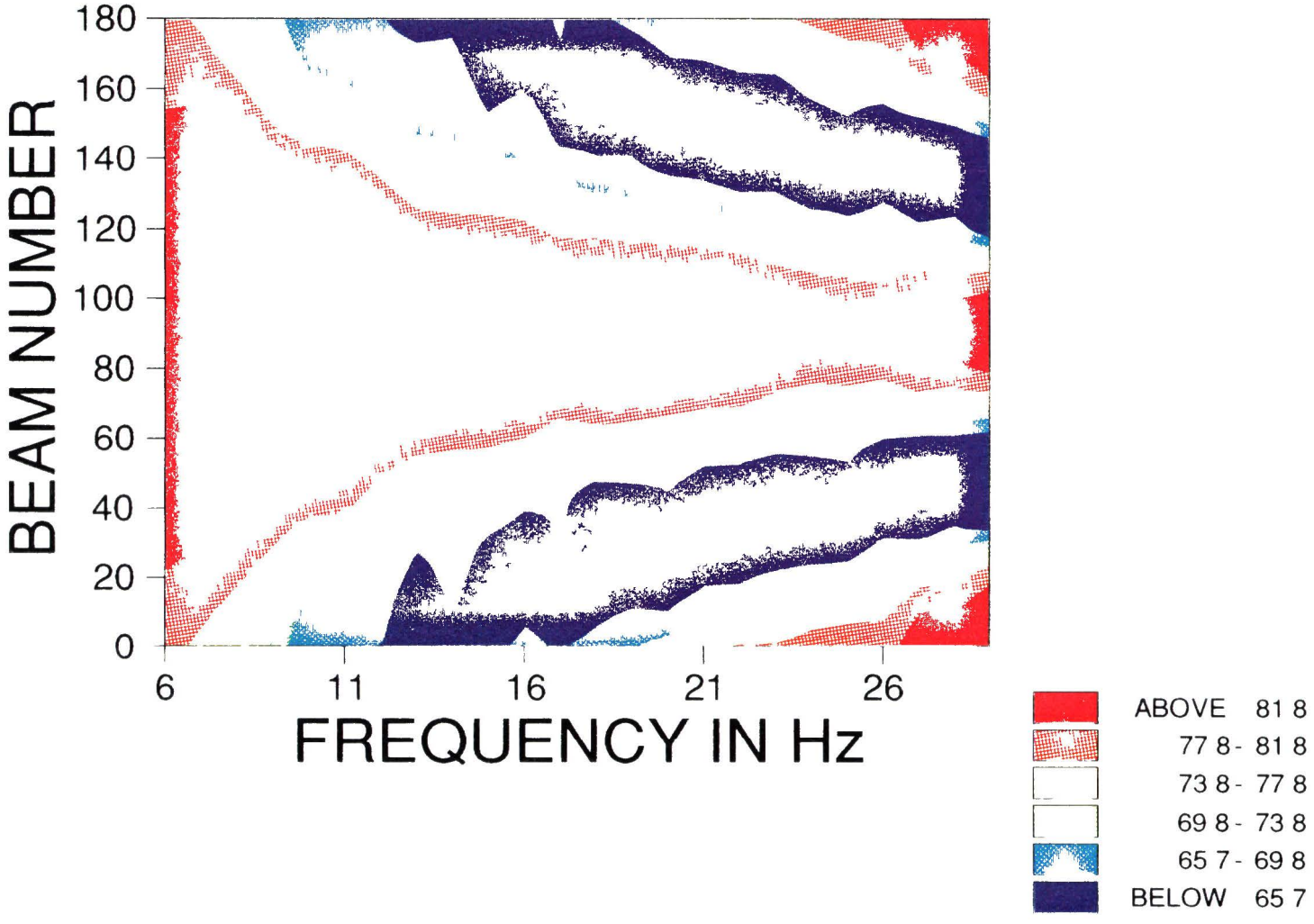

Figure 4 2 Representative contour plot for a 54m array

to identify contaminated data sets A high noise-level signal is apparent between beams 100 and 120 and frequencies of 11 to 15 Hz The scientific log-book for the experiment revealed that this was due to a sound source which was in operation at the time of the observation and was sweeping the frequency band 11-15 Hz The figure is also useful, however, in estimating the side-lobe rejection properties of the array to confirm that the Kaiser-Bessel spatial window function was having the desired effect of decreasing side-lobe levels At 12 Hz, the noise power in beam number 100 is greater than 91 dB, but in the end-fire beams it is between 60 and 68 dB This indicates a side-lobe suppression of at least 23 dB and possibly better

B. 18m Arrays

Figure 4 4 is a representative contour plot from an 18m array The pedestal structure in the vertical directionality is still apparent at some frequencies (most notable around 33 Hz and 35 Hz), but the plot shows signals at the horizontal and away from it which are contaminating the data in the end-fire beams This was true for all of the data from the 18m arrays and it was felt that these data were unreliable Much of the high-level shipping noise appears to be concentrated in the effective frequency range of the 18m arrays (approximately 30-45 Hz) and to study the vertical noise in this region, a larger aperture array than was used in this study is needed to decrease beam widths and make the spatial filter of the beamformer more effective at discriminating between the vertical noise and the noise at other angles

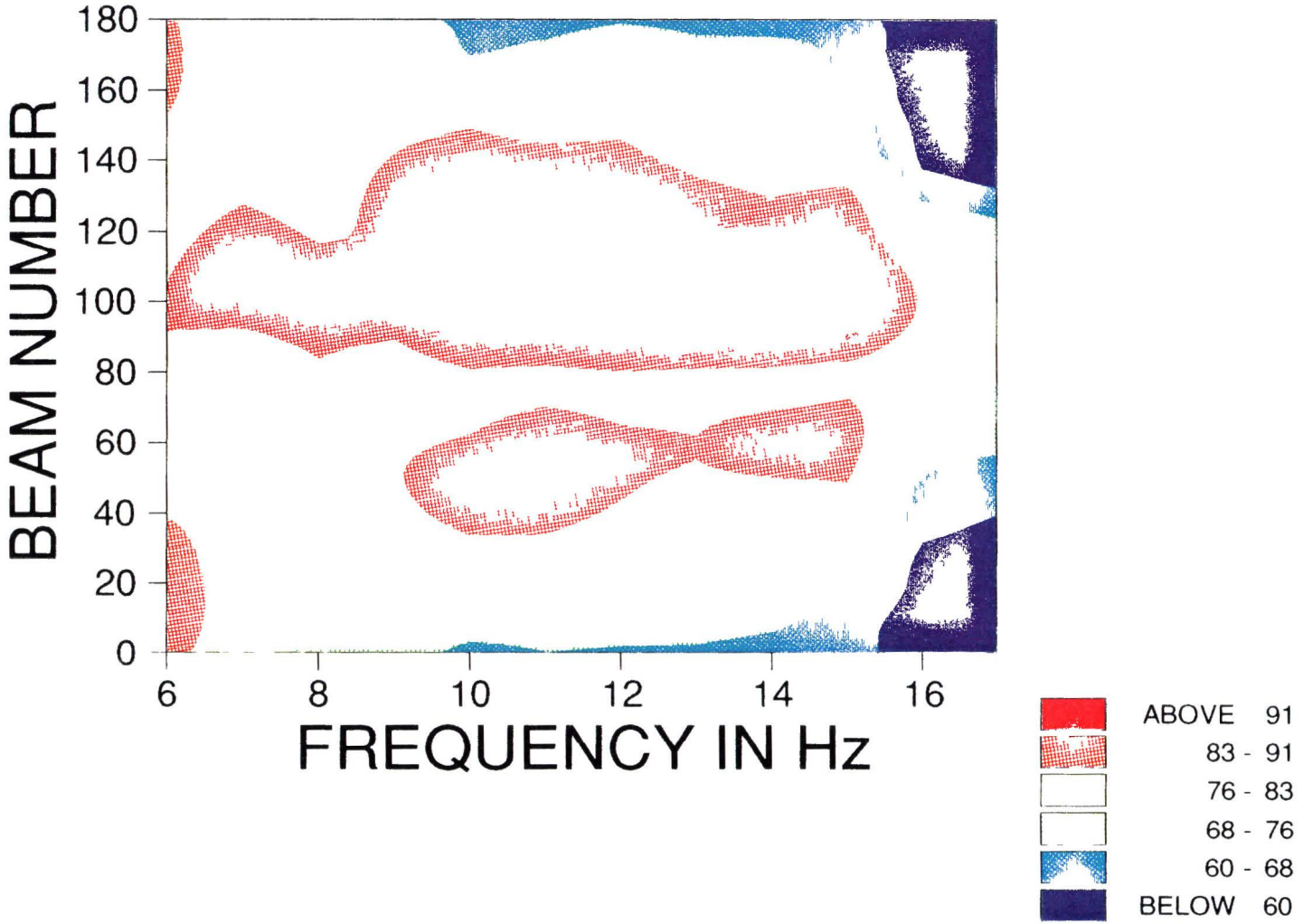

Figure 4 3 45m array contour plot showing contaminated data set

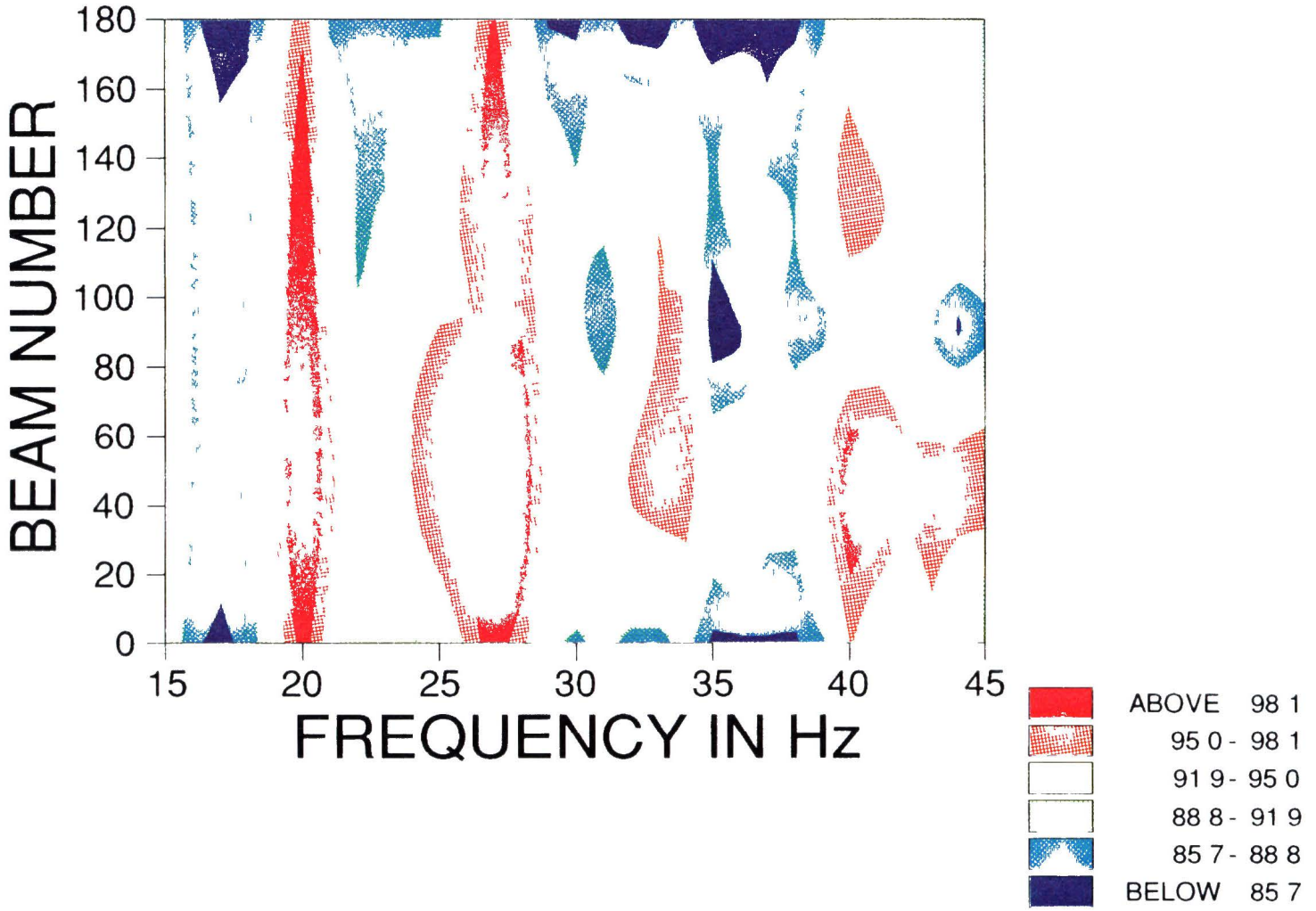

Figure 4 4 Representative contour plot for an 18m array

C. 6m Arrays

The frequency range for the 6m arrays (approximately between 50-80 Hz and 125 Hz depending on the aperture of the array) was the region for which the most data was available, including enough low wind-speed data to use the two-process model Figure 4 5 is a representative example of a contour plot from a 6m array The horizontal pedestal in the vertical directionality field is readily apparent at all frequencies, as is the decrease in noise level with increasing frequency Also apparent in this figure is the difference in noise level between the upward looking beam (beam 0) and the downward looking beam (beam 180) which was discussed in the introduction For example, at 90 Hz, the power in the downward-looking beam is below 62 dB, whereas the power in the upward-looking beam is between 62 dB and 68 dB At frequencies close to the cut-off frequency of the array (125 Hz in this case), this difference in power is no longer apparent in the figure This is due to the inability of the beamformer to distinguish between signals arriving from upwards or downwards end-fire as discussed in section 2 II E

Figure 4 6 is another example of how the contour plots were used to identify contaminated data sets In this case, a source or several sources were present which had steep arrival angles which could contaminate the end-fire data due to the width of the main lobe For this data set, the scientific log confirmed that there was a ship operating nearby at the time the measurements were taken The high arrival-angle

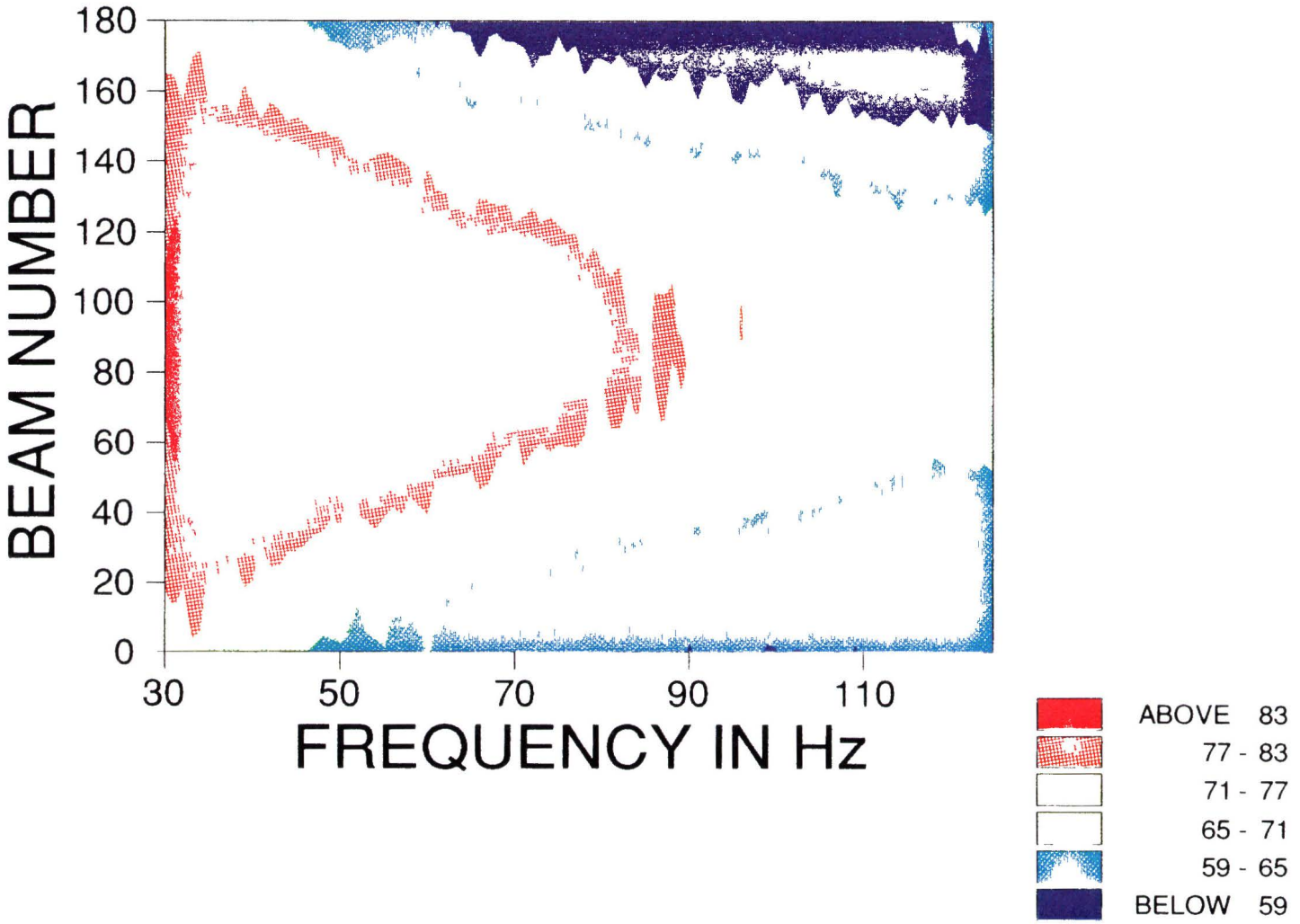

Figure 4 5 Representative contour plot for a 6m array

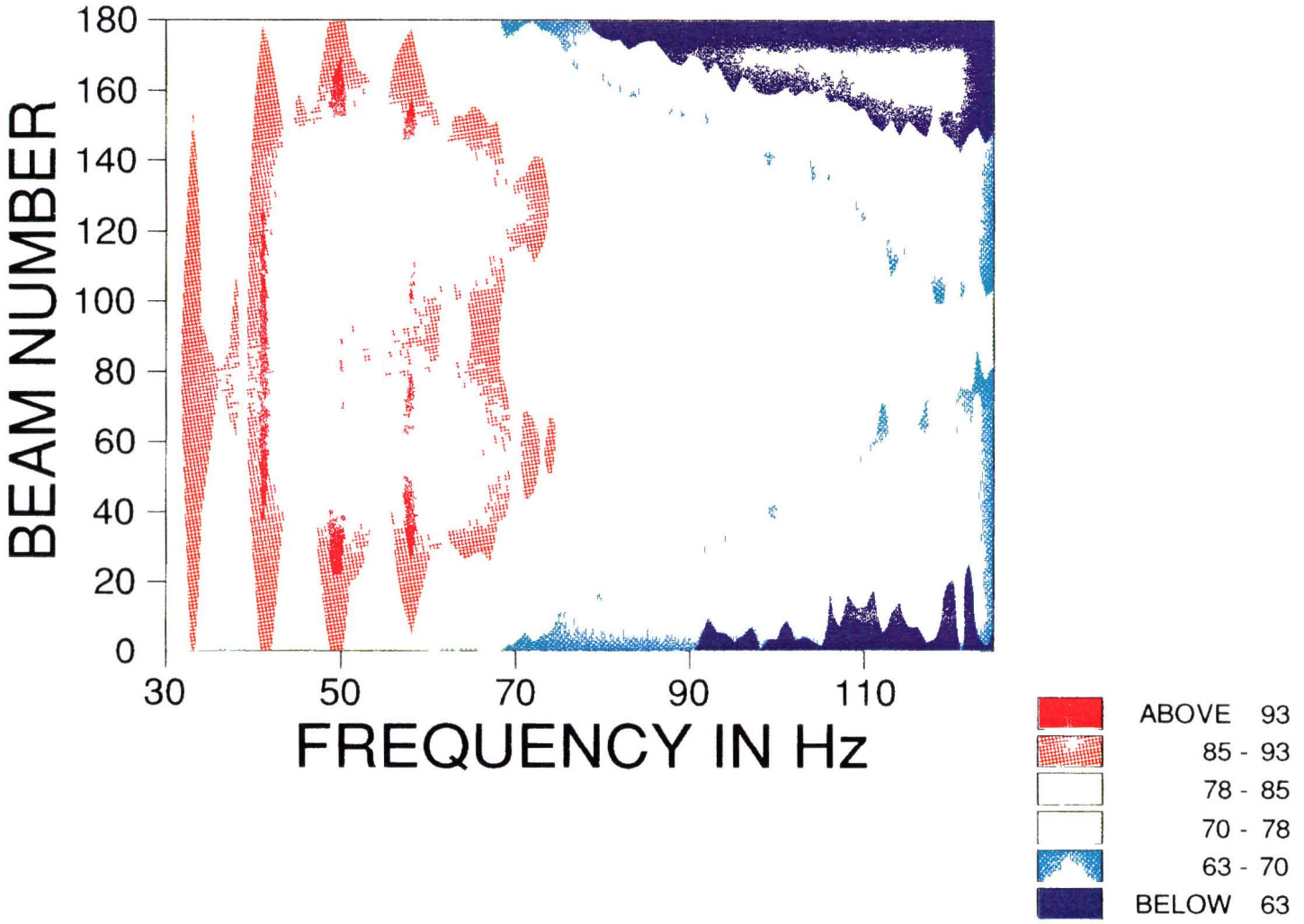

Figure 4 6 6m array contour plot showing contaminated data set

signals present in this plot were probably due to direct or bottom bounce arrival paths of sound from this ship

Figure 4 7 can be used to estimate the side-lobe suppression of the array There is a strong signal present at the horizontal at approximately 123 Hz with a strength of greater than 77 dB The observed power in the end-fire beams at this frequency is less than 53 dB, indicating a side-lobe suppression of greater than 24 dB

D. 3m Array

The 16 element, filled 3m array, deployed in 1986, had the largest effective frequency range (approximately 70-250 Hz) because of its relatively large aperture and number of elements Figure 4 8 is a representative example of a contour plot from this array The pedestal at 90° to the array in the vertical noise field is evident at all frequencies within the effective range, and the noise level decreases with increasing frequency The side-lobe suppression, estimated from the plot, is at least 21 dB for this array

E. 2m Arrays

Figure 4 9 is a representative example of a contour plot for the 2m arrays The effective frequency range for these arrays is between approximately 225 Hz and 350 Hz Once again, the pedestal effect is evident at all frequencies within this range and the noise level decreases with increasing frequency The difference in noise level between the upward and the downward looking beams is also apparent in this plot

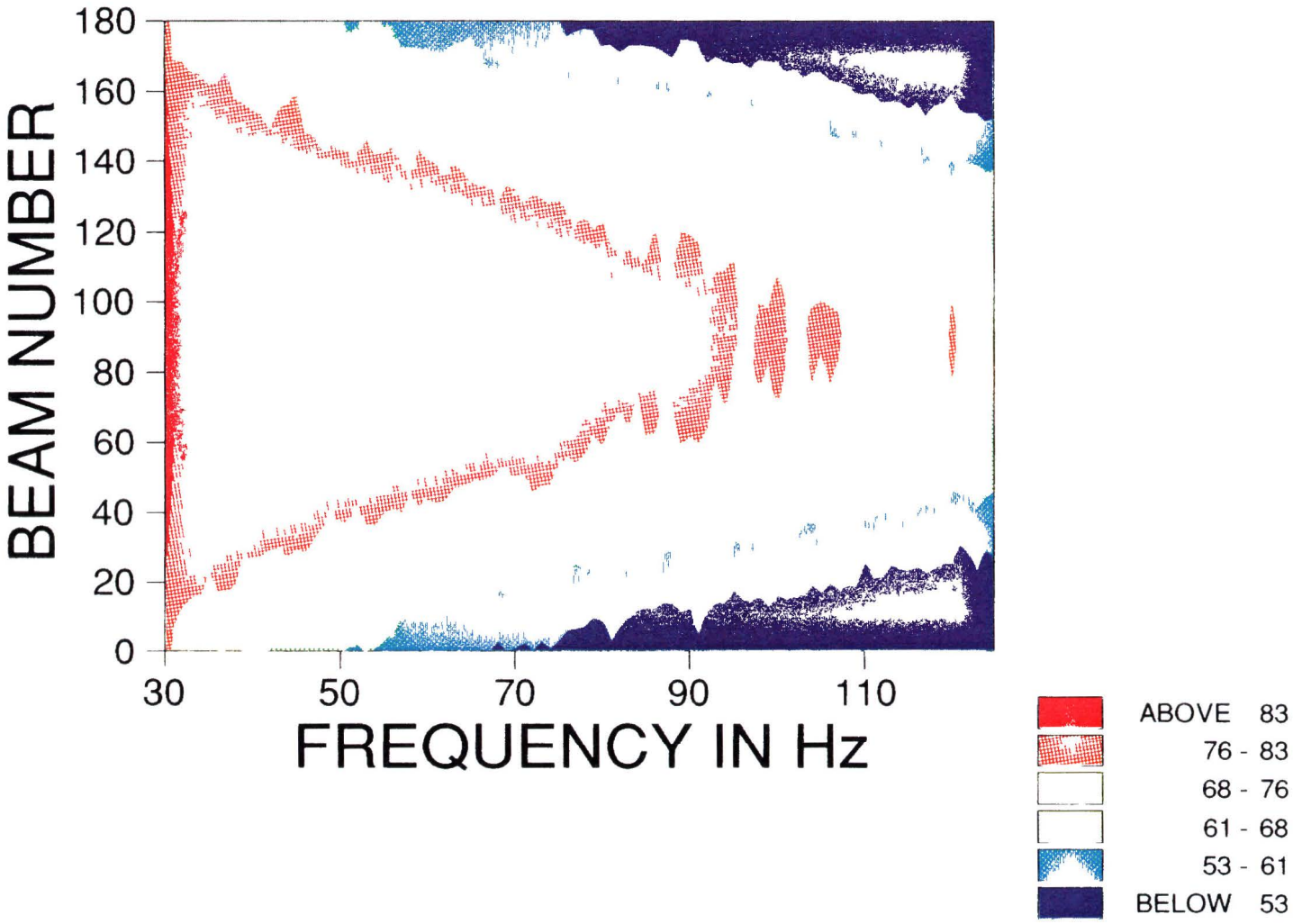

Figure 4 7 Contour plot for estimating side-lobe suppression in a 6m array

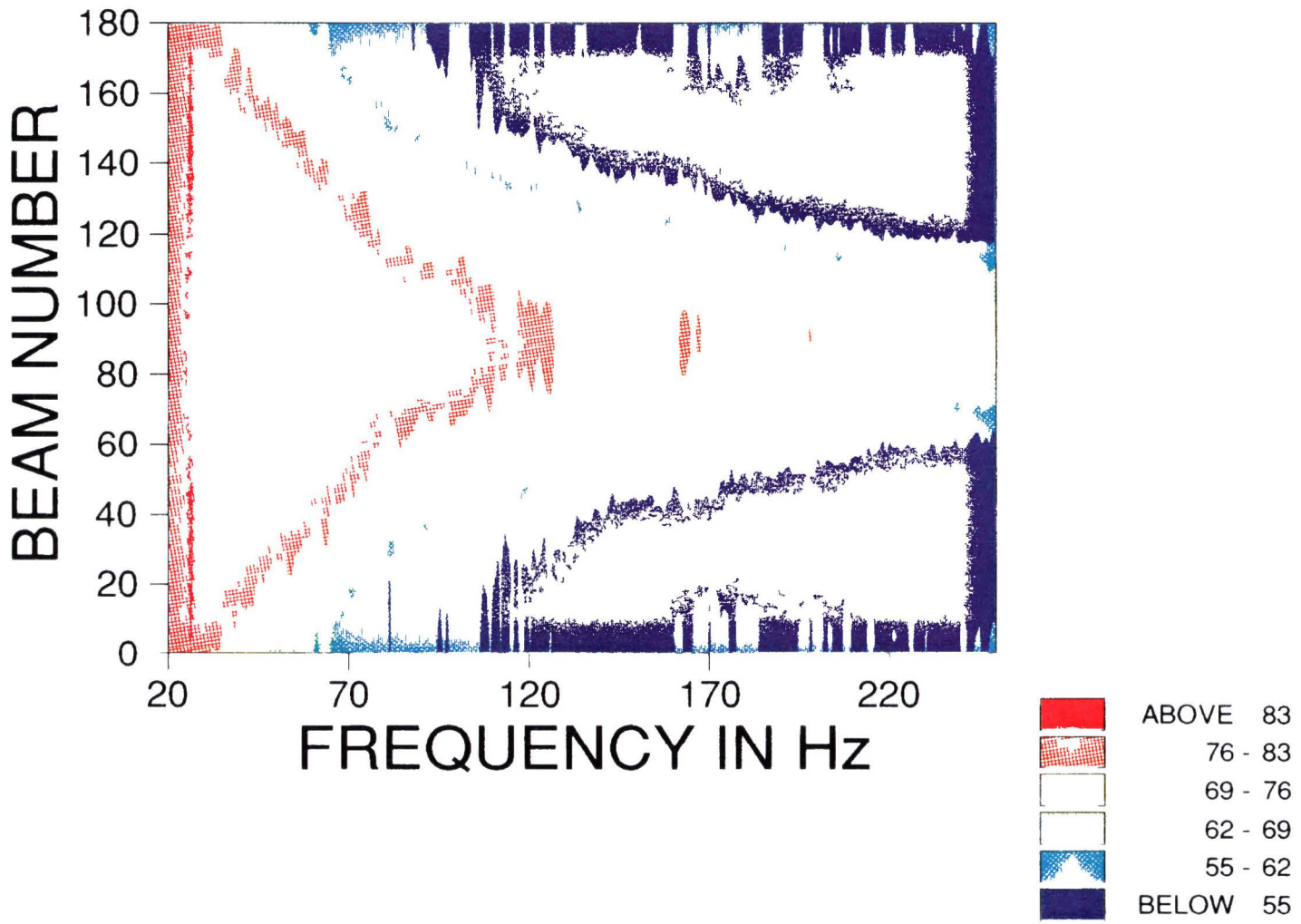

Figure 4 8 Representative contour plot for a 3m array

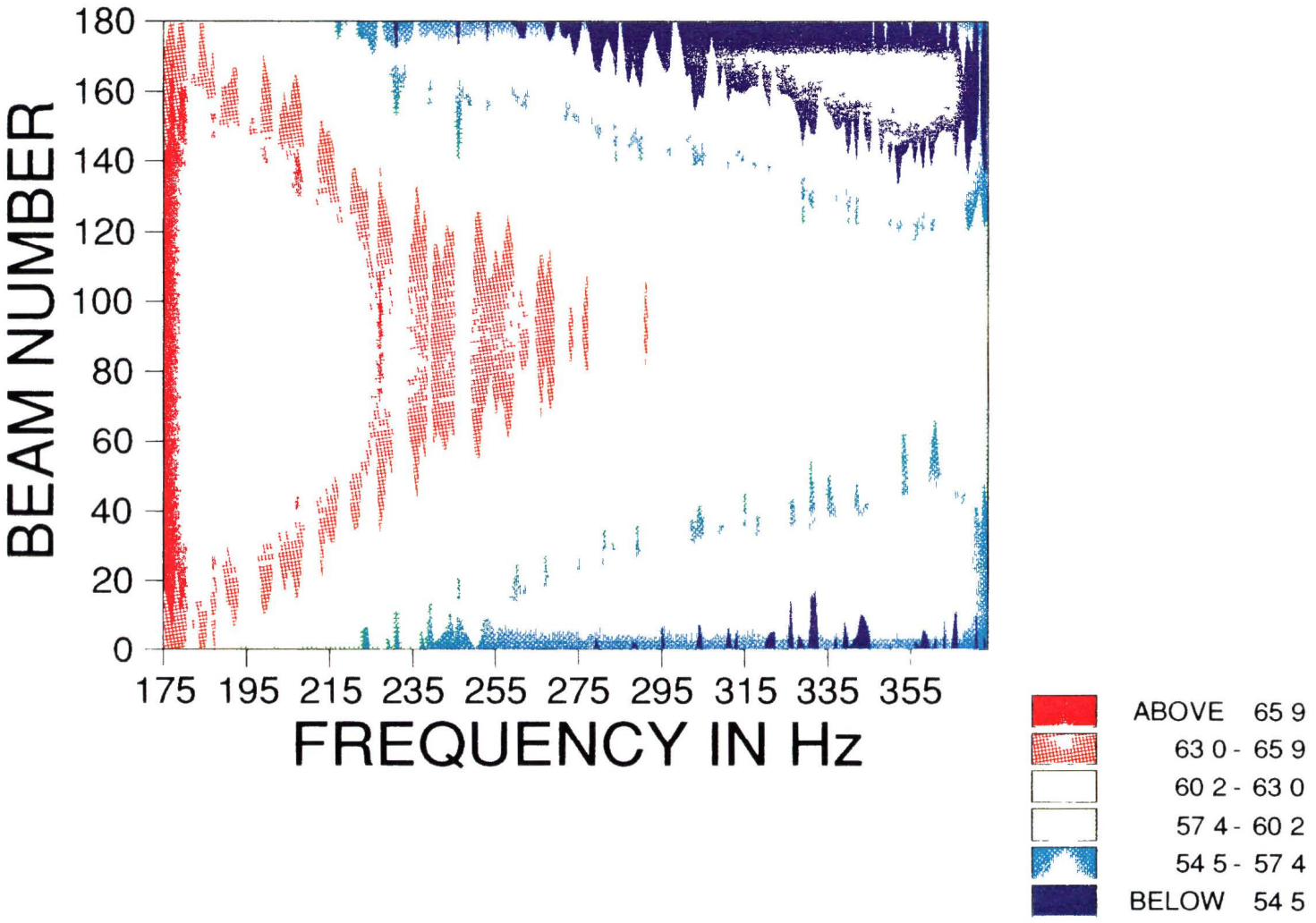

Figure 4 9 Representative contour plot for a 2m array

The best estimate of side-lobe suppression available from Figure 4 9 is that the suppression is greater than about 8 dB This is due to the fact that no strong signals were present to use as a reference and, as mentioned in the introduction in section IV, the difference between the noise level in the horizontal and the noise level in the vertical is less at these high frequencies than at lower ones Because of this the side-lobe suppression is not as critical at these high frequencies as it is at lower ones and the actual side-lobe suppression of the array is probably much greater than 8 dB

II. Estimates of Wind-Generated Noise Model Parameters

Plots of the measured surface source level vs the logarithm of the wind speed at various frequencies over the band studied are shown in Figures 4 10 to 4 27 The key to the symbols used to identify data from different sets is shown in Table II

Symbol	Year/Set	Symbol	Year/Set
	1977/1		1983
	1977/2		1984
	1978		1985
	1981		1986

Table 4 1 Key to symbols in noise level vs wind speed plots

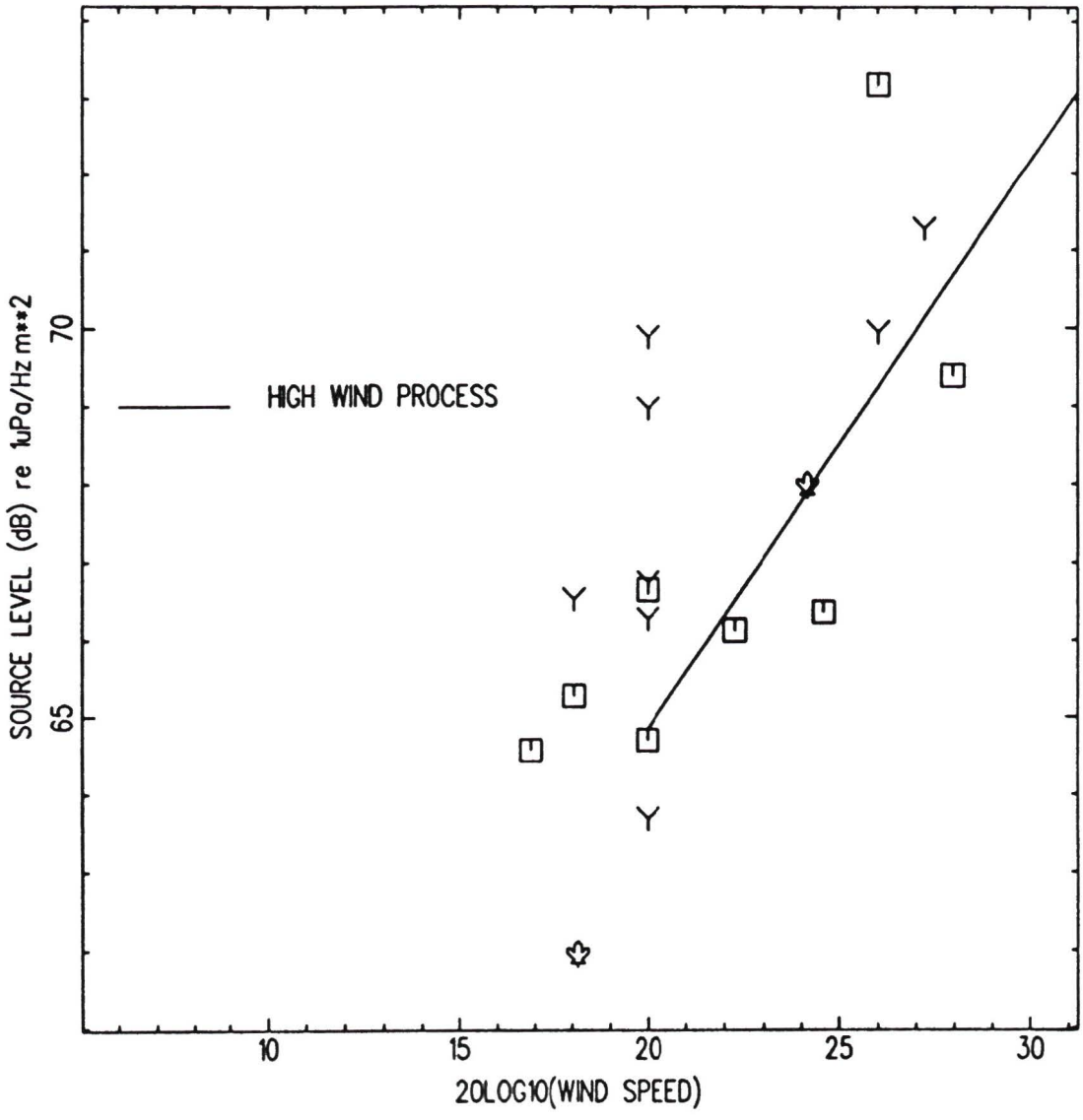

Figure 4 10 Surface noise level vs wind speed at 10 Hz

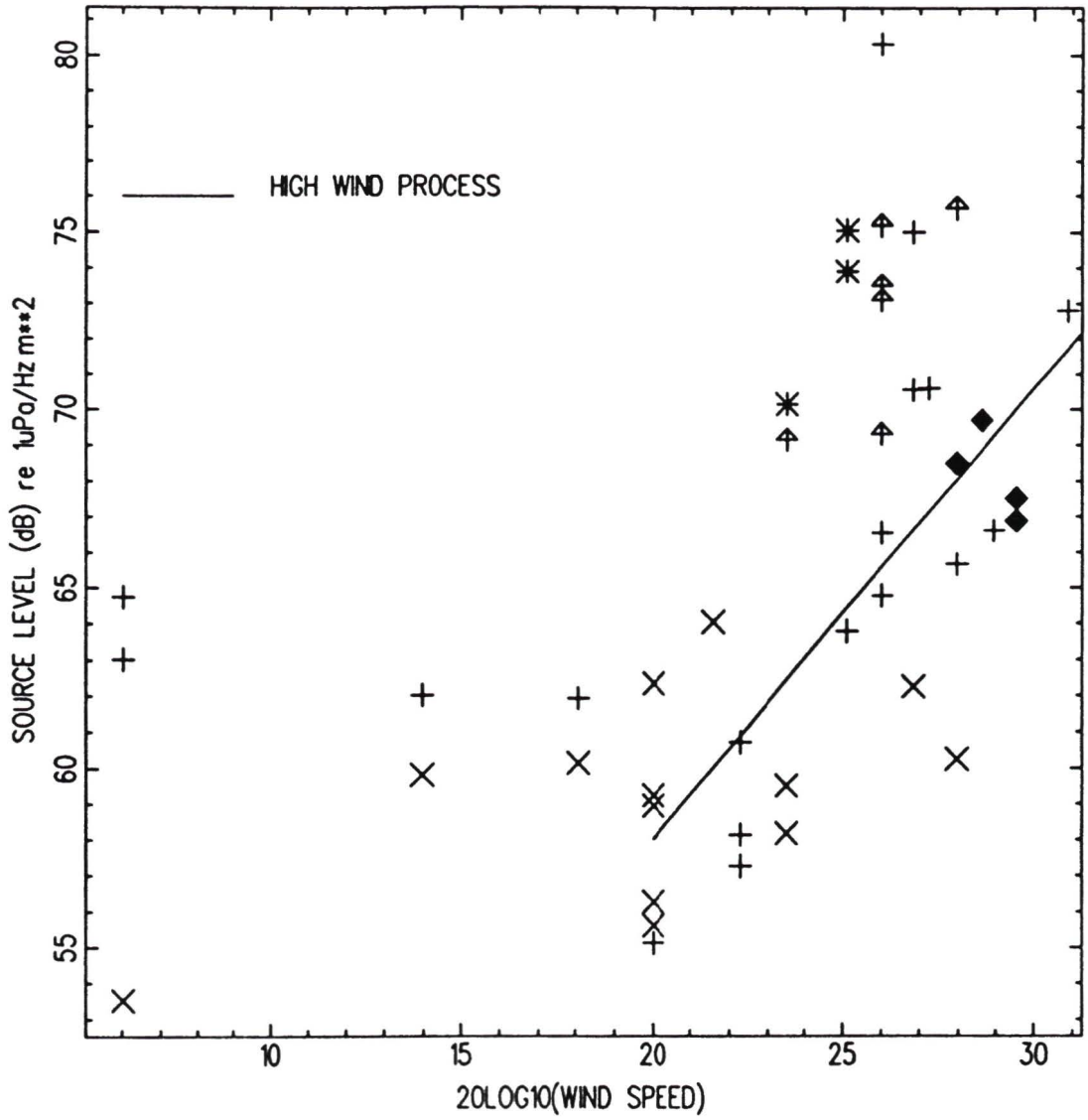

Figure 4 11 Surface noise level vs wind speed at 50 Hz

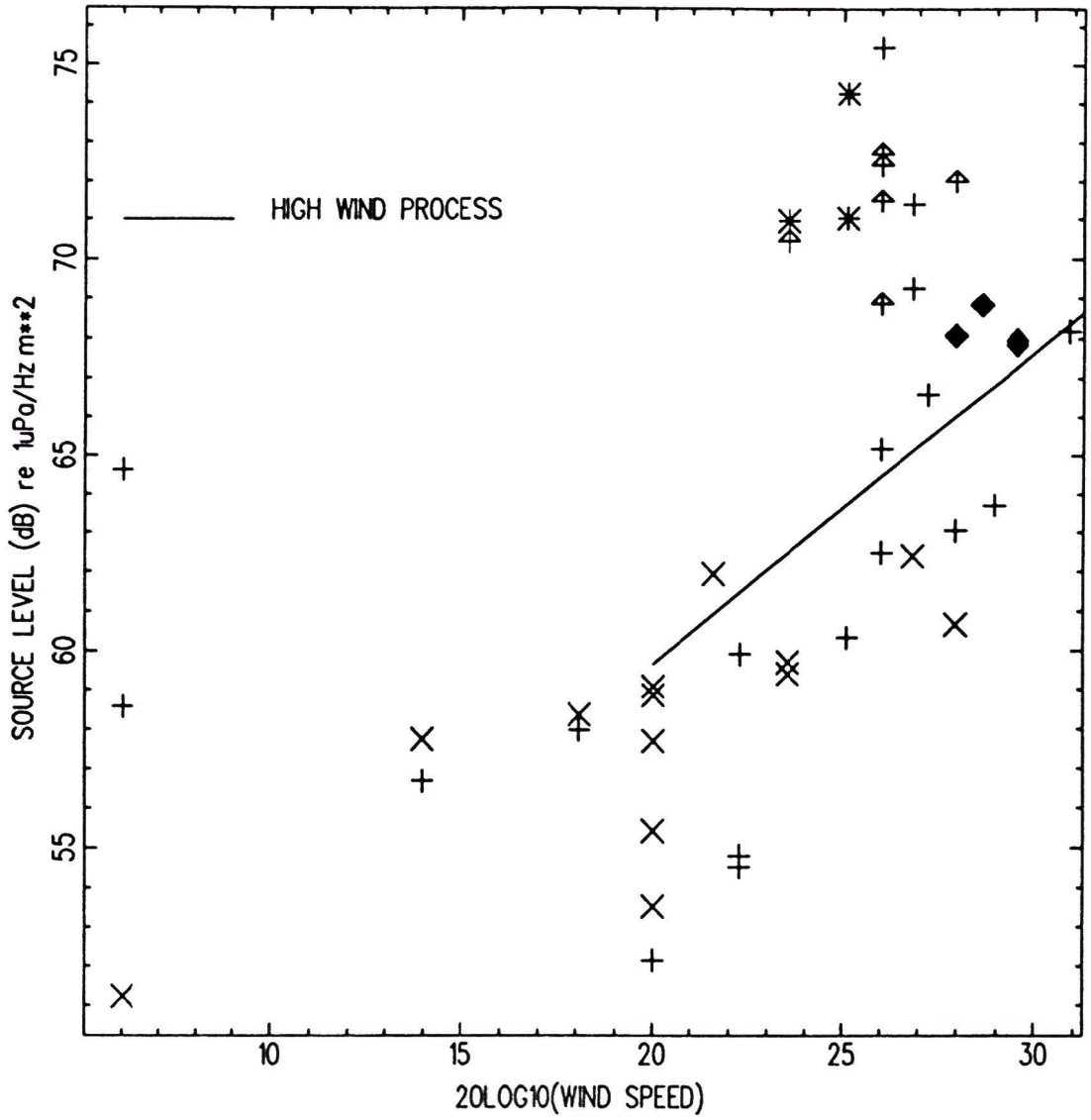

Figure 4 12 Surface noise level vs wind speed at 60 Hz

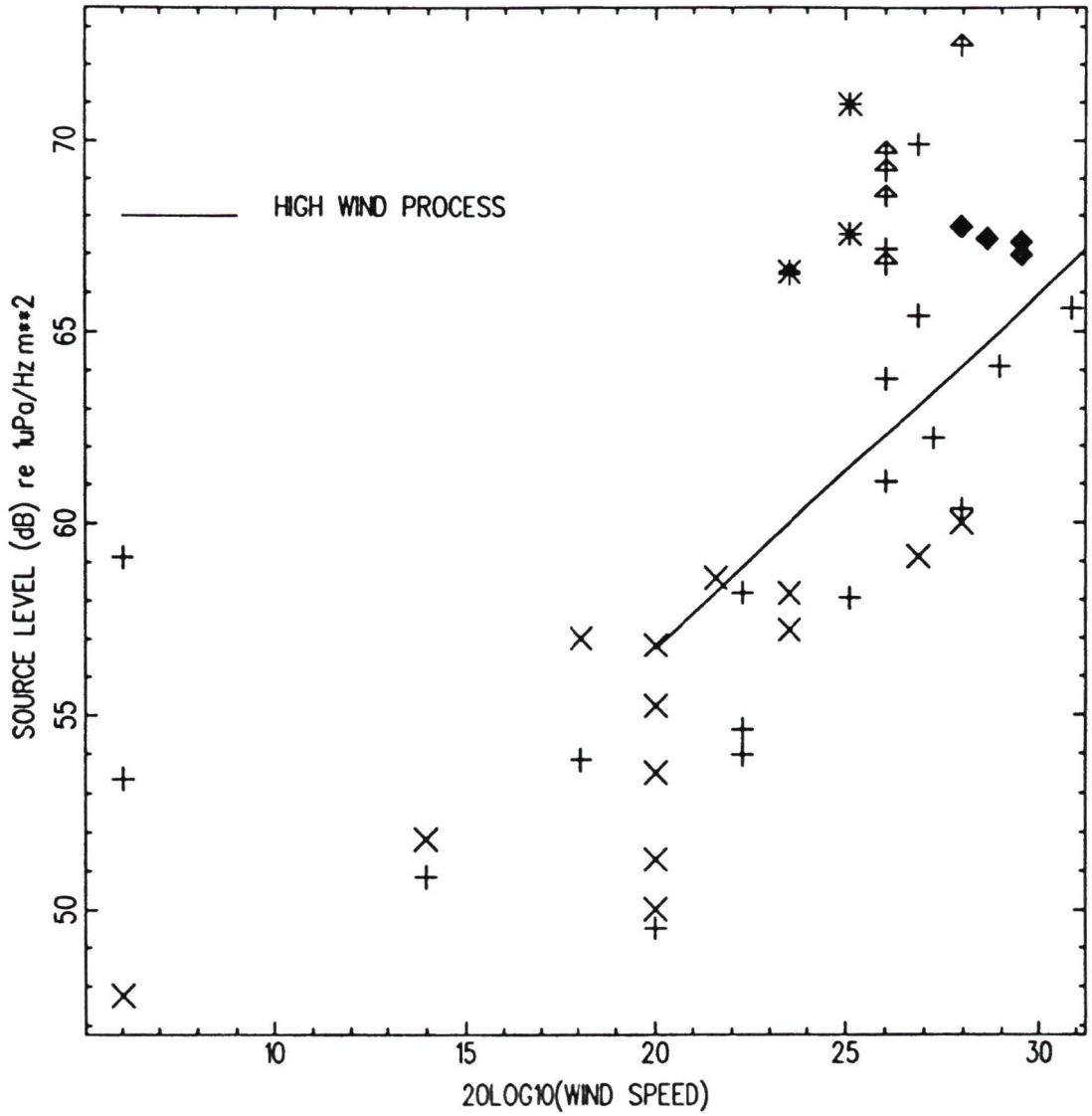

Figure 4 13 Surface noise level vs wind speed at 70 Hz

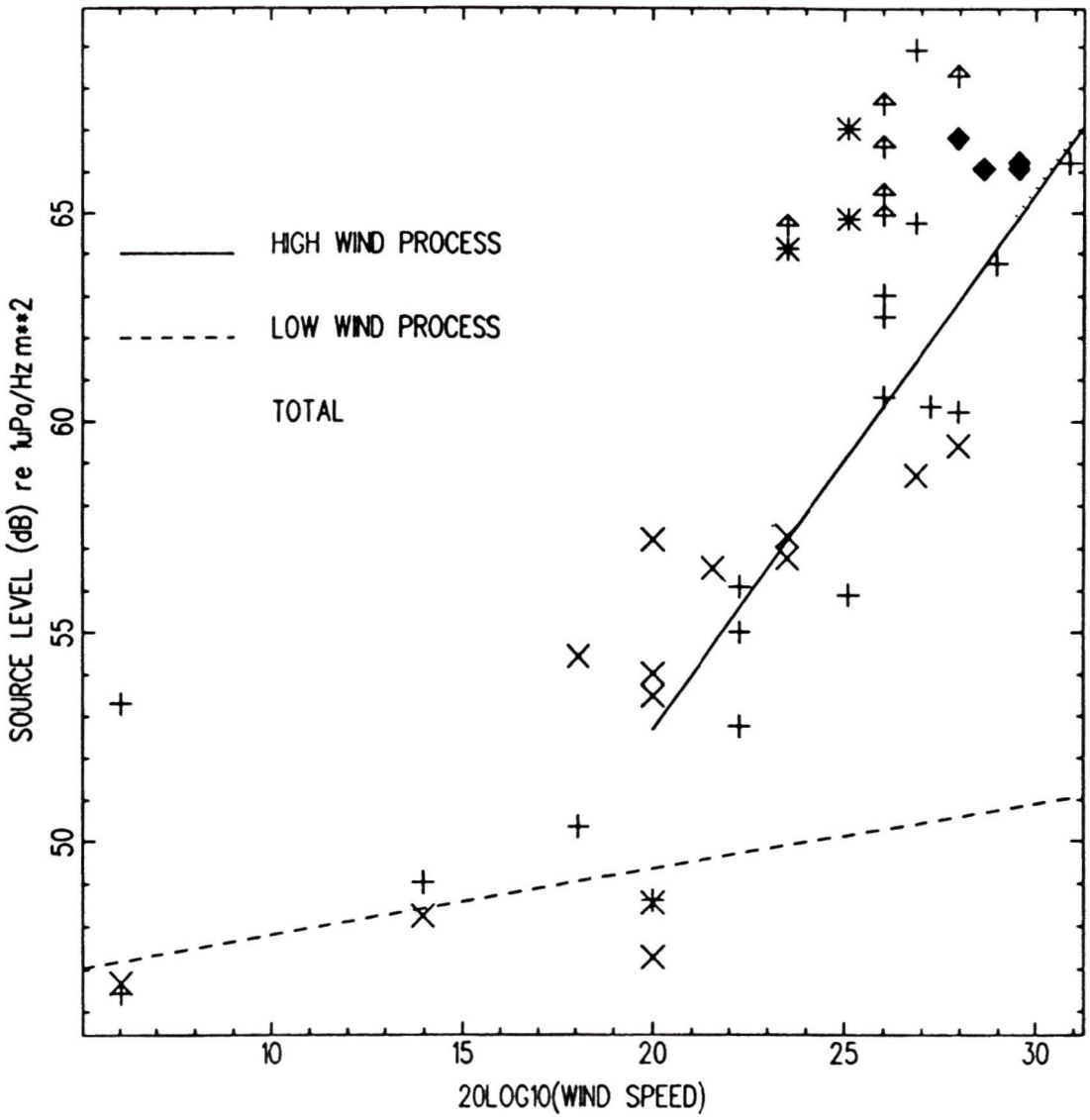

Figure 4 14 Surface noise level vs wind speed at 80 Hz

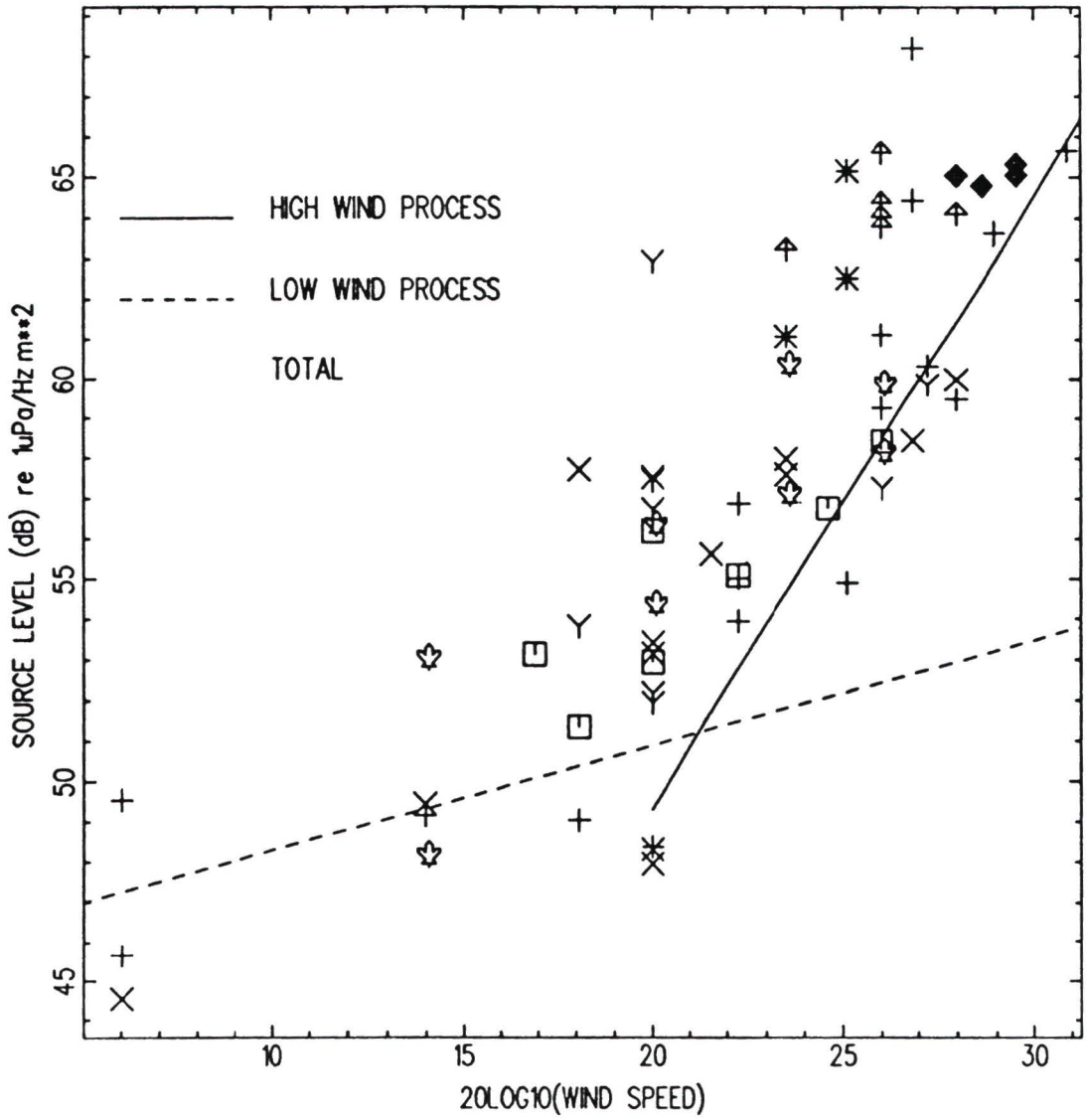

Figure 4 15 Surface noise level vs wind speed at 90 Hz

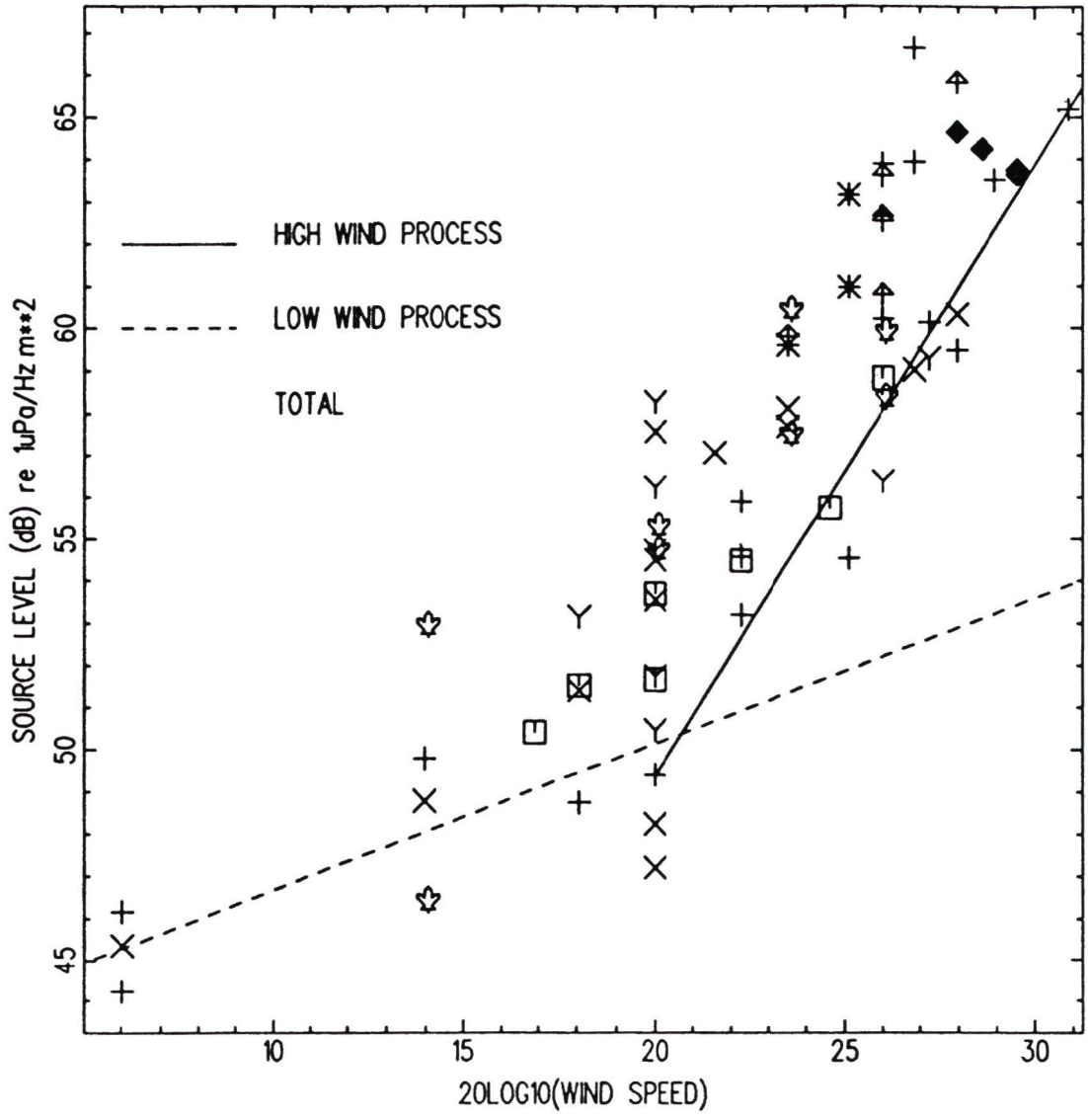

Figure 4 16 Surface noise level vs wind speed at 100 Hz

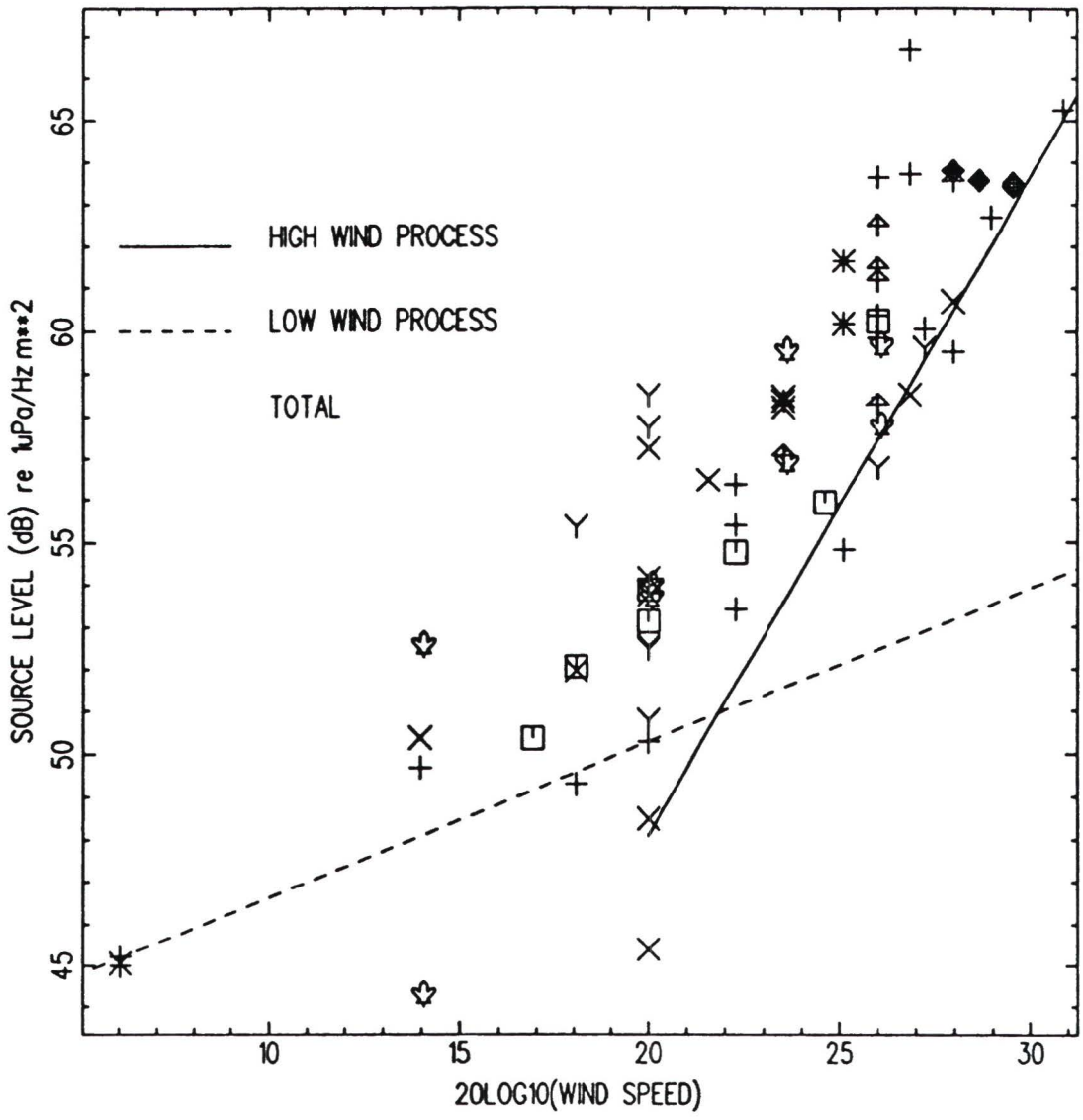

Figure 4 17 Surface noise level vs wind speed at 110 Hz

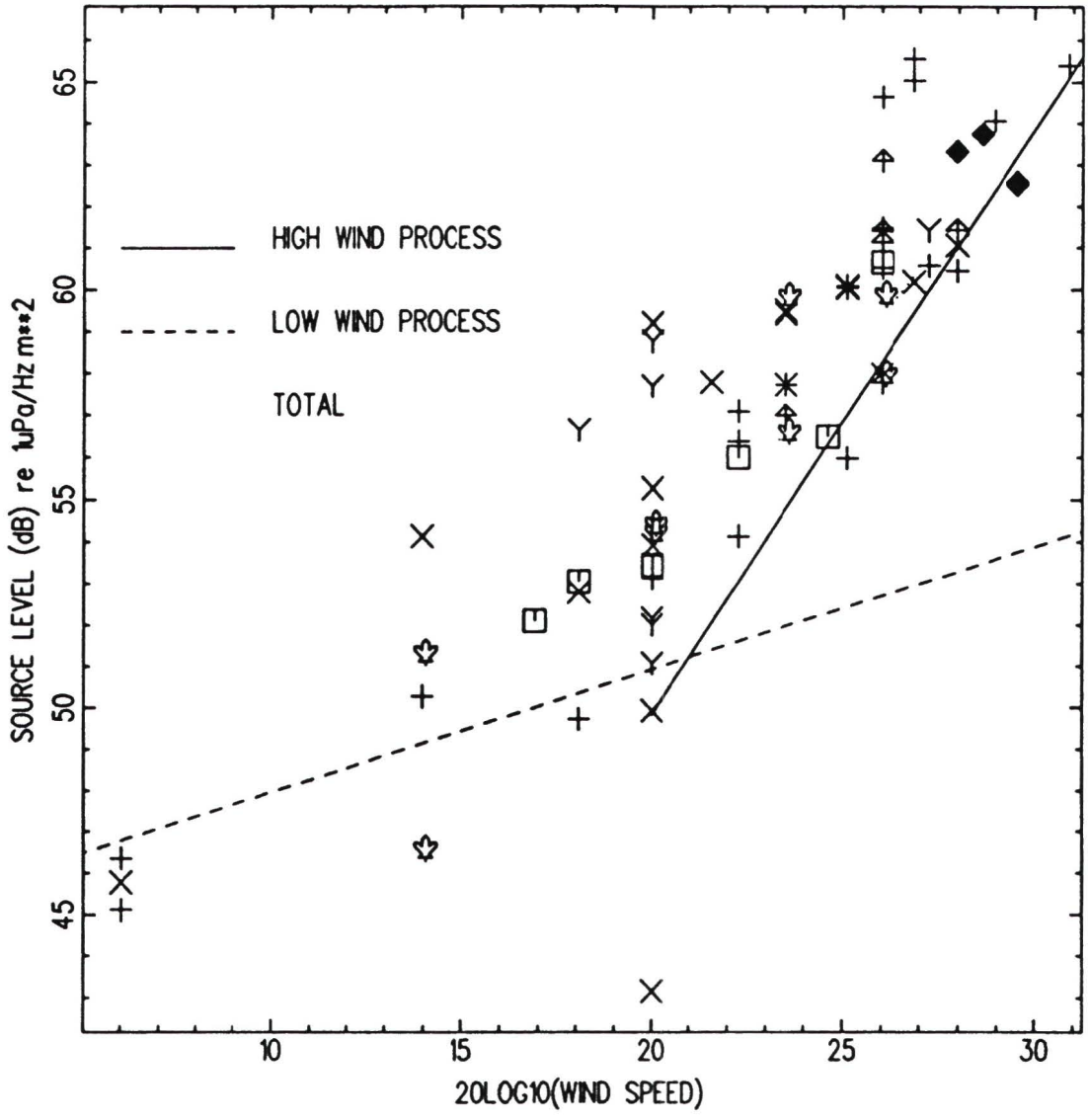

Figure 4 18 Surface noise level vs wind speed at 120 Hz

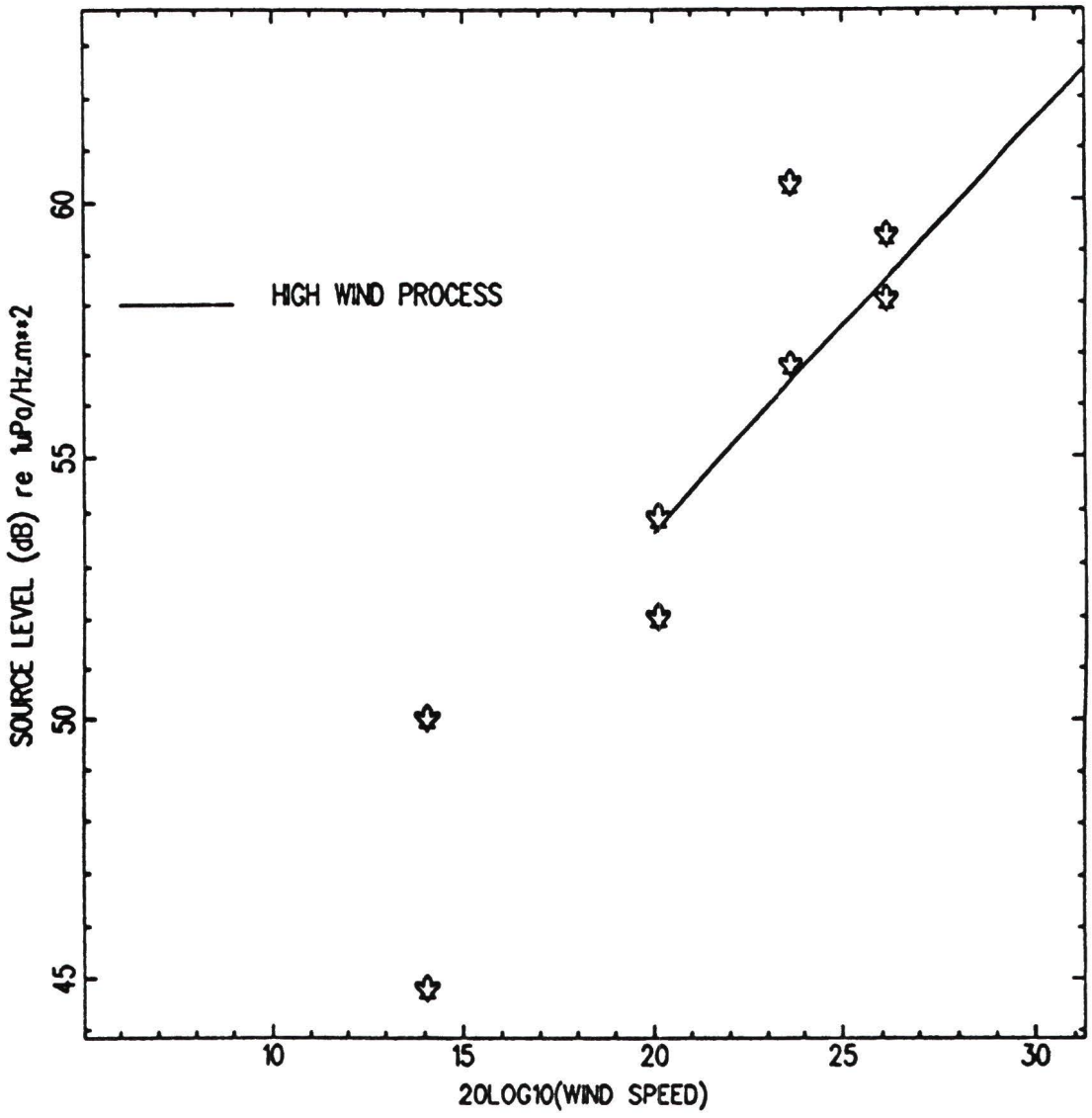

Figure 4 19 Surface noise level vs wind speed at 150 Hz

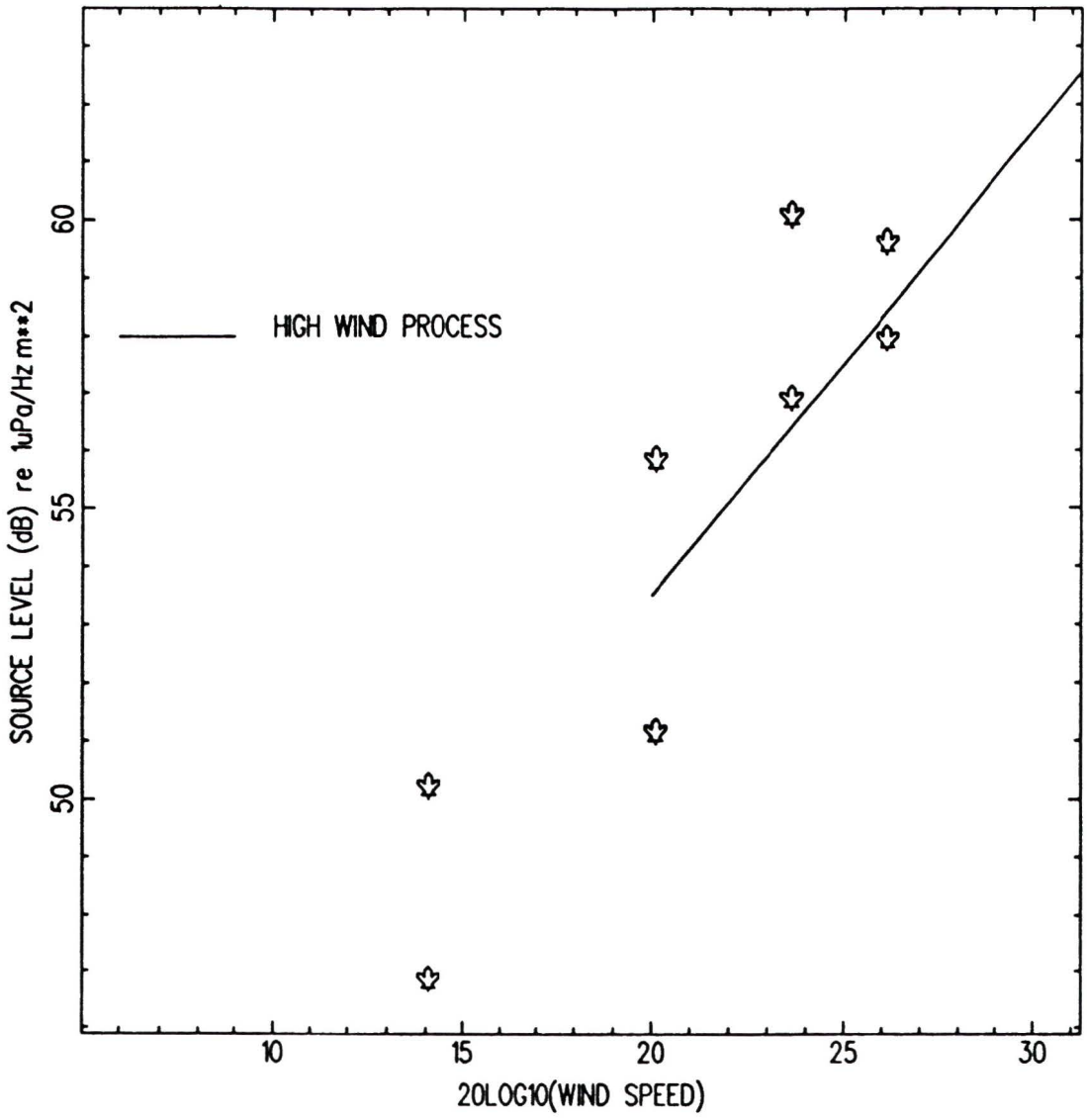

Figure 4 20 Surface noise level vs wind speed at 175 Hz

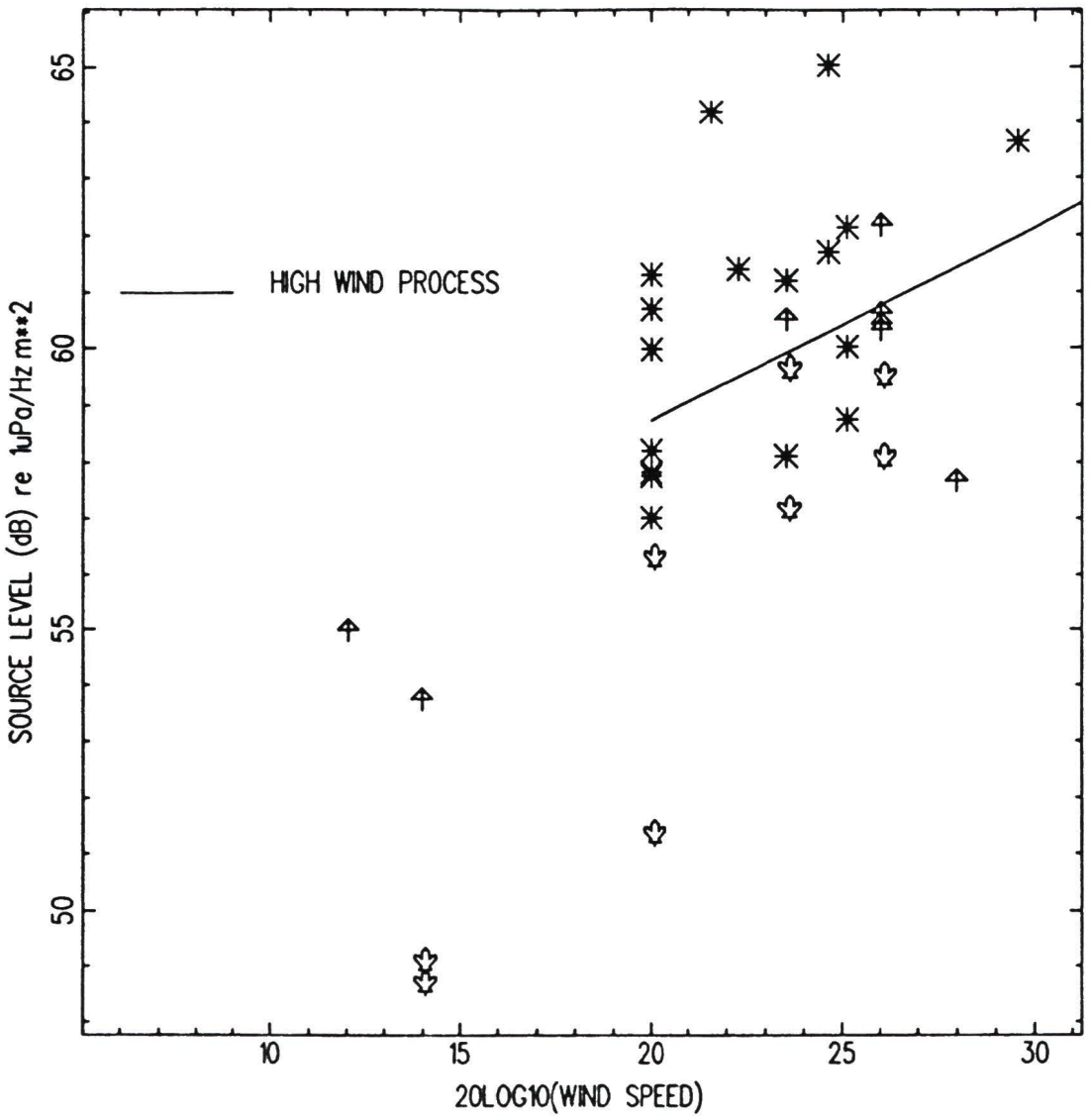

Figure 4 21 Surface noise level vs wind speed at 200 Hz

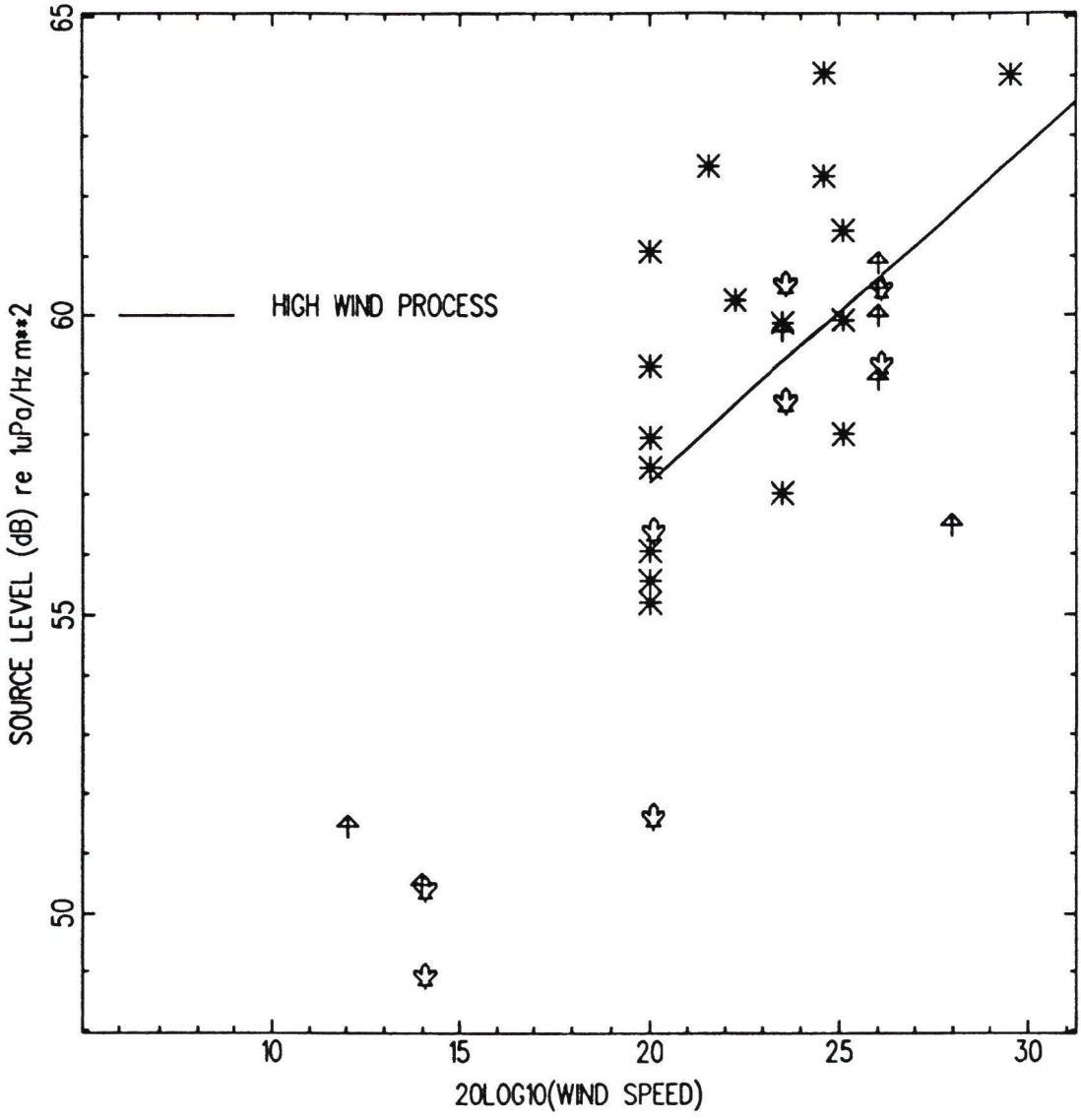

Figure 4 22 Surface noise level vs wind speed at 225 Hz

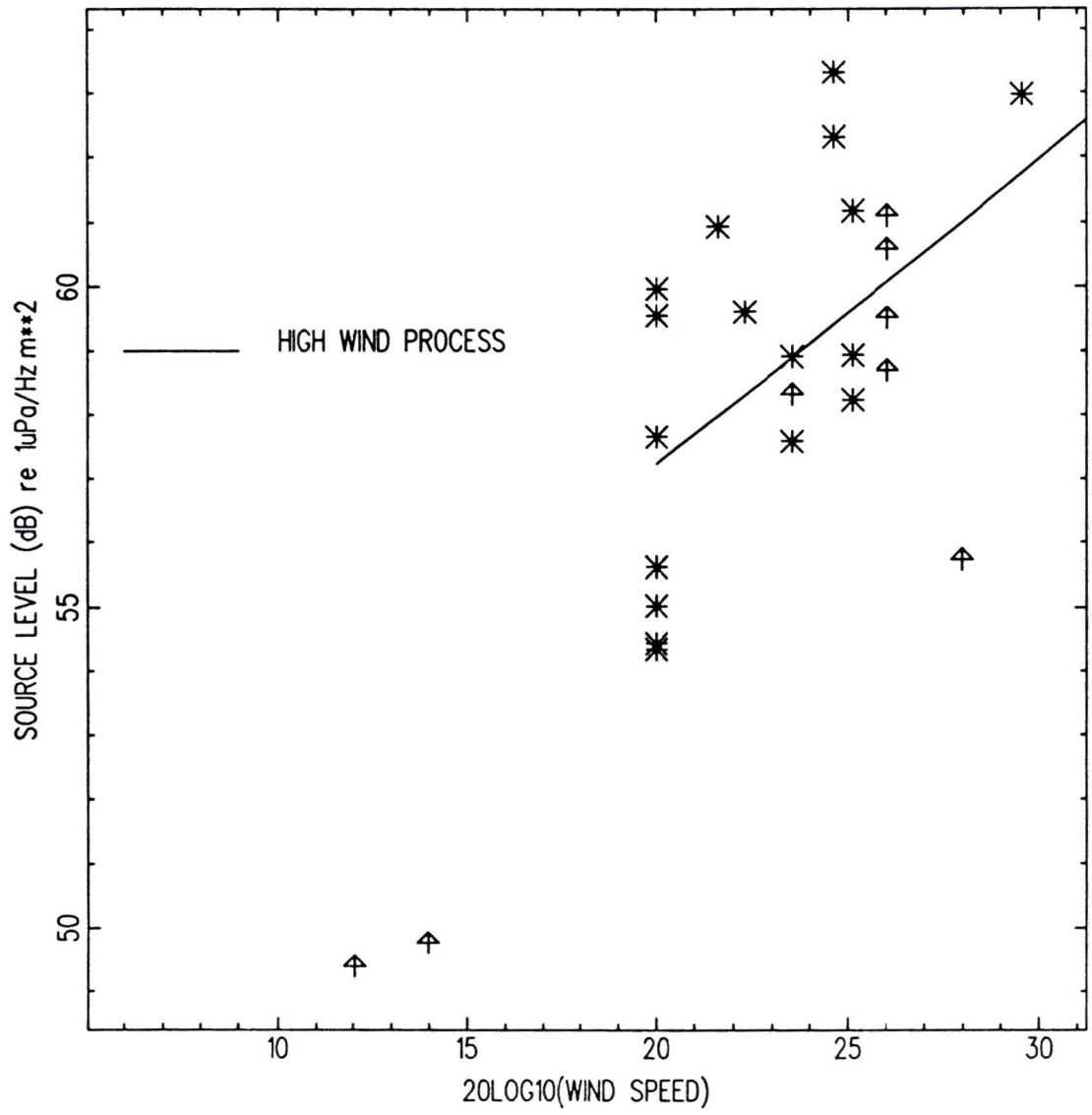

Figure 4 23 Surface noise level vs wind speed at 250 Hz

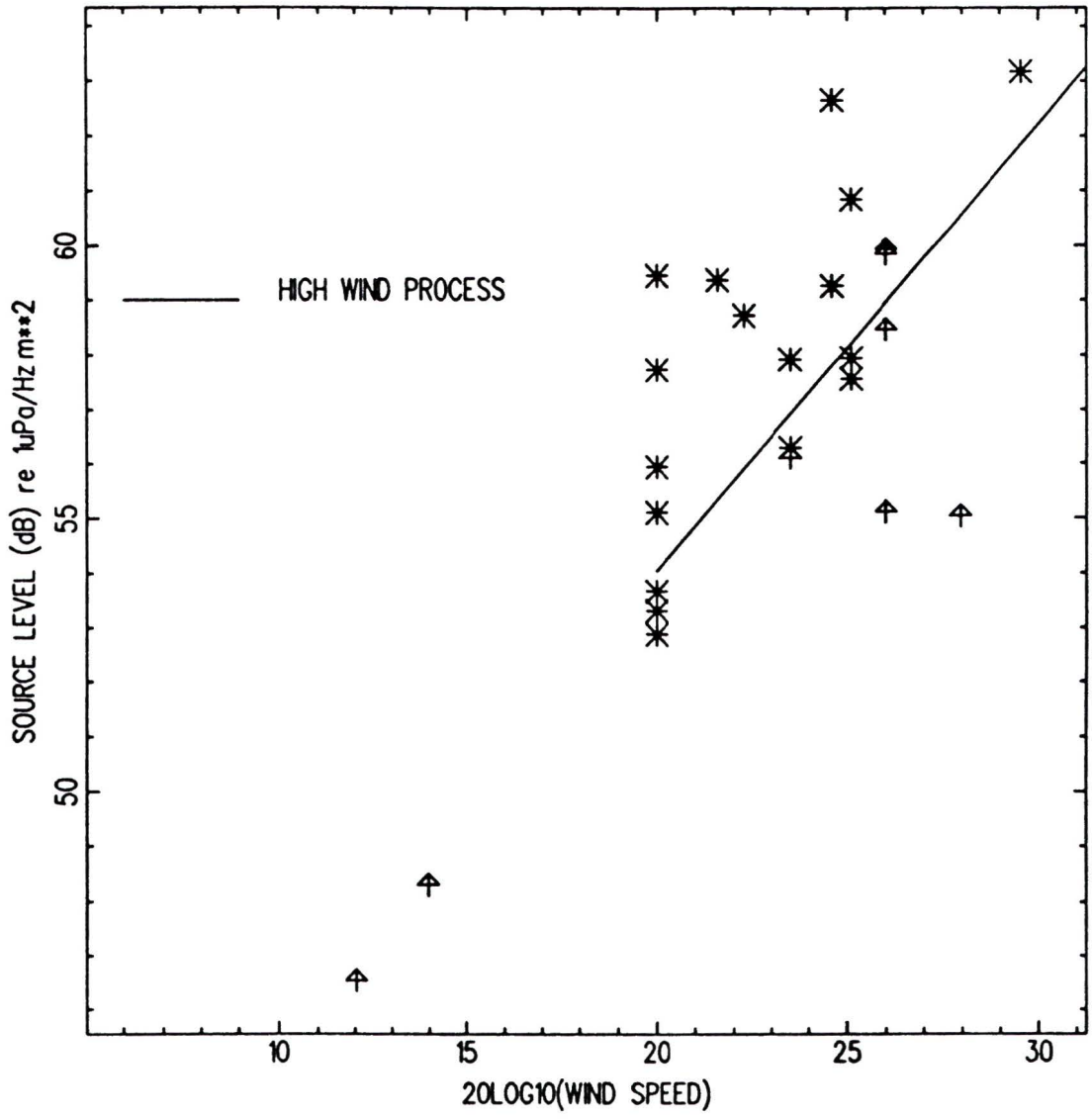

Figure 4 24 Surface noise level vs wind speed at 275 Hz

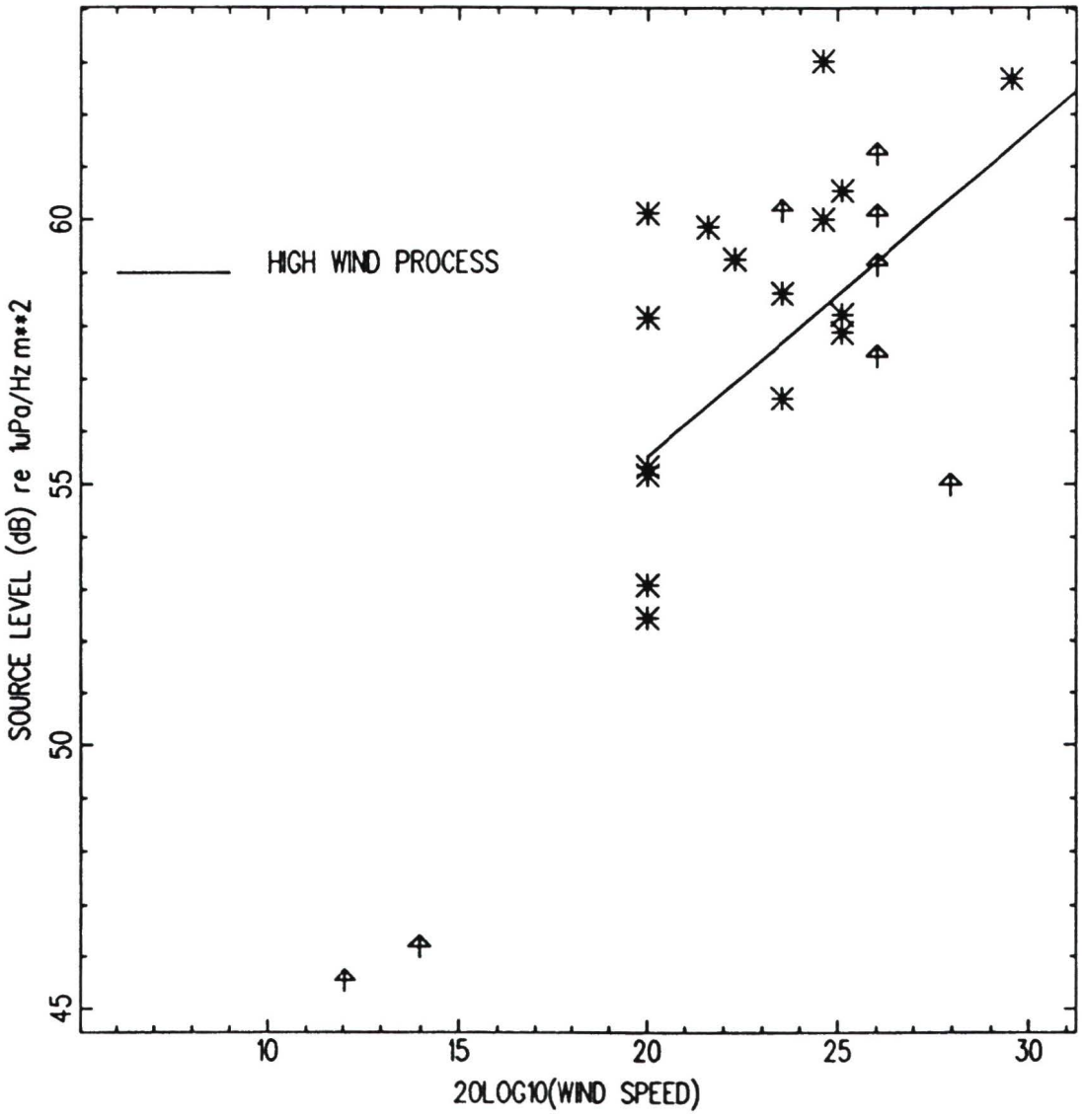

Figure 4 25 Surface noise level vs wind speed at 300 Hz

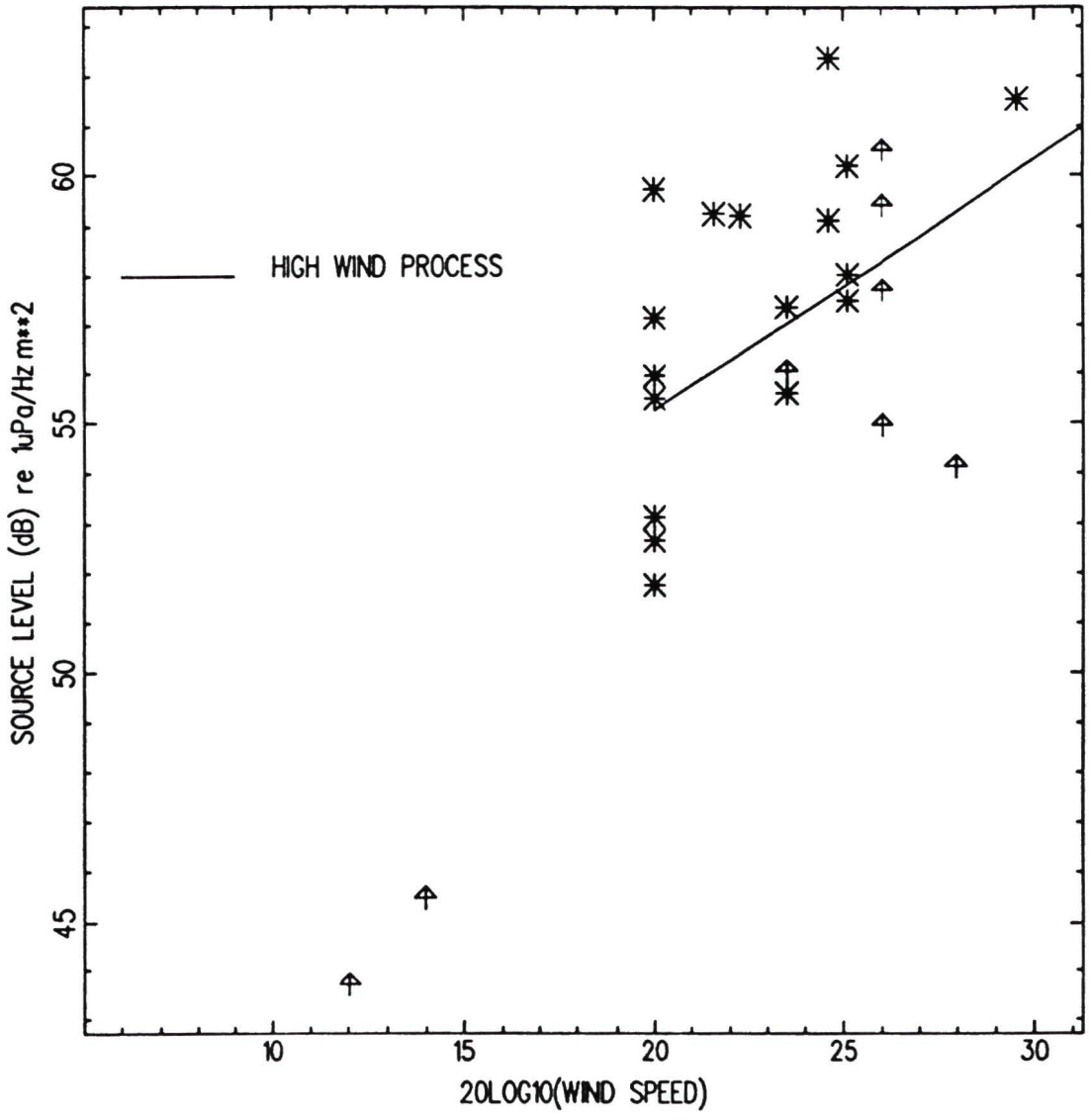

Figure 4 26 Surface noise level vs wind speed at 325 Hz

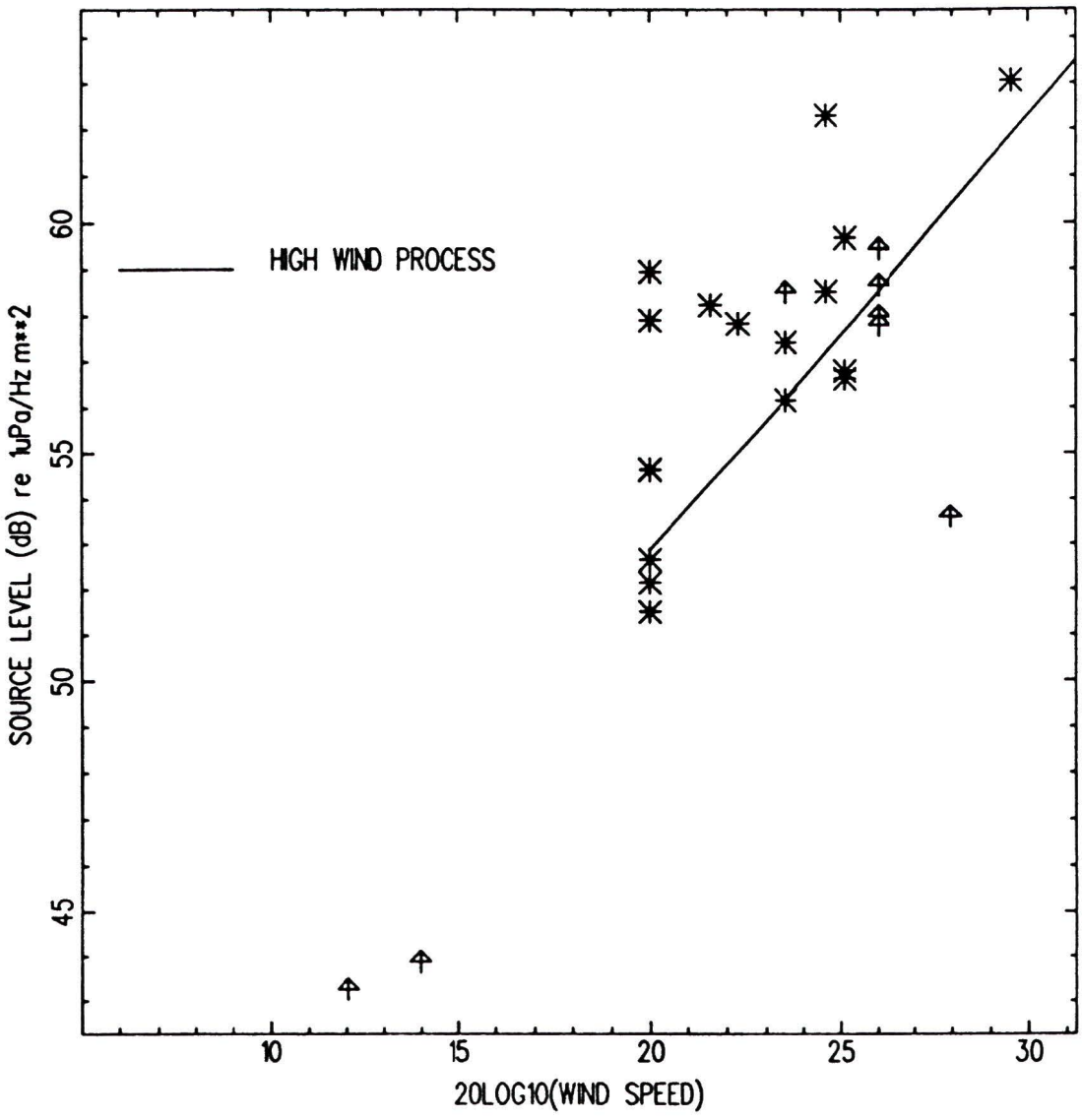

Figure 4 27 Surface noise level vs wind speed at 340 Hz

Included in these figures are the lines corresponding to the best fits to the parameters of the model outlined in section 3 II For the frequencies between 80 Hz and 100 Hz, three separate lines are included which are the estimated fits to the data for the low-wind process, the high-wind process, and the total noise For all other frequencies, only the high-wind process line is included as not enough low-wind data was available to calculate the parameters for the low-wind process The model parameters which were calculated by regression analysis from the measured data are summarized in Table III

As can be seen from the noise level vs wind speed plots, there is a fairly wide spread of noise levels at some of the wind speeds- most notable at wind speeds of 5, 10,15, and 20 knots This spread is larger than would be expected from just random variations in the noise generation and could cause errors in the values determined for the model parameters This spread could be due to a number of factors which could not be accounted for with the available data. The most obvious possibility is evidenced by the fact that the measured wind speeds are clustered around factors of 5 knots The wind speeds used in this study were derived from the bridge logs of the research vessel, where the deck officers were requested to record wind speeds from the ships anemometer If any estimation or rounding was done by the deck officers, the lower levels in the spread for any particular wind speed could have resulted from a rounding up of the wind speed measurements when they were recorded and vice-versa for the higher levels

Freq	A_L	n_L	r_L	A_H	n_H	r_H
10				50 17	0 73	0 94
50				32 83	1 26	0 99
60				43 69	0 80	0 98
70				38 29	0 92	0 97
80	46 26	0 16	0 99	27 04	1 28	0 97
90	45 70	0 26	0 99	18 77	1 53	0 98
100	43 21	0 35	0 99	20 27	1 45	0 98
110	43 00	0 36	0 99	16 93	1 56	0 98
120	44 99	0 30	0 99	21 72	1 41	0 97
150				37 69	0 81	0 96
175				37 39	0 81	0 96
200				51 91	0 34	0 84
225				45 92	0 56	0 85
250				47 74	0 47	0 86
275				37 65	0 82	0 90
300				43 22	0 62	0 91
325				45 00	0 51	0 90
340				33 88	0 95	0 91

Table 4 2 Estimates of wind-generated noise model parameters

Another possibility to be considered for explaining the spread in noise levels is the consideration that surface agitation is dependent not only on instantaneous wind velocities, but also on such factors as the fetch and duration of the wind and even, to a lesser extent, on the temperature and density of the air and water which determines the friction velocity [18] The fetch could be a major consideration, since no information was available on the spatial characteristics of the wind field and small scale weather systems might could result in a high measured wind speed with insufficient fetch to fully develop the surface agitation The duration of the wind could also be a major factor If, as Marrett and Chapman [10] found in their data and is also physically reasonable, there is a time lag between a change in wind velocity and a change in noise level, this could contribute to the spread in the data points

Finally, there are many noise generation mechanisms in the ocean other than wind speed which could conceivably arrive at angles to the array which would not be filtered out by the beamformer Such mechanisms include seismic noise (only at very low frequencies), biological noise, close-in shipping noise, and system self-noise

Some attempts were made to reduce the possibility of, or the effect of, contamination of the data by non wind-generated noise sources The contour plots of noise intensity vs elevation angle and frequency helped to eliminate data sets which showed strong signals at high vertical angles to the array Also, the data was weighted during the regression fit to emphasize the lower noise levels at a particular wind speed, assuming that any contamination would raise the level These attempts, however

do not preclude the possibity that sources other than wind-generated ones had some effect on the data.

In addition to the spread of the data values discussed above, there are other possible sources of error in the estimated model parameters These include the effect of side-lobe contamination, array tilt, sample size, and error in the high-wind model parameters for the frequencies where not enough low-wind data was available to use the two-process model

Contamination of the end-fire data by noise entering through the side-lobes of the array beam pattern was a major concern in the design of the arrays and the data-processing procedure As Burgess and Kewley [7] pointed out, it is important that the side-lobe rejection be greater than the difference between the noise level at the horizontal in the noise pedestal and the noise level in the vertical The side-lobe levels in the beam patterns for the arrays used in this study were reduced as much as was possible given the constraints mentioned in section 2 II C, and the examination of the contour plots discussed above suggest that Burgess and Kewley's [7] criterion was met However, if side-lobe contamination was present in the data, it could affect the estimates of all the model parameters By raising the measured noise level equally at all wind speeds, side-lobe contamination would not affect the values obtained for n in the fits, but would raise the values for the A's More likely, however, side-lobe contamination would raise the levels for the low wind speeds more than for the higher ones This is due to the fact that, as Axelrod et al [13] pointed out, the difference

between the horizontal noise levels and the vertical noise levels is greater at lower wind speeds In this case, side-lobe contamination would have the effect of biasing upwards the A values in the fit and biasing downwards the n values

A tilt in the array axis would cause the up end-fire beam to point away from directly at the surface by an angle equal to the tilt angle, which could affect the results if a highly directive array (i e one with very good angular resolution) was used The array tilt was measured and recorded for each data set used in this study, and it never exceeded 3-4° Since the beam widths of the arrays used were very broad (between 25° and 60°, it was assumed that array tilt had a negligible effect on the data presented

The effect of sample size on the results depends on whether the data is time stationary over the period of sampling Stationarity had to be assumed in order to perform the analysis, non-stationarity in the data would cause errors in the Fourier transform and therefore in the estimates of the model parameters In this study, 40 averages of the FFT's of blocks of 2048 data points were used in the determination of the covariance matrices, corresponding to a sampling period of approximately 55 seconds In order to confirm that this was a reasonable number of averages to work with, a simple check was made using a representative data set Beam powers for the upward looking beam were calculated using 10, 20, 40, 80 and 200 averages These beam powers were scaled and compared and are tabulated in Table IV The values fluctuated by as much as 2 5 dB for the lower averages, but remained constant to

Frequency (Hz)	Number of Averages				
	10	20	40	80	200
30	80 5	79 0	78 9	79 1	78 8
60	67 8	70 0	69 4	69 8	69 5
100	57 5	58 6	58 0	57 0	57 2
125	62 3	62 0	60 9	60 6	60 9

Table 4 3 Comparison of beam powers for various averages

within ±1 dB for 40, 80 and 200 averages

No independent statistical check was made on the stationarity of the data presented in this report, but the results of other researchers indicate that deep-ocean ambient noise data is stationary over much longer time periods than were used in this study (approximately 1 minute averaging time) Sotirin and Hodgkiss [16] examined the stationarity of their data with statistical checks and found that their data were stationary for up to 50 minutes at low wind speeds and 20 minutes at high wind speeds, Jobst and Adams [28] found stationarity in their data for up to 22 minutes for unreported wind speeds, and Arase and Arase [29] found stationarity for up to 3 minutes at wind speeds between 20 and 30 knots

Finally, for the frequencies where not enough low wind-speed data was available to calculate A_L and n_L, all that could be done was to fit a straight line to the high-wind data For these frequencies, if $n_L \gg 0\,0$, then the estimates of n_H would be biased

to lower values Without a larger data set to work from, nothing could be done to avoid this bias

III. Plot of Source Level vs Frequency at Various Wind Speeds

Using the estimated fits to the wind-generated noise model parameters at the selected frequencies, it was possible to produce a plot of the estimated source level of the wind-generated noise for various wind speeds This plot is shown in Figure 4 28 From this figure, it is evident that the measured surface noise level is dependent on the local wind speed at all frequencies studied The general trend evident between 10 Hz and 150 Hz is a decrease in noise level with increasing frequency Beyond about 150 Hz, the noise level appears to be approximately independent of frequency except for the peak at 200 Hz (most evident at the lower wind speeds) which could be insignificant due to the relatively small number of observations available at this frequency

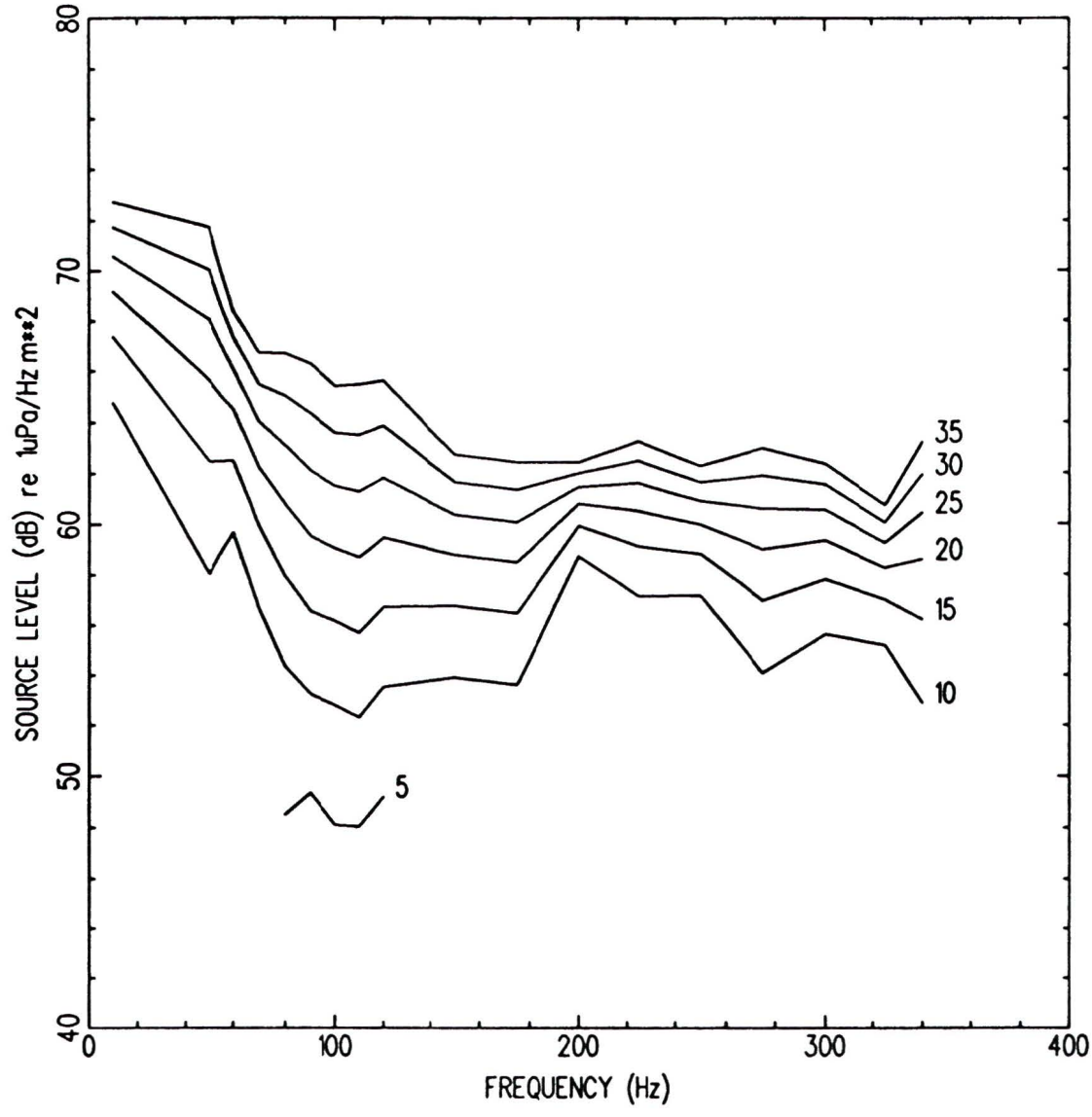

Figure 4 28 Plot of source level vs frequency at various wind speeds

Chapter 5

Discussion

In order to compare the results presented in this paper to those in the literature, a plot of source level vs frequency at various wind speeds was produced which included the results reported by other researchers for similar data as compiled by Kewley et al [2] This plot is shown as Figure 5 1 It is evident from the figure that the noise levels estimated from our data are, on average, slightly higher (approximately 3 dB) than those presented by Kewley et al [2] This could be due, in part, to contamination of our data by non wind-generated sources such as shipping, since mosts of Kewley et al 's data was collected in the southern hemisphere in areas of low shipping density The difference could also be due to the different approaches used in determining the source level Kewley et al used the difference in power between the upward-looking beam and the downward-looking beam to take out the effect of multiple bottom bounces as discussed in the introduction In our analysis,

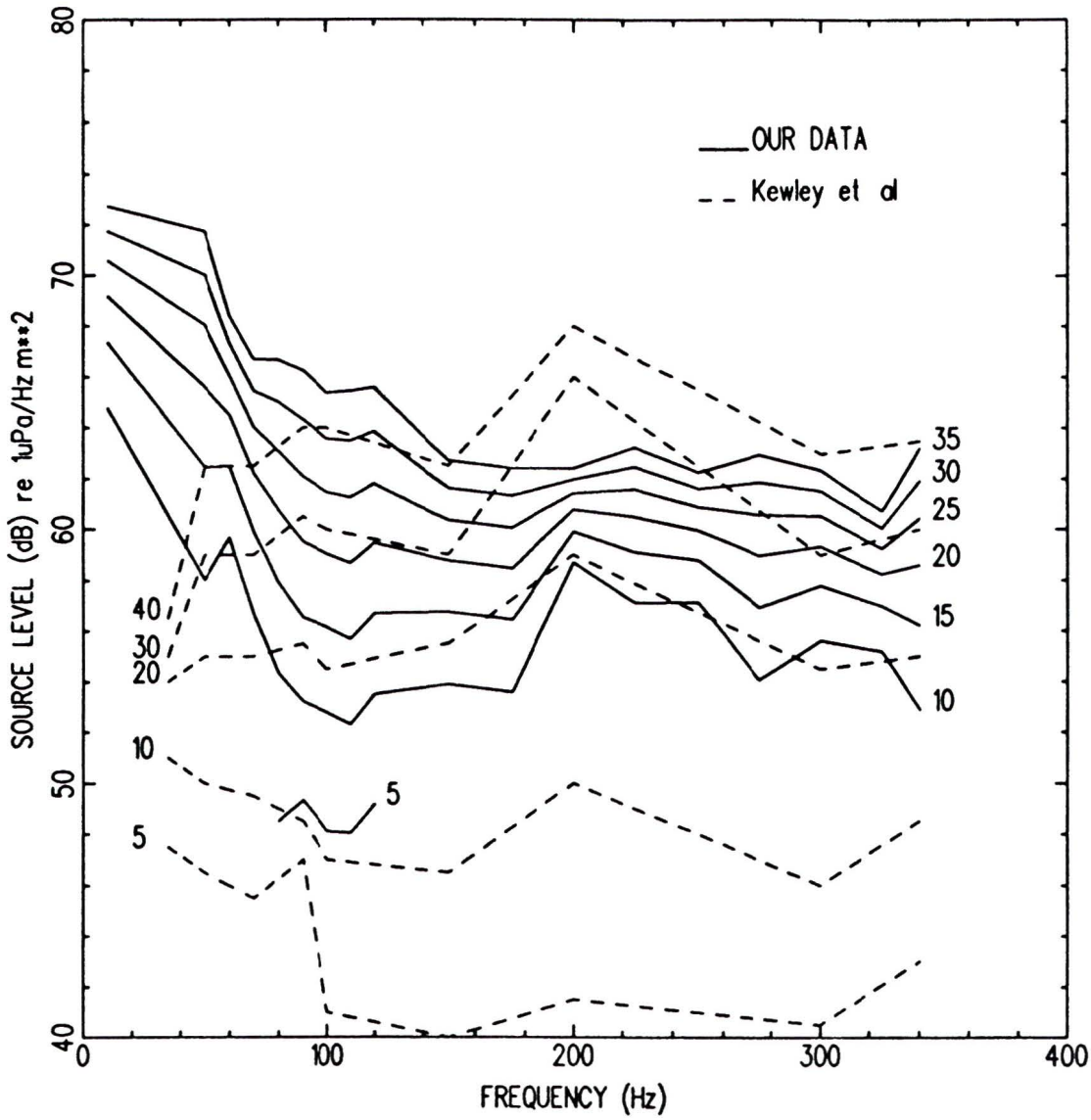

Figure 5 1 Plot of source level vs frequency at various wind speeds including data from other researchers

however, it was found that this difference was not consistent enough to rely upon, and actual bottom-loss measurements, in conjunction with a propagation model, were used to eliminate the effect of multiple bottom bounces

An interesting feature, apparent in the figure, is that Kewley et al also found a peak in the noise level at 200 Hz In their final presentation of the data, they showed a smoothed line at each wind speed which did not have this peak, assuming that it could be a result of experimental uncertainties Although not enough data were available in this study to confirm that this peak was significant, the fact that Kewley et al 's data show it as well suggests that further investigation could prove that this peak actually represents a real peak in the underlying process For example, the peak could correspond to the natural frequency of collective oscillation of bubble clouds This is supported by the theoretical results of Omta [30] He modelled the behaviour of clouds of bubbles disturbed by pressure fluctuations and found a resonant peak around 180 to 100 Hz for many different modelled bubble distributions

The results presented in this thesis seem to support the hypothesis of a two process model as discussed in section 3 II The plots of noise level vs wind speed for the frequencies from 80 to 100 Hz show an inflection point at a wind speed of 10 knots, with the slope of the noise level vs log of the wind speed line increasing past this point At the other frequencies, not enough low wind-speed data was available to comment on this feature More data, especially at the lower wind speeds would help to confirm the validity of this hypothesis

The importance of bottom-loss measurements to the determination of the source level of wind-generated ambient noise became readily apparent in the analysis of the data presented here If the bottom-loss correction described in section 3 I were not applied to the data, the result obtained for noise level in dB would be biased upwards by 10 $\log_{10}(1-b)$ where b is the bottom reflection coefficient If all the data were taken at the same location, only the value of the A parameters in the model would be affected and not the n (slope) values When using data from different areas, however, with different bottom reflection coefficients, the values of both A and n could be seriously affected by a failure to consider and remove the noise contributed by multiple bottom-bounce paths

Figure 4 28 represents the realization of one of the major objectives of this study in that it provides a means of estimating the surface noise level at a particular frequency given the local wind speed As mentioned in the introduction, this information is vital to the accurate study and prediction of total ambient noise fields in the ocean

Chapter 6

Suggestions for Further Research

The results obtained in this study from the available data suggest a need for further research in the area and indicate several avenues for future studies One of the difficulties encountered in processing the data derived from the fact that a relatively small number of hydrophones was used in the experiment Thus, when the spatial window was applied to reduce side-lobe levels in the beam patterns, the frequency range of the arrays were limited by the increase in beam width with the decrease in frequency This could be improved by employing more hydrophones in the array and thus increasing the array aperture

Increasing the array aperture (and thereby decreasing the beam width at all frequencies) would also aid in studying the fine structure of the vertical noise field This, in turn, would allow an investigation of the radiation pattern of the wind-generated noise sources This radiation pattern (represented by the $a(\theta)$ in Bannister's [12]

model) would help to identify the actual mechanism generating the noise and allow a determination of the source level independent of the source radiation pattern which was not possible in this study due to beam width limitations

In order to study the effect on measured noise level of the duration of the wind, as the data of Marrett and Chapman [10] suggest is an important factor, it would be very useful to have more frequent observations of both the surface noise level and the wind speed In this way, it would be possible to investigate the time-lagged cross-correlation between the two and to use this information to account for the affect on noise level of the duration of the wind

As pointed out by Prosperetti [18], the wind velocity and duration are not the only factors influencing surface agitation and therefore the noise generated Air and water temperature and density affect the wind friction velocity which, in turn, affects the surface agitation Measurements of these parameters are necessary to determine how important they are

Finally, to improve the statistical accuracy of the estimates of the model parameters, more data is needed for all wind speeds, especially the lower ones and better estimates of the wind speed are required This could be accomplished by deploying the array for a long period of time or during the passage of a weather system which could be expected to produce a good range of wind speeds and by using a more reliable and objective method of measuring the wind speeds such as a strip chart recorder

In order to accomplish these objectives, a large amount of ship time, manpower,

and processing power would have to be expended However, given the importance of accurate input estimates of wind-generated noise levels to the prediction of total noise levels in sophisticated prediction models [1, 2], it is felt that the results would be worth the effort

References

[1] J H Wilson, *Wind-Generated Noise Modeling,* Journal of the Acoustical Society of America, Vol 73, pp 211–216, January 1983

[2] D J Kewley, D G Browning and W M Carey, *Low Frequency Wind Generated Ambient Noise Source Levels,* Submitted to the Journal of the Acoustical Society of America.

[3] R.J Urick, *Principles of Underwater Sound,* McGraw-Hill Inc, New York, New York, 1983

[4] G M Wenz *Acoustic Ambient Noise in the Ocean Spectra and Sources,* Journal of the Acoustical Society of America, Vol 34, pp 1936–1956, December 1962

[5] D D Lemon, D M Farmer and D R. Watts, *Acoustic Measurements of Wind Speed and Precipitation Over A Continental Shelf,* Journal of Geophysical Research, Vol 89, pp 3462–3472, May 1984

[6] C L Piggott, *Ambient Sea Noise at Low Frequencies in Shallow Water of the Scotian Shelf,* Journal of the Acoustical Society of America, Vol 36, pp 2152–2163, November 1962

[7] A S Burgess and D J Kewley, *Wind-Generated Surface Noise Source Levels in Deep Water East of Australia,* Journal of the Acoustical Society of America, Vol 73, pp 201–210, January 1983

[8] A E Gill *Atmosphere-Ocean Dynamics,* Academic Press, Orlando, Florida, 1982

[9] J A Shooter and M L Gentry, *Wind Generated Noise in the Parece Vela Basin,* Journal of the Acoustical Society of America, Vol 70, pp 1757–1761, December 1981

[10] R. Marrett and N R. Chapman, *Low Frequency Ambient Noise Measurements in the South Fiji Basin,* Journal of the Acoustical Society of America, Vol 85, S127, 1989

[11] W A Kuperman and M C Ferla, *A Shallow Water Experiment to Determine the Source Spectrum Level of Wind-Generated Noise,* Journal of the Acoustical Society of America, Vol 77, June 1985

[12] R.W Bannister, A S Burgess and D J Kewley, *Estimation of Source Characteristics From Underwater Noisefield Measurements,* in Sea Surface Sound, B R. Kerman editor, NATO ASI Series, Kluwer Academic, Dordrecht, 1988

[13] E H Axelrod, B A Schoomer, and W A Von Winkle, *Vertical Directionality of Ambient Noise in the Deep Ocean at a Site Near Bermuda,* Journal of the Acoustical Society of America, Vol 37, pp 77–83, January 1965

[14] W M Carey and R.A Wagstaff *Low Frequency Noise Fields,* Journal of the Acoustical Society of America, Vol 80, pp 1523–1526, November 1986

[15] W S Hodgkiss and F H Fisher, *Vertical Directionality of Ambient Noise at* $32°N$ *as a Function of Longitude,* MPL Technical Memorandum 387-A, Scripps Institution of Oceanography, January 1988

[16] B J Sotirin and W S Hodgkiss, *Fine-Scale Measurements of the Vertical Ambient Noise Field,* Journal of the Acoustical Society of America, Vol 87, pp 2052–2063, May 1990

[17] B R. Kerman, *Underwater Sound Generation by Breaking Wind Waves,* Journal of the Acoustical Society of America, Vol 75, pp 149–165, January 1984

[18] A Prosperetti, *Bubble-Related Ambient Noise in the Ocean,* Journal of the Acoustical Society of America, Vol 84, pp 1042–1054, September 1988

[19] Priestly, *Spectral Analysis and Time Series,* Academic Press Ltd, San Diego, California, 1989

[20] W S Burdic, *Underwater Acoustic System Analysis,* Prentice-Hall Inc, Englewood Cliffs, New Jersey, 1984

[21] I Barrodale and M Greening, *Evaluation of Beamforming Algorithms Using Computer Simulation Techniques,* Contractors Report Series 85-3, Defense Research Establishment Pacific, March 1984

[22] H P Bucker, *Cross-Sensor Beam Forming With a Sparse Line Array,* Journal of the Acoustical Society of America, Vol 61, pp 494–498, February 1977

[23] F J Harris, *On the Use of Windows for Harmonic Analysis with the Discrete Fourier Transform,* Proceedings of the IEEE, Vol 66, pp 51–83, January 1978

[24] NAG Fortran Library Manual, Vol I

[25] D Hannay, *Processing of Low Frequency Bottom Loss Data,* Contractors Report Series 90-10, Defence Research Establishment Pacific, April 1990

[26] Crouch and Burt *The Logarithmic Dependence of Surface-Generated Ambient Sea-Noise Spectrum Level on Wind Speed,* Journal of the Acoustical Society of America, Vol 51, pp 1066–1072, July 1972

[27] W H Press, B P Flannery, S A Teukolsky, and W T Vettering, *Numerical Recipes, the Art of Scientific Computing,* Cambridge University Press, New York, New York, 1986

[28] W J Jobst and S L Adams, *Statistical Analysis of Ambient Noise,* Journal of the Acoustical Society of America, Vol 62, pp 63–71, July 1977

[29] T Arase and E M Arase, *Deep-Sea Ambient-Noise Statistics,* Journal of the Acoustical Society of America, Vol 44, pp 1679–1684, November 1968

[30] R. Omta *Oscillation of a cloud of bubbles of small and not so small amplitude,* Journal of the Acoustical Society of America, Vol 82, pp 1018–1033, September 1987

VITA

James William Joseph Cornish

Born 20 February 1963 at Calgary, Alberta

Educational Institutions Attended

Red-Deer College	1983 to 1984
Royal Roads Military College	1984 to 1988
University of Victoria	1988 to 1991

Degrees Awarded

B Sc (Honours)	Royal Roads Military College	1988

Honours and Awards.

Louise Mckinney Scholarship	1984-88
NSERC 1967 Science Scholarship	1988-90

PARTIAL COPYRIGHT LICENSE

I hereby grant the right to lend my thesis to users of the University of Victoria Library, and to make single copies only for such users or in response to request from the Library of any other university, or similar institution, on its behalf or for one of its users I further agree that permission for extensive copying of this thesis for scholarly purposes may be granted by me or a member of the University designated by me It is understood that copying or publication of this thesis for financial gain shall not be allowed without my written permission

Title of Thesis Measuring the Source Level of Wind-Generated Ambient Noise in the Ocean

Author 

J W CORNISH

23 Dec 90